

Vertical Accumulation of Ozone and Aerosol during the 2016 Southeastern U.S. Wildfires

Bo Wang¹, Shi Kuang², Gabriele G. Pfister³, Arastoo Pour-Biazar², Michael
J. Newchurch¹, Rebecca R. Buchholz³, Andrew O. Langford⁴

¹Department of Atmospheric and Earth Science, University of Alabama in Huntsville, Huntsville, AL,
USA

²Earth System Science Center, University of Alabama in Huntsville, Huntsville, AL, USA

³Atmospheric Chemistry Observations and Modeling Laboratory, NCAR, Boulder, CO, USA

⁴Chemical Sciences Division, NOAA Earth System Research Laboratory, Boulder, CO, USA

Key Points:

- WRF-Chem performance and emission inputs are evaluated against ozonesonde, UV DIAL, EPA PM2.5, EPA O₃, MODIS AOD, and fire inventories.
- (OC+BC)/CO ratios in fire inventories differ by a factor of 5.7 within fire region. Aerosol adjustment affects modeled PM2.5, aerosol extinction, and AOD.
- Fire emissions increase daytime net chemical ozone production by up to 25% in the upper air, and increase PM2.5 by up to 77% during daytime.

Abstract

The vertical accumulation of ozone and aerosol during an episode of the 2016 Southeastern United States Wildfires is analyzed by integrating a regional chemical transport model with ozonesonde, O₃ Differential Absorption Lidar (DIAL), ceilometer, surface monitors, and satellite products. The results indicate that measurements capture the vertical extent of the smoke plumes affecting the surface and upper air over Huntsville, AL, and also the enhanced ozone lamina in the plumes. Sensitivity simulations and tendency diagnostics characterize the chemical and physical processes affecting the vertical profiles downstream of the wildfires. The model results show that the net chemical ozone production (PO₃) dominates the daytime ozone accumulation by up to 19 ppb/10 hrs in the upper air over Huntsville. At the surface, the negative PO₃ is offset by positive O₃ contributions from vertical mixing and advection. Fire emissions increase the vertical ozone by affecting local chemical reactions, transportation, and vertical exchange. The dominant processes exhibit daily, diurnal, and vertical variability. Quantitatively, fire emissions increase the daytime positive PO₃ by up to 25% in the upper air, and increase the daytime PM_{2.5} by up to 77%. The capability of the regional model for reproducing the observations is explored. Increasing the fire aerosol emissions improves the model performance on domain-averaged PM_{2.5}. The model captures the well-mixed aerosol in the boundary layer but fails to fully reproduce the densest plumes seen in the DIAL and satellite. The discrepancies are associated with poor satellite observing condition due to clouds and with uncertainties in emission inventories.

1 Introduction

Biomass burning (BB) can release substantial aerosol and ozone (O₃) precursors that affect climate and air quality Akagi et al. (2011); Andreae and Merlet (2001); Crutzen and Andreae (1990); Crutzen, Heidt, Krasnec, Pollock, and Seiler (1979). In the past decades, observation and modeling studies have indicated that BB emissions contributed to local and regional air-quality problems Baker et al. (2016); Hodzic et al. (2007); D. A. Jaffe et al. (2013); Pfister, Wiedinmyer, and Emmons (2008); Wigder, Jaffe, and Saketa (2013), as well as to downwind air-quality problems by long-range transport Colarco et al. (2004); Cook et al. (2007); D. Jaffe et al. (2004); Lapina, Honrath, Owen, Val Martin, and Pfister (2006); Lindaas et al. (2017); Martin et al. (2006); McKeen et al. (2002); Morris et al. (2006); Oltmans et al. (2010); Rogers, Ditto, and Gentner (2020); Sapkota et al. (2005). The impacts of biomass burning on air quality vary dramatically over time and space.

Chemical transport models (CTMs) have been widely used for estimating fire impacts. CTMs can provide good spatio-temporal coverage, differentiate the impacts of specific sources, and support mechanism understanding of chemical and dynamical processes Baker et al. (2018). However, large uncertainties in fire-emission estimations and their treatment in models present challenges for estimating the variability of fire impacts. Uncertainties of fire-emission estimation can arise from inherent limitations of satellite detection (e.g., polar-orbiting detection, cloud/haze burden, small fires) and inherent uncertainties of empirical approaches for emission estimations Carter et al. (2020); Justice et al. (2002); Liu et al. (2020); Van Der Werf et al. (2017); Wang et al. (2018). The emission estimation uncertainties can affect simulated smoke loading in domain-averaged scale, and at local and hourly-to-daily scales in particular Cohen, Ng, Lim, and Chua (2018); Liu et al. (2020); Zhang et al. (2014). Inappropriate model treatment can induce misplacement of smoke plumes and O₃ vertically Baker et al. (2018); Cohen et al. (2018); Fast et al. (2016, 2006); Wu et al. (2017). Therefore, observation evaluation is essential to understand the model bias and emission uncertainties for a given fire event.

Although satellites and surface monitors make routine measurements of atmospheric O₃ concentration, balloon soundings and the lidar technique can provide precise vertically resolved O₃ observations throughout the troposphere and lower stratosphere Thomp-

son et al. (2011). This vertical information significantly benefits air-quality management and modeling improvement Cooper, Langford, Parrish, and Fahey (2015). We take advantage of both ozonesonde Newchurch, Ayoub, Oltmans, Johnson, and Schmidlin (2003) and ozone lidar Kuang, Burris, Newchurch, Johnson, and Long (2011) at the University of Alabama in Huntsville (UAH) to observe vertical profiles. The UAH ozone lidar is affiliated with the Tropospheric Ozone Lidar Network (TOLNet, <https://www-air.larc.nasa.gov/missions/TOLNet/>). Under a collaborative protocol, the TOLNet lidars have demonstrated their feasibility and capability in fire studies M. Johnson, Kuang, Wang, and Newchurch (2016); Kuang et al. (2017); A. Langford et al. (2015); Reid et al. (2017); Strawbridge et al. (2018) and extensive scientific projects Gronoff et al. (2019); Leblanc, Brewer, Wang, and Granados Muñoz (2018); Sullivan et al. (2019). The continuous profiling of ozone and aerosols provides details missed by isolated measurements and is an asset for model evaluation by coordinating measurements A. Langford et al. (2018); A. O. Langford et al. (2019). In addition, the ultraviolet (UV) backscatter (or extinction) profiles retrieved from ozone lidar can quantify the aerosol variability at high spatio-temporal resolution and these measurements serve as a tracer for fire smoke Kuang et al. (2020); A. O. Langford et al. (n.d.). To our best knowledge, there has been little or no attempt to evaluate CTMs using this range-resolved UV aerosol optical product.

Integrating vertical observations into CTMs can also improve our understanding of the fire impacts on vertical profiles. Due to multiple O_3 sources in troposphere and a lack of coincident measurements at sufficient spatial resolution, coordinating observations and modeling are often crucial for understanding O_3 production from fire emissions Fiore, Pierce, Dickerson, Lin, and Bradley (2014). The diagnostics of trace-gas tendencies in CTMs output are widely used to identify the drivers for ozone production due to varied anthropogenic and natural sources while fewer attempts for biomass burning sources occur Barth et al. (2012); Hu, Xue, Kong, and Zhang (2019); Lu et al. (2018); Pfister et al. (2019). In this study, the O_3 -tendency diagnostics, together with sensitivity simulations both with and without fire emissions, allow exploration of the roles of chemical and dynamical processes affecting vertical O_3 accumulation downstream of fires. The enhancement of local vertical O_3 due to fire emissions is expected to arise from multiple processes, including the local chemical reactions (e.g., photochemical reaction of input O_3 precursors from fire emissions), transportation (e.g., the transported higher O_3 produced by upwind smoke plumes), and the vertical exchange (e.g., redistribution of O_3 by interactions between surface and upper air). We are interested in understanding the impact of those processes on vertical O_3 variability in fire smoke.

With relatively flat topography in the SEUS region, Huntsville station was usually dominated by local anthropogenic/biogenic/agricultural burning at the surface and more frequent wildfire plumes in the free troposphere (FT) Reid et al. (2017). In this case study, we observed smoke affecting both surface and upper air over Huntsville downstream of the wildfires. Using comprehensive observations (Huntsville ground-based lidars, in-situ measurements, satellite) to evaluate the performance of regional model simulations results in a tool to estimate the vertical variability of fire impacts. Integrating vertical observations and modeling can benefit the evaluation work and scientific understanding. The following objectives comprise this study: (1) Evaluate the model performance against regional and local observations, especially vertical ozone and UV aerosol extinction profiles and understand the model capabilities and limitations to reproduce the observations. (2) Characterize the chemical and dynamical processes affecting the vertical ozone accumulation in smoke plumes and understand the roles of local chemical reactions, transportation, and vertical exchange. (3) Quantify vertically the contribution from fire emissions to net chemical ozone production and particulate matter.

2 Data and Methods

2.1 Wildfires Episode and Study Area

The 2016 Southeastern United States (SEUS) Wildfires series occurred along the Southern Appalachians throughout October and November 2016 and burned over 158,000 acres across six Southern states (see Table S1 in the supporting information). Multiple factors contributed to the extraordinary wildfires outbreak and spread, including the exceptional drought, deep leaf litter and duff layers, many human ignitions with few lightning strikes, episodic strong winds by frontal systems, and complex mountain landscapes Konrad and Knox (2017). We focus on a high-pollution episode when smoke influenced Huntsville station and the SEUS region in 12-14 November 2016. Figure 1a shows the locations and names of 14 largest active wildfires around this study period. Figure 1b shows the study domain with surface PM_{2.5} and O₃ monitoring sites. Huntsville station is located in North Alabama, with ground-based lidars and ozonesondes to be introduced in the following sections.

2.2 Huntsville Station Facilities

Both the Ceilometer and the ground-based O₃ Differential Absorption Lidar (DIAL) at the UAH campus (34.725°N, 86.645°W) detect the vertical aerosol structure. Balloon-borne Electrochemical Concentration Cell (ECC) ozonesonde launched from the UAH campus measures vertical O₃ concentration in smoke plume. Model simulations with both DIAL (aerosol extinction and O₃) and ozonesonde data assess how well the model captures the vertical distribution of O₃ and aerosol.

Although primarily designed for the detection of cloud heights, ceilometers have the potential capability for a quantitative retrieval of aerosol backscatter coefficient Wiegner et al. (2014). The Vaisala CL51 ceilometer used in this study is a pulsed diode-laser lidar (905 nm) in the UAH Mobile Integrated Profiling System (MIPS) Wingo and Knupp (2015). For this case, the ceilometer, located on the UAH campus, measures backscatter profiles up to 15 km above ground level (AGL) with high spatial and temporal resolution at 30 m and 15 s, respectively. Because the backscatter signal is dominated by the aerosol component at 905 nm, the total backscatter intensity serves as an indicator of relative aerosol loading during 12-14 November 2016.

The UAH campus also houses one of the TOLNet O₃ DIAL systems, named the Rocket-city O₃ Quality Evaluation in the Troposphere (RO₃QET) lidar. RO₃QET measures vertical O₃ profiles from 0.1 km up to 10 km above the ground using 289 and 299-nm lasers with an uncertainty of about $\pm 10\%$ Kuang et al. (2011). The temporal resolution of the lidar sampling is adjustable and is typically set at 10 minutes. The vertical resolution varies with altitude to obtain sufficient lidar signal-to-noise ratio and is between 150 and 300 m in the planetary boundary layer (PBL). Aerosol extinction coefficients at the non-absorption line (299 nm) are retrieved by assuming a constant aerosol extinction-to-backscatter ratio, which is 60 sr for this study. Validation experiments through comparing co-located high spectral resolution lidar (HSRL) observations suggest that the RO₃QET lidar is capable of capturing aerosol variability at high spatio-temporal resolution up to 6 km Kuang et al. (2020).

The Huntsville ECC ozonesonde attached with radiosonde provides vertical profiles of ozone, temperature, relative humidity (RH), and wind. In this study, the data derive from one of the weekly flights, which make observations from the surface up to 35 km with a vertical resolution of 100 m Newchurch et al. (2003) at the Huntsville ozonesonde station on the UAH campus. Measurements have precision better than $\pm 5\%$ and an accuracy better than $\pm 10\%$ for O₃ B. J. Johnson et al. (2002).

2.3 Surface Data and Satellite Products

Hourly PM_{2.5} and O₃ measurements retrieved from the Environmental Protection Agency (EPA) (<https://www.epa.gov/outdoor-air-quality-data>) are used to evaluate the model performance on surface air quality within the smoke-impacted region. Moderate Resolution Imaging Spectroradiometer (MODIS) Collection 6 Level 2 10 km aerosol optical depth (AOD) data onboard Terra and Aqua (MOD04_L2 and MYD04_L2) Levy, Hsu, et al. (2015) acquired from the NASA Earth Data Level-1 and Atmospheric Archive & Distribution System Distributed Active Archive Center (LAADS DAAC) website (<https://ladsweb.modaps.eosdis.nasa.gov>) are used to evaluate the model performance on horizontal plume extent. Supporting information (Text S1) details the AOD estimates from MODIS and the model. Visual images from MODIS and the Visible Infrared Imaging Radiometer Suite (VIIRS), available via NASA Worldview website (<https://worldview.earthdata.nasa.gov/>), qualitatively assess plume coverage and fire detections from fires and thermal anomalies products. The sensor resolutions of MODIS and VIIRS hotspot detections are 1 km and 375 m, respectively.

2.4 Model Description and Experiment Design

A fully coupled meteorology-chemistry model, the Weather Research and Forecasting with Chemistry model (WRF-Chem V3.9.1) is applied in this study. The model configurations are listed in Table 1. For this study we selected the Model for Ozone and Related chemical Tracers (MOZART) gas phase chemical scheme Emmons et al. (2010) coupled with the Georgia Institute of Technology–Goddard Global Ozone Chemistry Aerosol Radiation and Transport (GOCART) aerosol scheme Chin, Rood, Lin, Müller, and Thompson (2000), referred to as MOZCART Pfister et al. (2011). Other parameterizations include Morrison’s microphysics scheme, the Rapid Radiative Transfer Model (RRTM) long-wave and Goddard shortwave radiation schemes, the Monin-Obukhov surface layer, the Noah Land Surface Model, the Yongsei University (YSU) PBL, the New Grell cumulus scheme (G3), and the simplified Tropospheric Ultraviolet-Visible photolysis scheme (F-TUV). National Centers for Environmental Prediction (NCEP) North American Mesoscale (NAM) 12 km Analysis data (<https://rda.ucar.edu/datasets/ds609.0/>, accessed 7 Feb 2018) provide the initial and lateral boundary meteorological conditions. MOZART-4 global model outputs provide the initial and lateral chemical conditions. Biomass burning emissions are calculated using the Fire Inventory from NCAR (FINNv1.5) Wiedinmyer et al. (2011) and the online plume-rise model Freitas et al. (2007). FINNv1.5 are based on fire counts derived from the Moderate Resolution Imaging Spectroradiometer (MODIS). The hourly emissions are allocated using the standard WRAP diurnal profile WRAP (2005). Anthropogenic emissions for both area and point sources are obtained from the 2011 U.S. EPA national emissions inventory (NEI 2011 v2). Biogenic emissions are calculated online using the Model of Emissions of Gases and Aerosols from Nature (MEGAN) module Guenther et al. (2006).

Two nested domains cover CONUS and SEUS with 16 km and 4 km horizontal resolutions, respectively. The vertical coordinate comprises 60 unequally spaced layers below 50 hPa, with 12 layers below 2 km altitude and a center height of 28 m for the lowest layer (see vertical grids structure in Figure S1). The simulation time period ranges from 8 to 14 November 2016, for which the 12-14 November period in the inner domain serves to avoid the influence of the model spinup during the first 4 days. The modeled meteorology is reinitialized with analysis fields every 24 hours but the chemistry is recycled from the previous day. Three simulations estimate the wildfire impacts (Table 1): simulation CTRL contains no fire emissions; simulation FIREorig contains the original fire emissions (speciated from FINNv1.5 PM_{2.5}) without emissions correction; simulation FIREcorr contains the fire emissions with emissions adjustment (description in Section 3.2). In order to generate identical meteorology for the sensitivity analysis on fire-impacted O₃, the aerosol-radiation feedback is disabled.

2.5 Fire Inventories and Burn Area Products

The Monitoring Trends in Burned Severity database (MTBS; <https://www.mtbs.gov>) provides input for total burn acres since ignition for sorting large wildfires (Table S1). To investigate the emission inputs, the daily burn area is grouped for each wildfire by aggregating FINNv1.5 burn area in the geospatial bounding box from MTBS wildfire database. The fire emission inputs for this work (FIREorig and FIREcorr runs) are compared with three MODIS-based fire inventories: the FINNv1.5, the Global Fire Assimilation System version 1.2 (GFASv1.2) Kaiser et al. (2012), and the Quick Fire Emissions Database version 2.5_r1 (QFEDv2.5_r1) Darmenov and da Silva (2013).

3 Results

3.1 Horizontal and Vertical Plume Transport

In this section, analysis of the horizontal and vertical plume transport using satellite and ground-based lidars identifies the smoke-impacted period for model evaluation and diagnostic analysis later. This analysis also reveals that the daily and diurnal variations of smoke transport are mediated by synoptic weather and PBL evolution.

In Figure 2, MODIS AOD shows that the wildfires along the Southern Appalachians continued to burn and emitted a significant amount of smoke over SEUS region in 12-14 November 2016. Thus, we select 12-14 November to compare the model with MODIS AOD and surface monitors in later sections. NOAA WPC surface analysis (Figure S2) shows that a cold front passed over the wildfire region during 12-18 LT on 11 November. After the frontal passage, smoke stretched across portions of SEUS region by northeasterly wind on 12 November. As high-pressure circulation dominated the following two days, AOD shows less spreading but more concentrated pattern around the wildfires.

The UAH ceilometer captured the aerosol plumes downwind of the fires, as shown in Figure 3. The time-height curtain of backscatter intensity shows that several plumes passed over Huntsville in the nighttime residual layer (RL) (Figure 3a). Some plumes subsided toward surface before sunrise; others were entrained by a developing PBL in the morning and then mixed vertically throughout the PBL. This mixing provides a mechanism for fire emissions to contribute to the downwind air quality over night. In addition, an elevated aerosol plume stayed at ~ 2 km AGL from 12 UTC (6 LT) on 12 November to 12 UTC (6 LT) on 13 November, and it is likely to be fire smoke as MODIS shows obvious smoke spreading over Huntsville.

The most severe surface particulate air pollution at Huntsville occurred on 13 November, when an air-quality alert was issued for Madison and Morgan counties in the afternoon instigating DIAL measurement from 19:37 to 22:17 LT on 13 November under this high aerosol loading condition. The time-height curtain of aerosol extinction coefficient at 299 nm (Figure 3b) shows heavy background aerosols and relatively dense plumes within that domain. The background aerosols below the capping inversion layer (~ 0.5 /km below 1.5 km AGL) results from sufficient daytime mixing in the well-developed PBL. A relatively dense plume (>1.0 /km) features about 4 times higher extinction than that in usual aerosol loading conditions. At 22 LT, the dense plume extended across the whole RL column and evolved to be a thicker layer (~ 0.7 km thickness) between two finer layers. The specified fine structure is highly consistent with that observed by ceilometer backscatter (Figure 3c). Ozonesonde and DIAL are used to assess the model performance on 12 and 13 November, respectively.

3.2 Model Performance for AOD and Emissions Adjustment

In this section, the assessment of the model capability for reproducing the spatial pattern of smoke plumes as compared to satellite observations results in an adjustment

of emission inputs. We justify this adjustment by comparing our emission inputs with three fire inventories, which give different emission estimations.

Comparing WRF-Chem AOD to MODIS AOD in 12-14 November (see details in Text S2 and Figure S3) suggests that the model is able to reproduce the overall spatial pattern of smoke plumes over SEUS, with a spatial correlation coefficient between modeled and observed AOD 0.6 on average. However, the model underestimated the AOD magnitude. The domain-averaged observed AOD is about 3.6 times of the simulated AOD. The cause could be uncertainties in emission estimations Pereira et al. (2016); Zhang et al. (2014), inadequate assumptions of aerosol optical properties Curci et al. (2015), the use of simplified aerosol chemistry modules without secondary organic aerosol Fast et al. (2006), or misrepresentation of transport processes Aouizerats, Van Der Werf, Balasubramanian, and Betha (2015); Wu et al. (2017). In this case, the bias in predicting the frontal passage could cause uncertainties to the smoke transport on 12 November (Figure S2), and the aerosol scheme GOCART could also lead to uncertainties because it does not include secondary organic aerosols. However, quantifying each bias is a challenge beyond our scope. In this case study, we focus on exploring the uncertainties of emissions only and increase the original fire aerosol emissions (PM_{2.5}, PM₁₀, organic carbon, black carbon, and sulfate are speciated from PM_{2.5} in FINNv1.5) by a factor of 3.6, without changing the fire gas-phase emissions. Even though this approach does not rectify all the uncertainties in the emission estimates and may not reflect the temporal-spatial variations of smoke behavior, such a sensitivity study can help in constraining the emission estimates based on satellite observations.

To justify this method for scaling the aerosol emissions, we compare the original simulation (FIREorig) and the simulation with scaled aerosol emissions (FIREcorr) with the inter-inventory differences. Figure 4 shows the ratio of carbonaceous aerosol (both organic carbon OC and black carbon BC) and carbon monoxide CO in different fire inventories and our simulations. Each data point indicates the daily fire emission from the fire inventories or our model inputs, summed over the wildfire region of interest defined in 33.46-38.17°N and 78.75-86.25°W (see the selected region in Figure S4). The three inventories show considerable discrepancies in the emissions ratios in November 2016 over the wildfire area. The ratio is about 0.07, 0.09, and 0.4 in Gg/Gg for FINNv1.5, GFASv1.2, and QFEDv2.5_r1, respectively. Such a broad range of emission ratios justifies our choice to scale the emission input from 0.08 Gg/Gg to 0.3 Gg/Gg.

The discrepancies among fire inventories might arise from their different estimation processes. Although all of the three inventories are based on MODIS fire detections, FINNv1.5 turns MODIS fire counts into burned area based on some assumptions Wiedinmyer et al. (2011), GFASv1.5 assimilates MODIS Fire Radiative Power (FRP) Kaiser et al. (2012), and QFEDv2.5_r1 uses MODIS FRP directly combined with a scaling factor by a top-down constraint for different biomes Darmanov and da Silva (2013). Carter et al. (2020) showed that fire aerosol emissions from different inventories differ by a factor of 4 to 7 over North America. Liu et al. (2020) showed that temperate North America (TENA) has a coefficient of variation as high as 102% for mean annual OC+BC emissions among fire inventories. Our comparisons agree with previous assessment about the uncertainties in fire aerosol emissions. The (OC+BC)/CO ratios over the SEUS wildfire region differ by a factor of 5.7, within the discrepancy envelope of previous studies. Because the performance of an individual fire inventory also depends on the region and season, emission evaluation and adjustment is often necessary for a given fire event.

3.3 Model Performance for Surface PM_{2.5} and Vertical Extinction

Using the adjusted emission inventory, we assess how well the model can simulate surface PM_{2.5} and vertical aerosol loading through comparing the model results with observations by surface monitors, lidar, and satellite.

Figure 5 shows the time series of U.S. EPA PM_{2.5} and modeled PM_{2.5} in three sensitivity simulations. The FIREorig simulation shows obvious underestimation of observed PM_{2.5}. Quantitatively, the standard deviations normalized with respect to observations are much lower than 1.0 (see pattern statistics in Figure S5). After the emission adjustment, the FIREcorr simulation is able to capture the domain-averaged magnitude and reproduce the maximum hourly PM_{2.5} ($\sim 200 \mu\text{g}/\text{m}^3$ on 12 November at Site 1). Additionally, the improved model reveals dominant fire contributions to the observed PM_{2.5} exceedance of air quality standard ($35 \mu\text{g}/\text{m}^3$ for 24-hour limit), especially at the rural sites nearby wildfires. Therefore, it is reasonable to use the FIREcorr simulation to investigate the fire impacts on PM_{2.5}.

Despite the improvement on magnitude, a domain-averaged scaling factor cannot improve the model performance on the diurnal variations. Both FIREorig and FIREcorr simulations perform well in reproducing the diurnal cycle at Site 3-7 but poorly at Site 1, 2, and 8. Statistically, modeled and observed PM_{2.5} have a fairly strong to moderate correlation at Site 3-7 and weak correlation at Site 1, 2, and 8. This model bias in the diurnal fire behavior can be partly explained by satellites providing information at the overpass time only Wang et al. (2006), wind bias, and the domain-averaged scaling factor adopted here. Other potential error sources are discussed later.

Figure 6 shows the comparison between the DIAL-retrieved aerosol extinction (at 299 nm) and the simulated vertical aerosol extinction (at 300 nm) during 19-23 LT on 13 November. The FIREcorr simulation is able to capture the nocturnal boundary layer aerosol ($\sim 0.5/\text{km}$ below 1.5 km AGL), while the FIREorig simulation underestimated the magnitude. This comparison indicates that the improved simulation can reproduce the well-mixed smoke during the daytime PBL development. However, the FIREcorr simulation missed the densest plume ($> 1.0/\text{km}$ after 20 LT on 13 November) observed by DIAL, and it underestimated the highest MODIS AOD nearby wildfires (observed at noon on 13 November in Figure S3) and PM_{2.5} at individual site nearby wildfire (e.g., Site 2). A likely reason for the underestimate is missing fire sources.

To confirm this hypothesis, we examine both MODIS and NPP/VIIRS reflectance images with the fires and thermal anomalies product (Figure 7), and group the FINNv1.5 daily burn area by each wildfire (Figure 8). It was cloudy and hazy over the wildfires region on 13 November. Although some wildfires emitted visible dense smoke plumes (e.g., the Rough Bridge Fire in north Georgia) and were counted in the NPP/VIIRS night detection, the fires were not counted in MODIS by the abnormal thermal product. Subsequently, the burn areas of many wildfires are zero on 13 November in FINNv1.5 inventory. Two other MODIS-based inventories (GFASv1.2 and QFEDv2.5_r1) also have quite small aerosol and gas emissions on 13 November (Figure S7). These differences imply that the clouds and thick haze probably obscured the MODIS fire detection on 13 November. The detection limitation is probably associated with attenuated fire signal and solar heating during the day and the potential cloud/smoke classification issues Justice et al. (2002); Polivka, Wang, Ellison, Hyer, and Ichoku (2016). As a result, the model using the MODIS-based fire inventories could not reproduce some freshly-emitted smoke plumes.

3.4 Model Performance for Surface Ozone and Vertical Ozone

This section reports the modeled O₃ compared with surface monitors, ozonesonde, and DIAL measurements. Because the aerosol-radiation feedback has been turned off to generate identical meteorology, and MOZCART does not consider heterogeneous or aqueous chemistry, the modeled O₃ results in FIREorig and FIREcorr simulations are identical.

Figure 9 shows the time series of EPA O₃ and modeled O₃ in sensitivity simulations. Our model reproduced the observed surface O₃ level (below 60 ppb) during 12-

14 November at most sites. The results show consistent diurnal variations between simulated and observed O_3 at both rural and urban sites, with strong to moderate correlation coefficients (see pattern statistics in Figure S6). The model performance at Site 3 and 5 is weaker, indicated by a low correlation coefficient and high normalized root-mean-square (NRMS) error. The model bias on O_3 can be complicated by meteorology, emissions, and model parameterizations. In this case, uncertainty in fire emissions is not the only possible source for the surface O_3 bias. Other factors, such as transport bias during the frontal passage, model capability in reproducing nocturnal stable layer, and the accuracy of anthropogenic and biogenic gaseous emissions, might also induce larger model bias. The difference between FIREcorr and CTRL simulations suggests that the total fire impacts on surface O_3 concentration was smaller than 10 ppb at most sites.

An ozonesonde launched from UAH campus at 13 LT on 12 November. Figure 10 compares modeled results with the observed vertical profiles, including ozone volume mixing ratio, relative humidity, potential temperature (θ), horizontal wind speed, and horizontal wind direction. The ozonesonde reveals an enhanced O_3 lamina between two θ inversion layers between 1.4-2.3 km. It peaks at 1.8 km AGL with 56 ppb, ~ 12 ppb larger than PBL. This thick lamina co-existed with the elevated aerosol plume observed in ceilometer in light northeasterly wind. This coexistence of fire-impacted aerosol plume and enhanced O_3 suggests a fire-impacted ozone lamina above the PBL height ~ 1.4 km. Overall, WRF-Chem is able to reproduce vertical ozone and meteorological profiles in smoke below 3 km. In particular, the model reproduces the wet and ozone-rich lamina, and obtains temperature and wind field consistent with observations; however, it is limited in simulating finer inversion layers. The model predicts a lower PBL height of 1.2 km than the observed 1.4 km, and it does not resolve the upper θ inversion at 2.3 km well. This limitation is likely due to the relatively coarse vertical resolution at ~ 2 km and the bias in predicting wind shear when the wind turned sharply above the lamina, as observed by sonde. The underestimated O_3 in PBL is consistent with the underestimated surface O_3 at the nearby site. This underestimate can be due partly to the model bias in wind direction and relative humidity in PBL, as well as to other factors discussed. The model also reproduces the O_3 laminae observed by DIAL during 19-23 LT on 13 November (Figure 6), but it underestimates the O_3 magnitude in the nocturnal boundary layer, which underestimate might be caused by the uncertainties in emission inputs as discussed in the previous section.

3.5 Diagnosing Fire Impacts on Vertical O_3 and PM2.5 Distribution

Because the model performs well in simulating the vertical and surface ozone distributions and reproducing the well-mixed aerosol during daytime, the model calculations estimate the vertical ozone accumulation in fire smoke during daytime on 12 and 13 November 2016. We begin with a regional sensitivity analysis to show the overall fire impacts and the possible sources, and then apply the model's tendency diagnostics to further examine the processes contributing to the ozone accumulation over Huntsville. Fire-impacted PM2.5 indicates the altitude and strength of the fire smoke.

3.5.1 Regional Impacts at 13 LT on 12 and 13 November 2016

Figure 11 shows the modeled longitude-altitude curtain plots of O_3 , fire-impacted O_3 , and fire-impacted PM2.5 at 13 LT (19 UTC) on 12 November over the SEUS region. The curtain shows that an enhanced O_3 lamina at 2 km ASL spreads widely from 78° W to 88° W and passes over the Huntsville station (Figure 11a). This thick layer is spreading above PBL and is capped below 3 km by a strong wind shear when the wind turns strongly westerly above ~ 3 km. Figure 11b and 11c show the modeled fire impacts (FIREcorr minus CTRL) on O_3 and PM2.5, respectively. The simulations show enhanced O_3 concentration within the elevated smoke plume, which are consistent with our observation analysis. Quantitatively, the fire emissions result in an O_3 enhancement of 2-5 ppb and

PM2.5 enhancement of 10-20 $\mu\text{g}/\text{m}^3$ at 13 LT. In 85-86° W, the enhancements in O_3 and PM2.5 can be much larger than 5 ppb and 20 $\mu\text{g}/\text{m}^3$, respectively. Using the modeled hourly PM2.5 and AOD (not shown here), we estimate that the smoke plume is transported to Huntsville from multiple wildfires that occurred during the frontal passage on 11 November (see the large active wildfires in Figure 8 and wildfire map in Figure 1a). The wind-shear structure caps the mixed smoke plume with enhanced O_3 in the lowest level of FT. Below the elevated plume, there is slightly lower PBL O_3 enhancement (1-2 ppb) and PM2.5 enhancement (5-15 $\mu\text{g}/\text{m}^3$) in 86-88° W. The smoke in the PBL is relatively fresh with < 6 hrs transport time and is likely emitted from nearby small fire on 12 November.

As the weather condition turns to high-pressure circulation on 13 November, a new pattern emerges with concentrated fire impacts from the surface up to 2 km ASL on a regional scale (Figure 12). PBL O_3 increases in the stagnant air, and fire emissions contribute more to O_3 and PM2.5. Quantitatively, the fire emissions result in a dominant O_3 enhancement by 4-10 ppb or higher and PM2.5 enhancement by 40-80 $\mu\text{g}/\text{m}^3$ or higher at 13 LT (Figure 12b and 12c). A large portion of the well-mixed PBL smoke is emitted from 12 November, when the wildfires are most active during our study period (Figure 8). As illustrated in the observation analysis, the smoke remains in the residual layer overnight and can effectively be transported to affect other locations on the next day.

3.5.2 Local Impacts in 7-17 LT on 12 and 13 November 2016

The sensitivity simulations confirm that fire emissions impacted the vertical ozone contribution over Huntsville on 12 and 13 November. This local enhancement could be caused by the transport of ozone and/or its precursors from fire emissions. The modeled results also imply that fire is not an exclusive source contributing to the observed ozone laminae. This result brings up two questions: (1) What are the relative roles of chemical and dynamical processes on the vertical ozone accumulation? (2) What is the relative contribution of fire emissions to the total net photochemical ozone production? To address these questions, we analyze the processes affecting vertical ozone distribution through WRF-Chem tendency diagnostics, including net chemical ozone production PO_3 (Chem), horizontal and vertical advection of ozone (AdvH+AdvZ), and vertical mixing of ozone (Vmix). The daytime ozone tendency output from the sensitivity simulations with fire emissions (FIREcorr) and without fire emissions (CTRL) is used to explore the fire contribution. The following model results are averaged over 5×5 horizontal grids (20 km \times 20 km) over Huntsville for a better representativeness.

Figure 13a and 13b show daytime-integrated (7-17 LT) O_3 process tendencies and PM2.5 over Huntsville in the FIREcorr and CTRL simulations on 12 and 13 November, respectively. The absolute O_3 process tendencies show similar patterns on both days. In the upper air (0.2-2.0 km AGL), the positive PO_3 dominates the daytime ozone accumulation on both days. The total PO_3 peaks on 13 November in the middle PBL by up to 19 ppb/10 hrs at 0.5 km. In the surface layer below 0.2 km, pronounced negative PO_3 is caused by the quick NO_x titration near the surface (modeled $\text{NO}_x \sim 15$ ppb). The negative PO_3 is offset by positive O_3 contributions from vertical mixing and advection processes. Vertical mixing contributes positively near the surface yet negatively in the upper air, because it tends to disperse the enhanced O_3 from the upper air to the surface Hu et al. (2019). The results imply that local chemical processes dominates the upper air ozone accumulation while dynamical processes directly contribute to the build-up of ground-level ozone over Huntsville.

Figure 13c and 13d extract the relative O_3 tendencies and PM2.5 contributed by fire emissions (FIREcorr minus CTRL) on 12 and 13 November, respectively. Here FIREcorr-CTRL SumTend (SumTend means the sum of all process tendencies) indicates the daytime-integrated ozone change due to fire emissions (Figure S8). During 12-13 November, fire

emissions increase the vertical O_3 concentrations by affecting local chemical reactions, transportation, and the vertical exchange. The total daytime ozone increase due to fire emissions is similar on both days, with largest contributions at lower altitude (up to ~ 8 ppb). However, the dominant processes contributing to the total signals show daily and vertical variability. On 12 November, an increase of positive PO_3 dominates the upper-level (above 1.2 km) fire-impacted O_3 accumulation, while the transport process dominates at the lower level. In contrast, on 13 November, an increase in PO_3 (either through increased ozone chemical production or a decrease in ozone chemical loss) dominates the lower level (below 1.0 km), while the transport processes dominate at the upper level. The decrease of negative PO_3 in the surface layer (i.e., PO_3 is more negative in CTRL compared to FIREcorr below 0.2 km) is affected by the additional NO_x and VOCs from the fire emissions.

Quantitatively, the percentage contribution from fire emissions to the net chemical ozone production is calculated by (FIREcorr-CTRL)/FIREcorr results during daytime over Huntsville. Fire emissions contribute 14% to the highest daytime PO_3 on 12 November (2 ppb out of 17 ppb at 1.6 km) and 25% on 13 November (5 ppb out of 19 ppb at 0.5 km). This different photochemical production is associated with the varied fire emissions and smoke transport. The smoke strength is indicated by the fire-impacted $PM_{2.5}$ here. The percentage contribution from fire emissions to vertical hourly $PM_{2.5}$ peaks at 51% on 12 November ($10 \mu g/m^3$ out of $19 \mu g/m^3$ at 1.8 km) and 77% on 13 November ($37 \mu g/m^3$ out of $48 \mu g/m^3$ at 1.0 km). The results suggest an increased fire contribution to the enhancement of ozone and particulate matter from day to day.

Diurnal variability of process tendencies can be affected by the boundary layer evolution, transport changes over the course of the day, and photochemistry. To examine how the different processes vary over the day, we analyze the total and fire-impacted process tendencies for 7-9 LT, 11-13 LT, and 15-17 LT in Figure 14. The total PO_3 clearly peaks in the middle of the day. The total advection term dominates in the late afternoon on 12 November and the middle of the day on 13 November when the largest inflow of ozone occurred. The total vertical mixing process is strongest when the PBL is built up in the middle of the day, and it dominates the surface ozone accumulation by dispersing considerable upper air ozone downward.

The diurnal variability of the total tendency terms can help explain what processes drive the ozone increase from fire emissions during different times of the day. On 12 November, transport process in the late afternoon drives the largest fire impacts on O_3 accumulation (~ 4 ppb/2 hrs near the surface), which is associated with the freshly emitted smoke plume discussed. Fire-impacted PO_3 from morning to the middle of the day is not intensive, yet this local chemical reaction dominates the ozone increase in the elevated smoke plume (compared to little dynamical process tendencies). On 13 November, the middle of the day drives the largest ozone increase (> 4 ppb/2 hrs), with highest PO_3 and inflow of O_3 from fire emissions, as well as the strongest vertical mixing that dispersing O_3 to the lower level. The combined effect of chemical reaction, transport, and vertical mixing on O_3 accumulation is pronounced in the middle of the day when fire smoke impacted the boundary layer.

4 Conclusions

This case study for the 2016 Southeastern Wildfires illustrates the high spatio-temporal variations of smoke impacts on air quality at both regional and local scales. Integrating vertical aerosol and O_3 profiles with modeling and multi-platform observations can fill the knowledge gap at altitudes above ground to improve our understanding of the fire impacts on vertical aerosol and O_3 distribution. In particular, the fire-impacted processes and fire-source contributions on 12 and 13 November are demonstrated by sensitivity simulations and tendency diagnostics: (1) Fire emissions increase the vertical ozone concen-

trations downstream of the fires by affecting local net chemical ozone production, inflow and outflow of ozone, and vertical ozone exchange. The dominant process has daily, diurnal, and vertical variability due to the PBL evolution, photochemistry, and smoke transport changes over the course of the day. On 12 November, local photochemical ozone production over Huntsville dominates the fire-impacted ozone enhancement in the elevated plume; while transport process dominates the boundary layer ozone accumulation in the late afternoon. (2) In this study, biomass burning is not a dominant source contributing to the local chemical ozone production (positive PO_3 is increased by up to 25% in the upper air), but can still play an important role in changing the O_3 concentrations because of additional impacts of vertical mixing and advection processes. The combined effect of chemical and dynamical processes lead to an increase of O_3 concentration by up to ~ 8 ppb during daytime at lower altitude. In the upper air, the increased concentration is smaller than 8 ppb, but the relative contribution from fire emissions to the total O_3 increase can be dominant. Fire emissions contribute significantly to the vertical accumulation of $\text{PM}_{2.5}$ (by up to 77%) during daytime. Besides the freshly emitted smoke plumes, relatively aged plumes emitted from previous day contribute considerably to the local $\text{PM}_{2.5}$ accumulation.

In this case, WRF-Chem can capture the general day-to-day AOD pattern, air quality variations, vertical structure of aged plumes, and enhanced ozone lamina. Three main avenues for future work: (1) Discrepancies in fire emission estimations need to be considered for model inputs. (OC+BC)/CO emission ratios in FINNv1.5, GFASv1.2, and QFEDv2.5_r1 fire inventories differ by a factor of 5.7 (in Gg per Gg) over the 2016 SEUS wildfire regions. A scaling ratio of 3.6 on aerosol emissions (derived from FINNv1.5 $\text{PM}_{2.5}$), within the spanned range of the emission ratios in different inventories, can improve the modeled magnitude of surface $\text{PM}_{2.5}$, vertical aerosol extinction, and AOD, but this was tested in only a single case study. (2) After the emission adjustment, underestimation of the densest plume in DIAL and highest AOD in MODIS is partly due to missing fire detections under clouds on 13 November. Adding extra satellite detections (e.g., FINNv2.2 includes VIIRS information) or filling in the gap of missing fire counts in emission estimation algorithms could be considered; (3) The density, continuity, and species of vertical measurements are relatively limited for modeling evaluation in this case study. Combining larger samples of vertical measurements (ground-based and airborne) with ambient data will benefit regional-model evaluation in future fire studies.

Acknowledgments

This work was supported by the TOLNet program developed by National Aeronautics and Space Administration (NASA)'s Science Mission Directorate, and the National Center for Atmospheric Research (NCAR), which is a major facility sponsored by the National Science Foundation under Cooperative Agreement No. 1852977. The views, opinions, and findings contained in this work are those of the authors and should not be construed as an official position, policy, or decision. We acknowledge use of the WRF-Chem preprocessor tools provided by the Atmospheric Chemistry Observations and Modeling Lab (ACOM) of NCAR. We appreciate the developers of the FINNv1.5, GFASv1.2, and QFEDv2.5_r1 fire inventories. We acknowledge the use of imagery from the NASA Worldview application (<https://worldview.earthdata.nasa.gov>), part of the NASA Earth Observing System Data and Information System (EOSDIS). The authors would like to thank Kevin Knupp and Dustin Phillips for providing Ceilometer data, Michael Graham for launching the ozonesonde, and Peiyang Cheng for extracting surface air-quality data in model evaluation. Helpful discussions with Udaysankar Nair, Zhixin Xue, Andrew White, Paula Tucker, Yonghua Wu, and the ACOM lab are gratefully acknowledged. The ceilometer backscatter datasets used in this study are archived at <https://www.nsstc.uah.edu/mips/data/data/>. The ozonesonde and DIAL datasets used in this study are available at <https://github.com/BoWang11/jgr2020>. Surface ozone and $\text{PM}_{2.5}$ datasets are downloaded from the Environmental Protection Agency (EPA) website (<https://www.epa.gov/outdoor-air-quality-data>). MODIS AOD

573 data is acquired from the NASA Earth Data Level-1 and Atmospheric Archive & Dis-
574 tribution System Distributed Active Archive Center (LAADS DAAC) website (<https://ladsweb.modaps.eosdis.nasa.gov>)
575 The WRF-Chem preprocessor tools and emission inputs used in this study are available
576 via <https://www2.aom.ucar.edu/wrf-chem/wrf-chem-tools-community>.

Table 1. Key Configurations for the WRF-Chem v3.9.1 Simulations

Simulations	1. CTRL (fire off)	2. FIREorig (fire on)	3. FIREcorr (fire on, correction)
Vertical	60 vertical levels from the surface to 50 hPa (vertical grids in Figure S1)		
Horizontal	D01: 16 km \times 16 km, D02: 4 km \times 4 km		
Emissions	Fire: FINNv1.5, Anthropogenic: NEI 2011 v2, Biogenic: MEGAN		
IC&BC	Met: NAM 12 km, Chemical: MOZART global		
Chemistry	MOZART gas, GOCART aerosol		
Physics	Goddard, RRTM, Morrison's, Monin-Obukhov, Noah, YSU, G3, F-TUV		

References

- Akagi, S., Yokelson, R. J., Wiedinmyer, C., Alvarado, M., Reid, J., Karl, T., ... Wennberg, P. (2011). Emission factors for open and domestic biomass burning for use in atmospheric models. *Atmospheric Chemistry and Physics*, 11(9), 4039–4072.
- Andreae, M. O., & Merlet, P. (2001). Emission of trace gases and aerosols from biomass burning. *Global biogeochemical cycles*, 15(4), 955–966.
- Aouizerats, B., Van Der Werf, G. R., Balasubramanian, R., & Betha, R. (2015). Importance of transboundary transport of biomass burning emissions to regional air quality in southeast asia during a high fire event. *Atmospheric Chemistry & Physics*, 15(1).
- Baker, K., Woody, M., Tonnesen, G., Hutzell, W., Pye, H., Beaver, M., ... Pierce, T. (2016). Contribution of regional-scale fire events to ozone and pm_{2.5} air quality estimated by photochemical modeling approaches. *Atmospheric Environment*, 140, 539–554.
- Baker, K., Woody, M., Valin, L., Szykman, J., Yates, E., Iraci, L., ... others (2018). Photochemical model evaluation of 2013 california wild fire air quality impacts using surface, aircraft, and satellite data. *Science of the Total Environment*, 637, 1137–1149.
- Barth, M., Lee, J., Hodzic, A., Pfister, G., Skamarock, W., Worden, J., ... Noone, D. (2012). Thunderstorms and upper troposphere chemistry during the early stages of the 2006 north american monsoon. *Atmospheric Chemistry & Physics*, 12(22).
- Carter, T. S., Heald, C. L., Jimenez, J. L., Campuzano-Jost, P., Kondo, Y., Moteki, N., ... others (2020). How emissions uncertainty influences the distribution and radiative impacts of smoke from fires in north america. *Atmospheric Chemistry and Physics*, 20(4), 2073–2097.
- Chin, M., Rood, R. B., Lin, S.-J., Müller, J.-F., & Thompson, A. M. (2000). Atmospheric sulfur cycle simulated in the global model gcart: Model description and global properties. *Journal of Geophysical Research: Atmospheres*, 105(D20), 24671–24687.
- Cohen, J. B., Ng, D. H. L., Lim, A. W. L., & Chua, X. R. (2018). Vertical distribution of aerosols over the maritime continent during el niño. *Atmospheric Chemistry and Physics*, 18(10), 7095–7108. Retrieved from <https://www.atmos-chem-phys.net/18/7095/2018/> doi: 10.5194/acp-18-7095-2018
- Colarco, P., Schoeberl, M., Doddridge, B., Marufu, L., Torres, O., & Welton, E. (2004). Transport of smoke from canadian forest fires to the surface near washington, dc: Injection height, entrainment, and optical properties. *Journal of Geophysical Research: Atmospheres*, 109(D6).
- Cook, P. A., Savage, N. H., Turquety, S., Carver, G. D., O'Connor, F. M., Heckel, A., ... others (2007). Forest fire plumes over the north atlantic: p-tomcat model simulations with aircraft and satellite measurements from the itop/icartt campaign. *Journal of Geophysical Research: Atmospheres*, 112(D10).
- Cooper, O. R., Langford, A. O., Parrish, D. D., & Fahey, D. W. (2015). Challenges of a lowered us ozone standard. *Science*, 348(6239), 1096–1097.
- Crutzen, P. J., & Andreae, M. O. (1990). Biomass burning in the tropics: Impact on atmospheric chemistry and biogeochemical cycles. *Science*, 250(4988), 1669–1678.
- Crutzen, P. J., Heidt, L. E., Krasnec, J. P., Pollock, W. H., & Seiler, W. (1979). Biomass burning as a source of atmospheric gases co, h₂, n₂o, no, ch₃cl and cos. *Nature*, 282(5736), 253.
- Curci, G., Hogrefe, C., Bianconi, R., Im, U., Balzarini, A., Baró, R., ... others (2015). Uncertainties of simulated aerosol optical properties induced by assumptions on aerosol physical and chemical properties: An aqmeii-2 perspec-

- 698 tive. *Atmospheric Environment*, *115*, 541–552.
- 699 Darnenov, A., & da Silva, A. (2013). The quick fire emissions dataset (qfed)–
700 documentation of versions 2.1, 2.2 and 2.4. *NASA Technical Report Series on*
701 *Global Modeling and Data Assimilation*, *NASA TM-2013-104606*, *32*, 183.
- 702 Emmons, L., Walters, S., Hess, P., Lamarque, J., Pfister, G., Fillmore, D., ... others
703 (2010). *Description and evaluation of the model for ozone and related chemical*
704 *tracers, version 4 (mozart-4)*, *geosci. model dev.*, *3*, 43–67.
- 705 Fast, J. D., Berg, L. K., Zhang, K., Easter, R. C., Ferrare, R. A., Hair, J. W., ...
706 others (2016). Model representations of aerosol layers transported from north
707 america over the atlantic ocean during the two-column aerosol project. *Journal*
708 *of Geophysical Research: Atmospheres*, *121*(16), 9814–9848.
- 709 Fast, J. D., Gustafson Jr, W. I., Easter, R. C., Zaveri, R. A., Barnard, J. C., Chap-
710 man, E. G., ... Peckham, S. E. (2006). Evolution of ozone, particulates, and
711 aerosol direct radiative forcing in the vicinity of houston using a fully cou-
712 pled meteorology-chemistry-aerosol model. *Journal of Geophysical Research:*
713 *Atmospheres*, *111*(D21).
- 714 Fiore, A. M., Pierce, R. B., Dickerson, R. R., Lin, M., & Bradley, R. (2014). Detect-
715 ing and attributing episodic high background ozone events. *AQAST Special Is-*
716 *sue of Environmental Manager*.
- 717 Freitas, S. R., Longo, K. M., Chatfield, R., Latham, D., Silva Dias, M., Andreae,
718 M., ... Carvalho Jr, J. (2007). Including the sub-grid scale plume rise of
719 vegetation fires in low resolution atmospheric transport models. *Atmospheric*
720 *Chemistry and Physics*, *7*(13), 3385–3398.
- 721 Gronoff, G., Robinson, J., Berkoff, T., Swap, R., Farris, B., Schroeder, J., ... others
722 (2019). A method for quantifying near range point source induced o3 titra-
723 tion events using co-located lidar and pandora measurements. *Atmospheric*
724 *Environment*, *204*, 43–52.
- 725 Guenther, A., Karl, T., Harley, P., Wiedinmyer, C., Palmer, P., & Geron, C. (2006).
726 Estimates of global terrestrial isoprene emissions using megan (model of emis-
727 sions of gases and aerosols from nature). *Atmospheric Chemistry and Physics*,
728 *6*(11), 3181–3210.
- 729 Hodzic, A., Madronich, S., Bohn, B., Massie, S., Menut, L., & Wiedinmyer, C.
730 (2007). Wildfire particulate matter in europe during summer 2003: meso-scale
731 modeling of smoke emissions, transport and radiative effects. *Atmospheric*
732 *Chemistry and Physics*, *7*(15), 4043–4064.
- 733 Hu, X.-M., Xue, M., Kong, F., & Zhang, H. (2019). Meteorological conditions
734 during an ozone episode in dallas-fort worth, texas, and impact of their mod-
735 eling uncertainties on air quality prediction. *Journal of Geophysical Research:*
736 *Atmospheres*, *124*(4), 1941–1961.
- 737 Jaffe, D., Bertschi, I., Jaeglé, L., Novelli, P., Reid, J. S., Tanimoto, H., ... Westphal,
738 D. L. (2004). Long-range transport of siberian biomass burning emissions
739 and impact on surface ozone in western north america. *Geophysical Research*
740 *Letters*, *31*(16).
- 741 Jaffe, D. A., Wigder, N., Downey, N., Pfister, G., Boynard, A., & Reid, S. B. (2013).
742 Impact of wildfires on ozone exceptional events in the western us. *Environmental*
743 *science & technology*, *47*(19), 11065–11072.
- 744 Johnson, B. J., Oltmans, S. J., Vömel, H., Smit, H. G., Deshler, T., & Kröger, C.
745 (2002). Electrochemical concentration cell (ecc) ozonesonde pump efficiency
746 measurements and tests on the sensitivity to ozone of buffered and unbuffered
747 ecc sensor cathode solutions. *Journal of Geophysical Research: Atmospheres*,
748 *107*(D19), ACH–8.
- 749 Johnson, M., Kuang, S., Wang, L., & Newchurch, M. (2016). Evaluating summer-
750 time ozone enhancement events in the southeast united states. *Atmosphere*,
751 *7*(8), 108.
- 752 Justice, C., Giglio, L., Korontzi, S., Owens, J., Morissette, J., Roy, D., ... Kaufman,

- Y. (2002). The modis fire products. *Remote Sensing of Environment*, 83(1-2), 244–262.
- Kaiser, J., Heil, A., Andreae, M., Benedetti, A., Chubarova, N., Jones, L., . . . others (2012). Biomass burning emissions estimated with a global fire assimilation system based on observed fire radiative power. *Biogeosciences*, 9(1), 527–554.
- Konrad, C., & Knox, P. (2017). The southeastern drought and wildfires of 2016. *NIDIS Rep.*, <https://sercc.com/NIDISDroughtAssessmentFINAL.pdf>.
- Kuang, S., Burris, J. F., Newchurch, M. J., Johnson, S., & Long, S. (2011). Differential absorption lidar to measure subhourly variation of tropospheric ozone profiles. *IEEE Transactions on Geoscience and Remote Sensing*, 49(1), 557–571.
- Kuang, S., Newchurch, M. J., Johnson, M. S., Wang, L., Burris, J., Pierce, R. B., . . . Feng, N. (2017, Jan). Summertime tropospheric ozone enhancement associated with a cold front passage due to stratosphere-to-troposphere transport and biomass burning: Simultaneous ground-based lidar and airborne measurements. *Journal of Geophysical Research (Atmospheres)*, 122(2), 1293–1311. doi: 10.1002/2016JD026078
- Kuang, S., Wang, B., Newchurch, M. J., Tucker, P., Eloranta, E. W., Garcia, J. P., . . . Natraj, V. (2020). Evaluation of uv aerosol retrievals from an ozone lidar. *Atmospheric Measurement Techniques Discussions*, 2020, 1–20. Retrieved from <https://www.atmos-meas-tech-discuss.net/amt-2020-40/> doi: 10.5194/amt-2020-40
- Langford, A., Alvarez II, R., Brioude, J., Evan, S., Iraci, L., Kirgis, G., . . . others (2018). Coordinated profiling of stratospheric intrusions and transported pollution by the tropospheric ozone lidar network (tolnet) and nasa alpha jet experiment (ajax): Observations and comparison to hysplit, raqms, and flexpart. *Atmospheric environment*, 174, 1–14.
- Langford, A., Senff, C., Alvarez II, R., Brioude, J., Cooper, O., Holloway, J., . . . others (2015). An overview of the 2013 las vegas ozone study (lvos): Impact of stratospheric intrusions and long-range transport on surface air quality. *Atmospheric environment*, 109, 305–322.
- Langford, A. O., Alvarez, I., Raul, J., Kirgis, G., Senff, C. J., Caputi, D., . . . others (2019). Intercomparison of lidar, aircraft, and surface ozone measurements in the san joaquin valley during the california baseline ozone transport study (cabots). *Atmospheric Measurement Techniques*, 12(3), 1889–1904.
- Langford, A. O., Alvarez, R. J., Brioude, J., Caputi, D., Conley, S. A., Evan, S., . . . others (n.d.). Ozone production in the soberanes smoke haze: implications for air quality in the san joaquin valley during the california baseline ozone transport study. *Journal of Geophysical Research: Atmospheres*, e2019JD031777.
- Lapina, K., Honrath, R., Owen, R., Val Martin, M., & Pfister, G. (2006). Evidence of significant large-scale impacts of boreal fires on ozone levels in the midlatitude northern hemisphere free troposphere. *Geophysical Research Letters*, 33(10).
- Leblanc, T., Brewer, M. A., Wang, P. S., & Granados Muñoz, M. J. (2018). Validation of the tolnet lidars: the southern california ozone observation project (scoop). *Atmospheric measurement techniques*, 11, 6137–6162.
- Levy, R., Hsu, C., et al. (2015). *Modis atmosphere l2 aerosol product, nasa modis adaptive processing system, goddard space flight center, usa*.
- Lindaas, J., Farmer, D. K., Pollack, I. B., Abeleira, A., Flocke, F., Roscioli, R., . . . Fischer, E. V. (2017). Changes in ozone and precursors during two aged wildfire smoke events in the colorado front range in summer 2015. *Atmospheric Chemistry and Physics*, 17(17), 10691–10707.
- Liu, T., Mickley, L. J., Marlier, M. E., DeFries, R. S., Khan, M. F., Latif, M. T., & Karambelas, A. (2020). Diagnosing spatial biases and uncertainties in global fire emissions inventories: Indonesia as regional case study. *Remote Sensing of*

- Environment*, 237, 111557.
- Lu, X., Zhang, L., Liu, X., Gao, M., Zhao, Y., & Shao, J. (2018). Lower tropospheric ozone over india and its linkage to the south asian monsoon. *Atmospheric Chemistry and Physics*, 18(5), 3101–3118.
- Martin, M. V., Honrath, R., Owen, R. C., Pfister, G., Fialho, P., & Barata, F. (2006). Significant enhancements of nitrogen oxides, black carbon, and ozone in the north atlantic lower free troposphere resulting from north american boreal wildfires. *Journal of Geophysical Research: Atmospheres*, 111(D23).
- McKeen, S., Wotawa, G., Parrish, D., Holloway, J., Buhr, M., Hübler, G., . . . Meagher, J. (2002). Ozone production from canadian wildfires during june and july of 1995. *Journal of Geophysical Research: Atmospheres*, 107(D14), ACH-7.
- Morris, G. A., Hersey, S., Thompson, A. M., Pawson, S., Nielsen, J. E., Colarco, P. R., . . . others (2006). Alaskan and canadian forest fires exacerbate ozone pollution over houston, texas, on 19 and 20 july 2004. *Journal of Geophysical Research: Atmospheres*, 111(D24).
- Newchurch, M., Ayoub, M., Oltmans, S., Johnson, B., & Schmidlin, F. (2003). Vertical distribution of ozone at four sites in the united states. *Journal of Geophysical Research: Atmospheres*, 108(D1).
- Oltmans, S., Lefohn, A., Harris, J., Tarasick, D., Thompson, A., Wernli, H., . . . others (2010). Enhanced ozone over western north america from biomass burning in eurasia during april 2008 as seen in surface and profile observations. *Atmospheric Environment*, 44(35), 4497–4509.
- Pereira, G., Siqueira, R., Rosário, N. E., Longo, K. L., Freitas, S. R., Cardozo, F. S., . . . Wooster, M. J. (2016). Assessment of fire emission inventories during the south american biomass burning analysis (sambba) experiment. *Atmospheric Chemistry and Physics*.
- Pfister, G., Avise, J., Wiedinmyer, C., Edwards, D., Emmons, L., Diskin, G., . . . Wisthaler, A. (2011). Co source contribution analysis for california during arctas-carb. *Atmospheric Chemistry and Physics*, 11(15), 7515–7532.
- Pfister, G., Wang, C.-T., Barth, M., Flocke, F., Vizuete, W., & Walters, S. (2019). Chemical characteristics and ozone production in the northern colorado front range. *Journal of Geophysical Research: Atmospheres*.
- Pfister, G., Wiedinmyer, C., & Emmons, L. (2008). Impacts of the fall 2007 california wildfires on surface ozone: Integrating local observations with global model simulations. *Geophysical Research Letters*, 35(19).
- Polivka, T. N., Wang, J., Ellison, L. T., Hyer, E. J., & Ichoku, C. M. (2016). Improving nocturnal fire detection with the viirs day–night band. *IEEE Transactions on Geoscience and Remote Sensing*, 54(9), 5503–5519.
- Reid, J. S., Kuehn, R. E., Holz, R. E., Eloranta, E. W., Kaku, K. C., Kuang, S., . . . others (2017). Ground-based high spectral resolution lidar observation of aerosol vertical distribution in the summertime southeast united states. *Journal of Geophysical Research: Atmospheres*, 122(5), 2970–3004.
- Rogers, H. M., Ditto, J. C., & Gentner, D. R. (2020). Evidence for impacts on surface-level air quality in the northeastern us from long-distance transport of smoke from north american fires during the long island sound tropospheric ozone study (listos) 2018. *Atmospheric Chemistry and Physics*, 20(2), 671–682.
- Sapkota, A., Symons, J. M., Kleissl, J., Wang, L., Parlange, M. B., Ondov, J., . . . Buckley, T. J. (2005). Impact of the 2002 canadian forest fires on particulate matter air quality in baltimore city. *Environmental science & technology*, 39(1), 24–32.
- Strawbridge, K. B., Travis, M. S., Firanski, B. J., Brook, J. R., Staebler, R., & Leblanc, T. (2018). A fully autonomous ozone, aerosol and nighttime water vapor lidar: a synergistic approach to profiling the atmosphere in the canadian

- oil sands region. *Atmospheric Measurement Techniques*, 11(12), 6735–6759.
- Sullivan, J. T., Berkoff, T., Gronoff, G., Knepp, T., Pippin, M., Allen, D., ... others (2019). The ozone water–land environmental transition study: An innovative strategy for understanding chesapeake bay pollution events. *Bulletin of the American Meteorological Society*, 100(2), 291–306.
- Thompson, A. M., Oltmans, S. J., Tarasick, D. W., von der Gathen, P., Smit, H. G., & Witte, J. C. (2011). Strategic ozone sounding networks: Review of design and accomplishments. *Atmospheric Environment*, 45(13), 2145–2163.
- Van Der Werf, G. R., Randerson, J. T., Giglio, L., Van Leeuwen, T. T., Chen, Y., Rogers, B. M., ... others (2017). Global fire emissions estimates during 1997–2016. *Earth System Science Data*, 9(2), 697–720.
- Wang, J., Christopher, S. A., Nair, U., Reid, J. S., Prins, E. M., Szykman, J., & Hand, J. L. (2006). Mesoscale modeling of central american smoke transport to the united states: 1. A top-down assessment of emission strength and diurnal variation impacts. *Journal of Geophysical Research: Atmospheres*, 111(D5).
- Wang, J., Yue, Y., Wang, Y., Ichoku, C., Ellison, L., & Zeng, J. (2018). Mitigating satellite-based fire sampling limitations in deriving biomass burning emission rates: Application to wrf-chem model over the northern sub-saharan african region. *Journal of Geophysical Research: Atmospheres*, 123(1), 507–528.
- Wiedinmyer, C., Akagi, S., Yokelson, R. J., Emmons, L., Al-Saadi, J., Orlando, J., & Soja, A. (2011). The fire inventory from near (finn): a high resolution global model to estimate the emissions from open burning. *Geoscientific Model Development*, 4(3), 625.
- Wiegner, M., Madonna, F., Biniotoglou, I., Forkel, R., Gasteiger, J., Geiß, A., ... Thomas, W. (2014). What is the benefit of ceilometers for aerosol remote sensing? an answer from earlinet. *Atmospheric Measurement Techniques*, 7(7), 1979–1997.
- Wigder, N., Jaffe, D., & Saketa, F. (2013). Ozone and particulate matter enhancements from regional wildfires observed at mount bachelor during 2004–2011. *Atmospheric Environment*, 75, 24–31.
- Wingo, S. M., & Knupp, K. R. (2015). Multi-platform observations characterizing the afternoon-to-evening transition of the planetary boundary layer in northern alabama, usa. *Boundary-Layer Meteorology*, 155(1), 29–53.
- WRAP. (2005). (western regional air partnership): 2002 fire emission inventory for the wrap region-phase ii. *Project No. 178-6, available at: https://www.wrapair.org/forums/fejfd/documents/WRAP_2002_PhII_EI_Report_20050722.pdf (last access: 17 January 2020)*.
- Wu, Y., Han, Y., Voulgarakis, A., Wang, T., Li, M., Wang, Y., ... Li, S. (2017). An agricultural biomass burning episode in eastern china: Transport, optical properties, and impacts on regional air quality. *Journal of Geophysical Research: Atmospheres*, 122(4), 2304–2324.
- Zhang, F., Wang, J., Ichoku, C., Hyer, E. J., Yang, Z., Ge, C., ... others (2014). Sensitivity of mesoscale modeling of smoke direct radiative effect to the emission inventory: a case study in northern sub-saharan african region. *Environmental Research Letters*, 9(7), 075002.

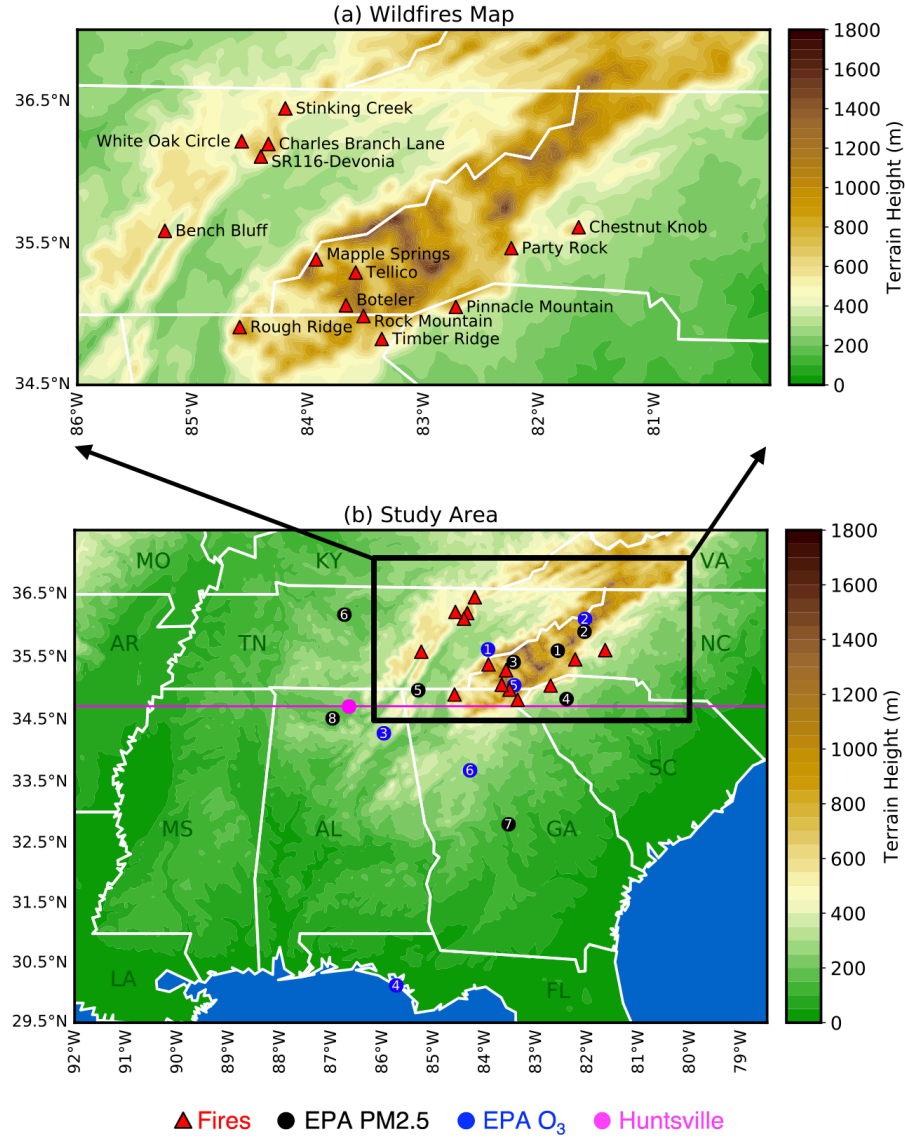


Figure 1. (a) Map of 14 active wildfires (red triangles) during 11-14 November, 2016 (see Table S1 for details). Here the names of wildfires are defined by the Monitoring Trends in Burn Severity project (MTBS; www.mtbs.gov). (b) WRF-Chem inner domain (D02) and terrain height (m). Black dots, blue dots, and magenta dot represent the 8 EPA PM2.5 sites, 6 EPA O₃ sites, and Huntsville station, respectively. The magenta line indicates the cross section of D02 across Huntsville station used for Figure 11.

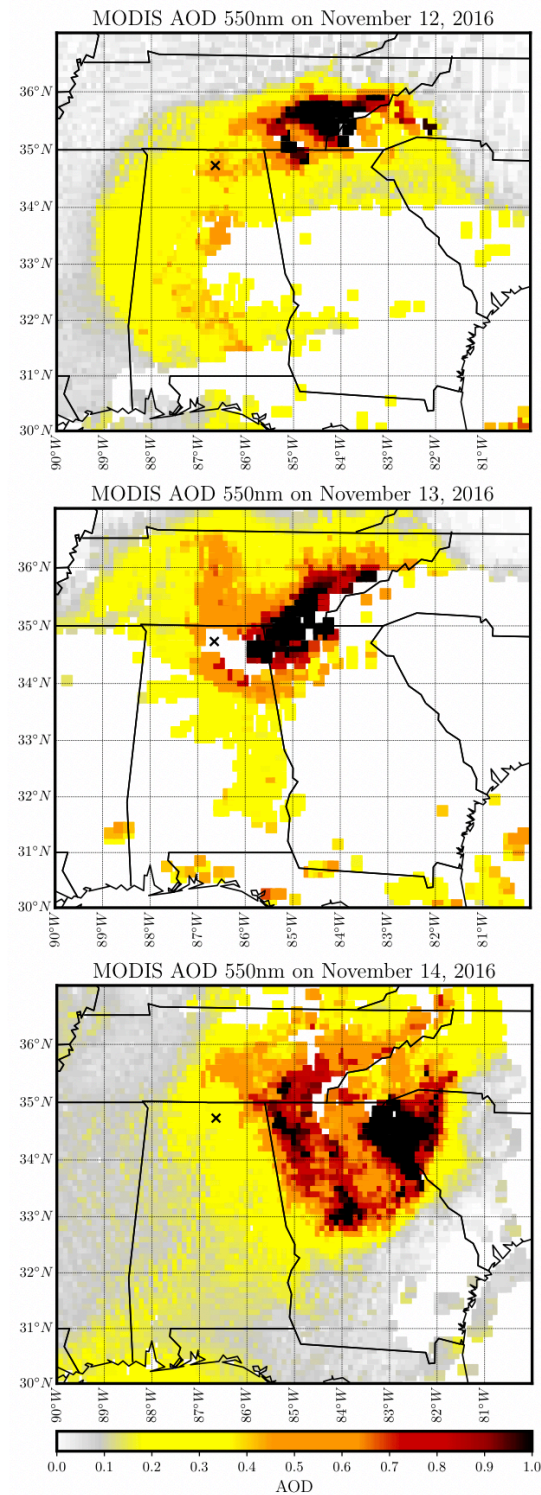


Figure 2. MODIS aerosol optical depth (AOD) at 550 nm in SEUS region on 12, 13, and 14 November 2016, respectively. MODIS AOD is calculated by mean of Aqua AOD at 19 UTC (13 LT) and Terra AOD at 17 UTC (11 LT) (or 16 UTC (10 LT) on 13 November). Cross marker indicates Huntsville location.

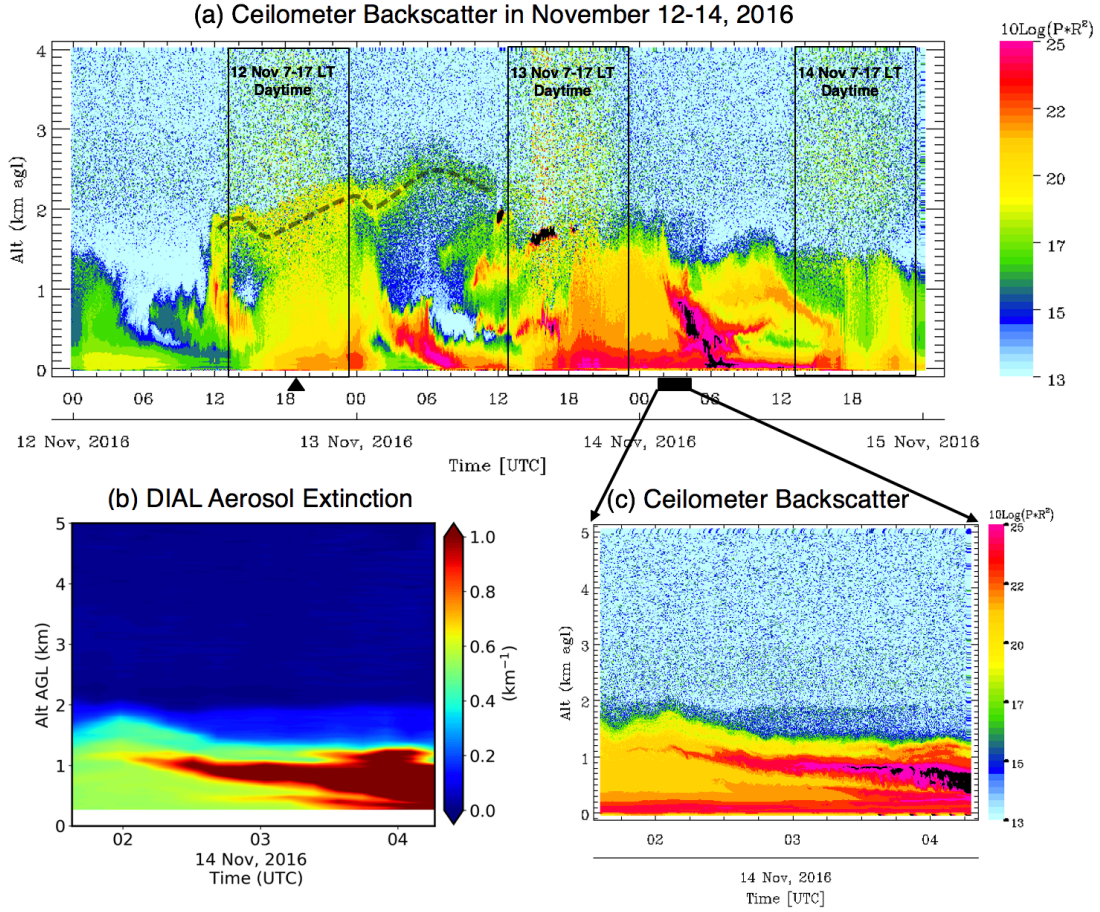


Figure 3. (a) Time-height curtain of UAH CT25K ceilometer backscatter intensity in 12-14 November 2016 (courtesy of Kevin Knupp). Here UTC time minus 6 hours is local time. The black triangle indicates the launch time of an ozonesonde. The black rectangle indicates the measurement time of DIAL. (b) Time-height curtain of DIAL aerosol extinction coefficient at 299 nm in 1:37-4:17 UTC on 14 November (19:37 to 22:17 LT 13 November). (c) Same time period with (b), but for ceilometer backscatter intensity at 905 nm.

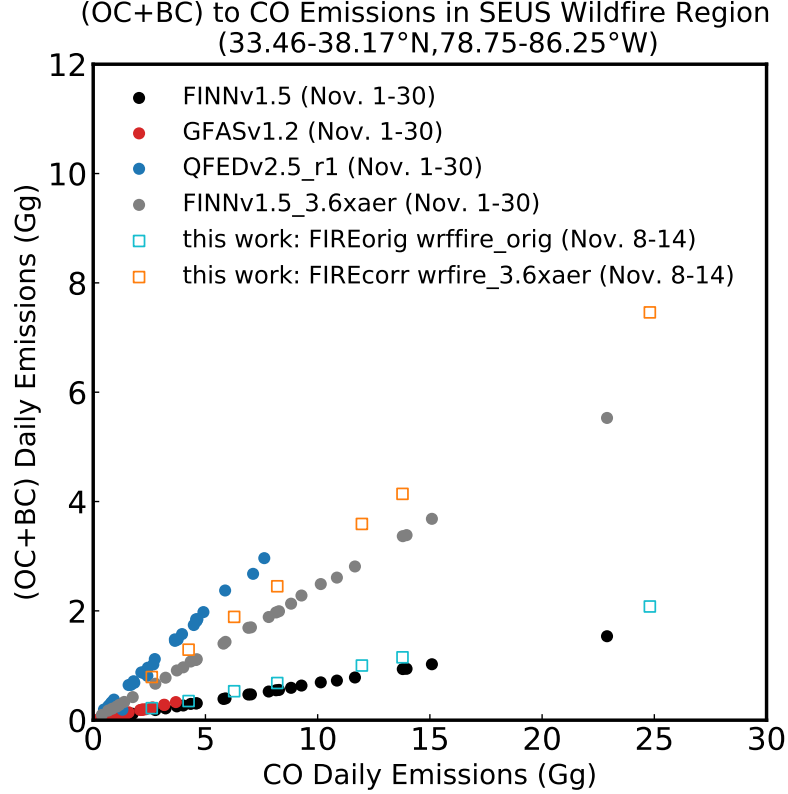


Figure 4. Comparison of fire emission ratios for (OC+BC) versus CO between this work and the different inventories. Daily emissions in the wildfire region are summed up within the latitude and longitude boundary 33.46-38.17° N and 78.75-86.25° W (Figure S4). The black, red, and blue dots represent daily emissions in 1-30 November 2016 from FINNv1.5, GFASv1.2, and QFEDv2.5_r1 inventories, respectively. Unfilled aqua and orange squares represent daily emissions in 8-14 November 2016 from FIREorig and FIREcorr runs, respectively. The gray dots denote a scaling by 3.6 on the original FINNv1.5 aerosols for a reference.

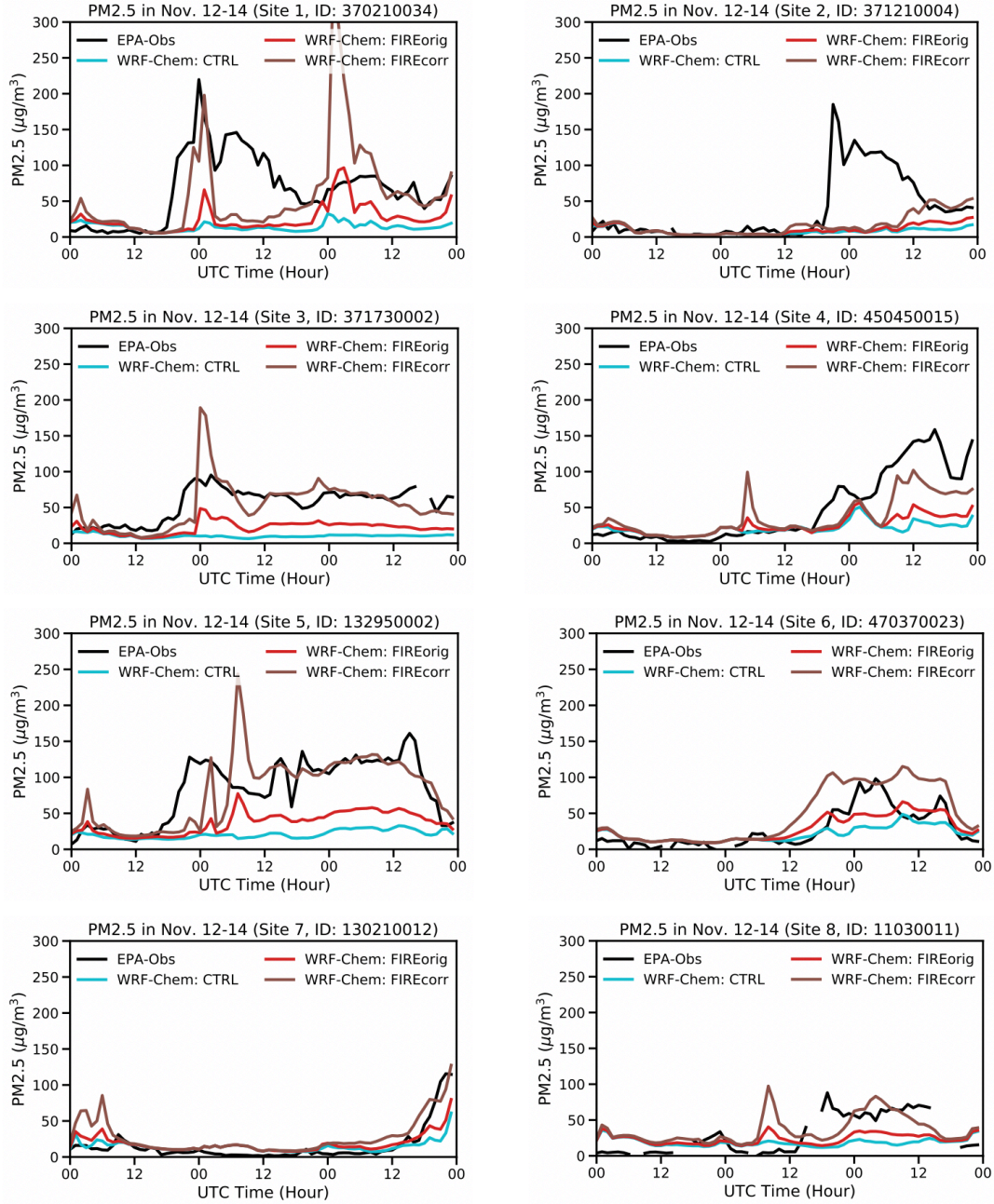
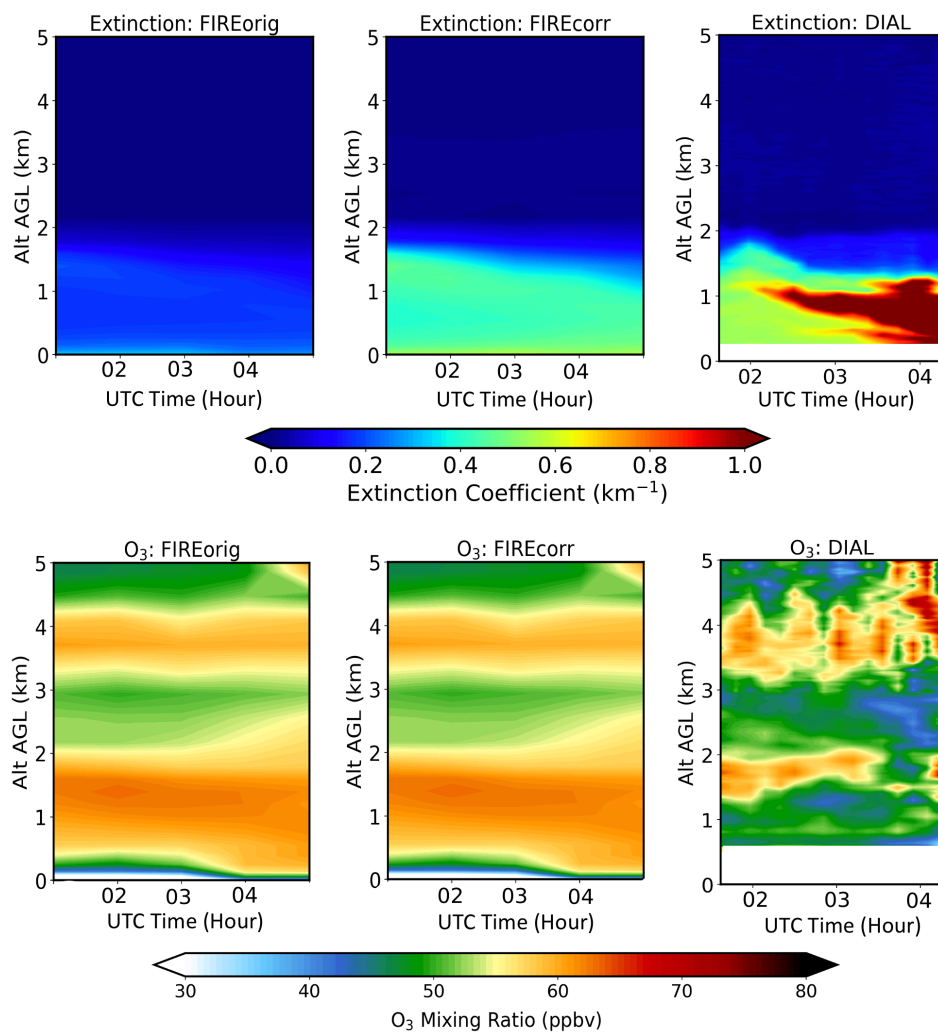
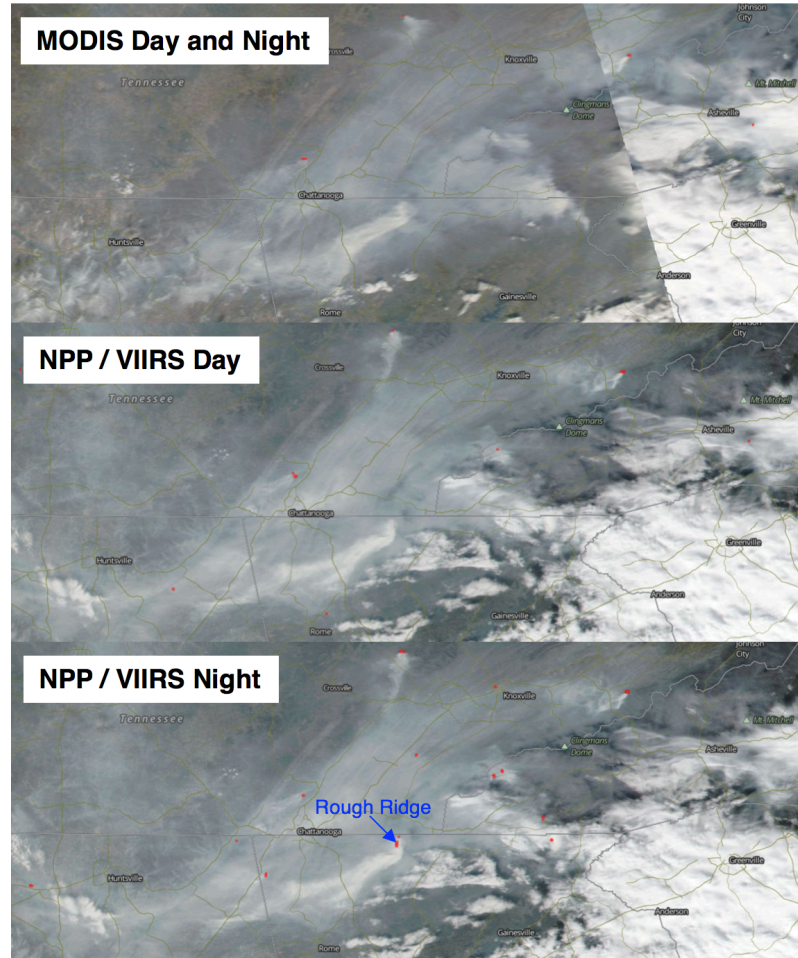


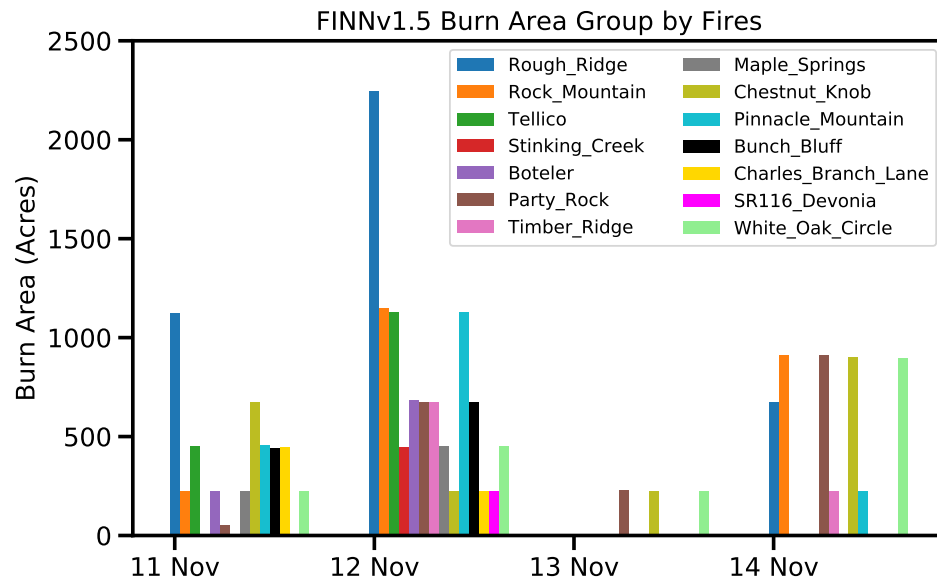
Figure 5. Comparison between 8 EPA sites (black line) and WRF-Chem hourly PM_{2.5} in 12-14 November 2016 for control run CTRL (aqua), before the emissions adjustment FIREorig (red), and after the emissions adjustment FIREcorr (brown). The control run is performed to show the modeled PM_{2.5} without fire impacts. Pattern statistic can be seen in Figure S5. 8 EPA PM_{2.5} sites include: 1. Asheville, NC, 2. Mitchell, NC, 3. Swain, NC, 4. Greenville-Anderson-Mauldin, SC, 5. Chattanooga, TN-GA, 6. Nashville-Davidson-Murfreesboro-Franklin, TN, 7. Macon, GA, 8. Decatur, AL.



607 **Figure 6.** Modeled time-height curtain of aerosol extinction coefficient (at 300 nm) and ozone
 608 before (FIREorig) and after (FIREcorr) the emissions adjustment in 1-5 UTC on November 14
 609 (19-23 LT on 13 November), compared with DIAL aerosol extinction (at 299 nm) and ozone.



610 **Figure 7.** Corrected Reflectance, Fires and Thermal Anomalies on 13 November 2016 from
 611 (upper) Terra and Aqua/MODIS (Day and Night); (middle) NPP/VIIRS (Day, 375 m); (bottom)
 612 NPP/VIIRS (Night, 375 m). Image source: NASA Worldview.



613 **Figure 8.** FINNv1.5 daily burn area (acres) group by individual wildfire during 11-14 Novem-
 614 ber 2016. The daily burn area is aggregated in the geospatial boundary box of each wildfire that
 615 defined by MTBS database.

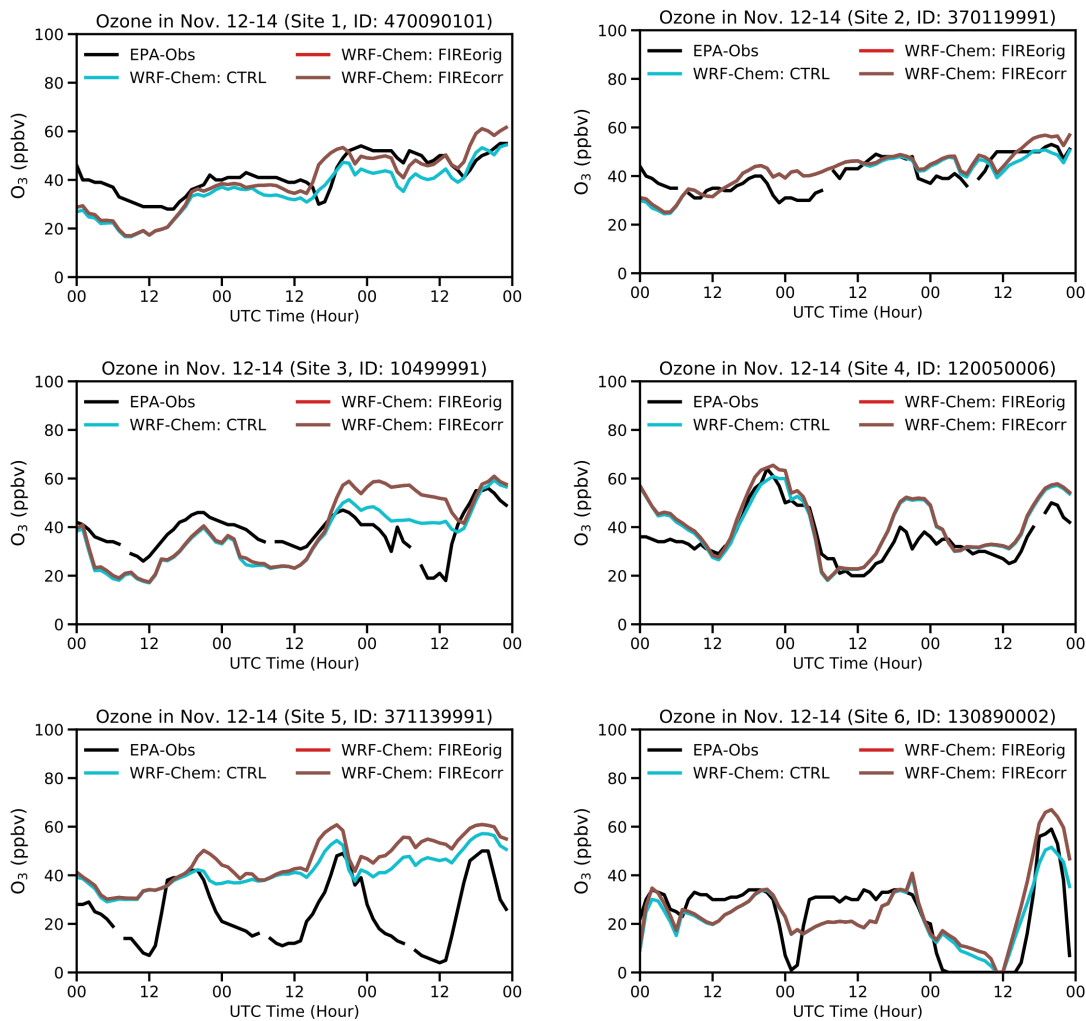


Figure 9. Comparison between EPA (black line) and WRF-Chem ozone in 12-14 November 2016 for control run (light blue), before correction (red), and after correction (brown). Pattern statistic can be seen in Figure S6. 6 EPA O₃ sites include: 1. Great Smoky Mountains NP-Look Rock, TN, 2. Cranberry, NC, 3. Sand Mountain, AL, 4. St.Andrews State Park, Panama City Beach, FL, 5. Coweeta, NC, 6. South DeKalb, GA.

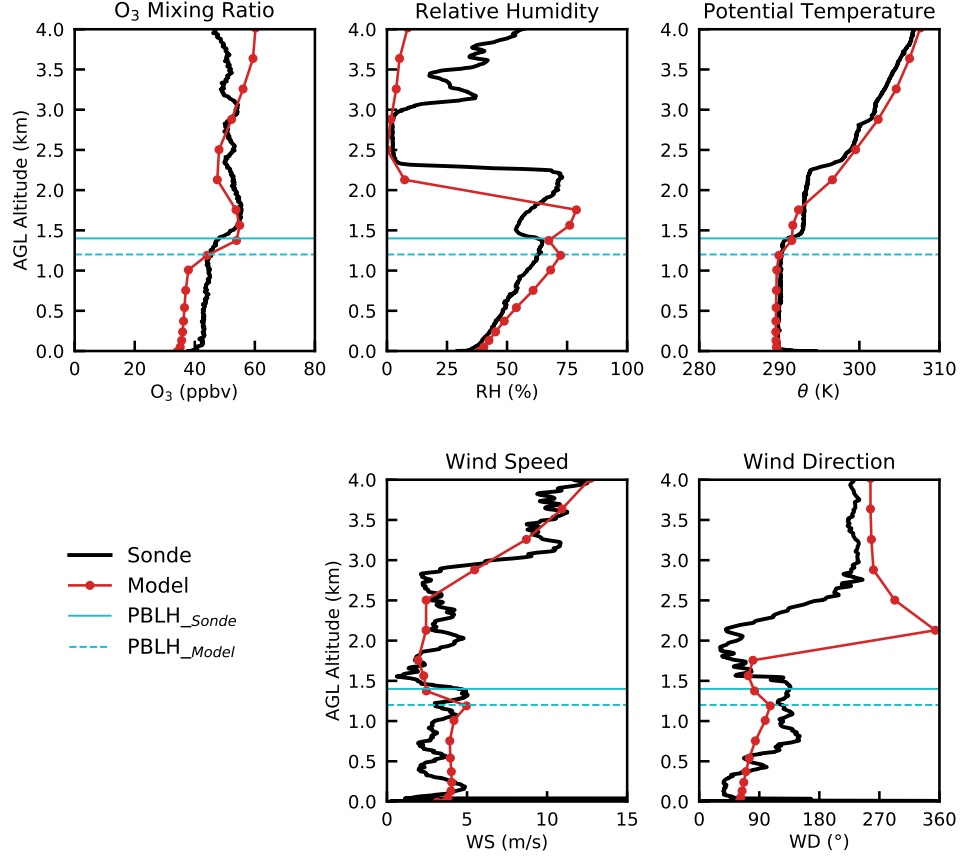


Figure 10. Comparison between ozonesonde (black color) and WRF-Chem FIREcorr simulation (red color) at 19 UTC (13 LT) on 12 November 2016. Ozone volume mixing ratio (O₃), relative humidity (RH), potential temperature (θ), horizontal wind speed (WS), and horizontal wind direction (WD) are displayed respectively. The aqua lines represent the PBL heights from sonde (solid line) and model (dashed line).

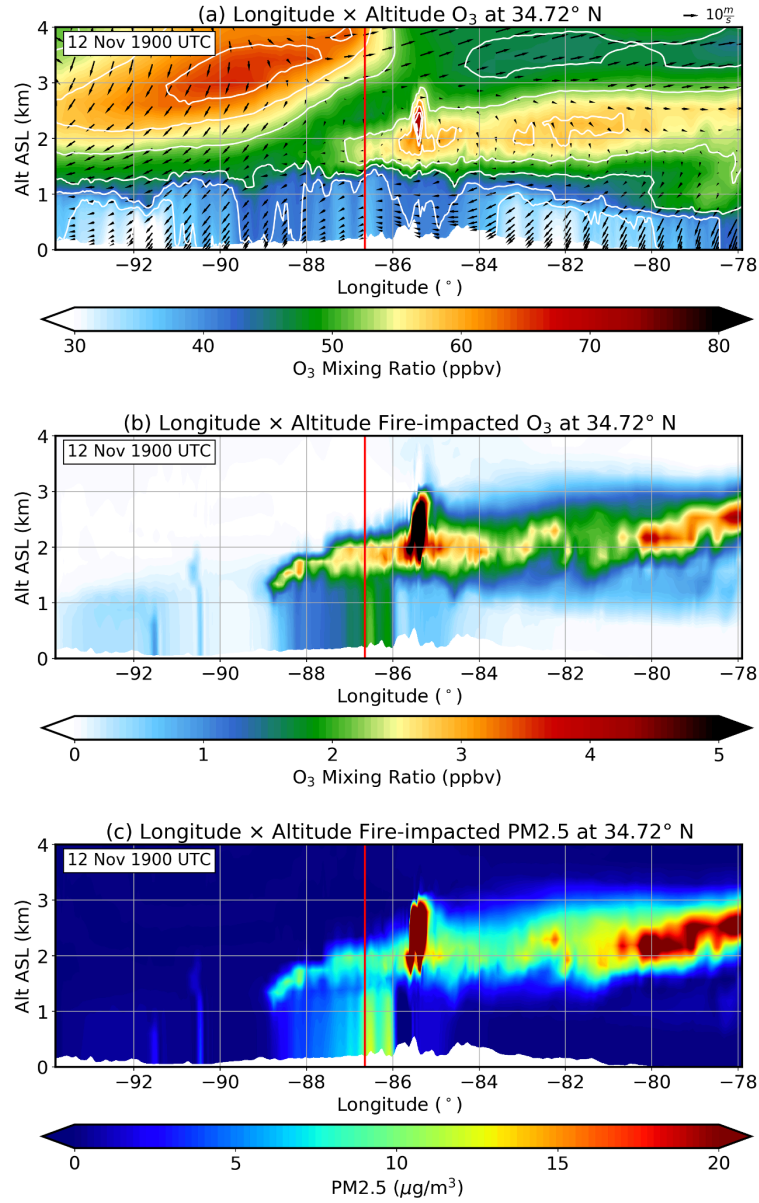
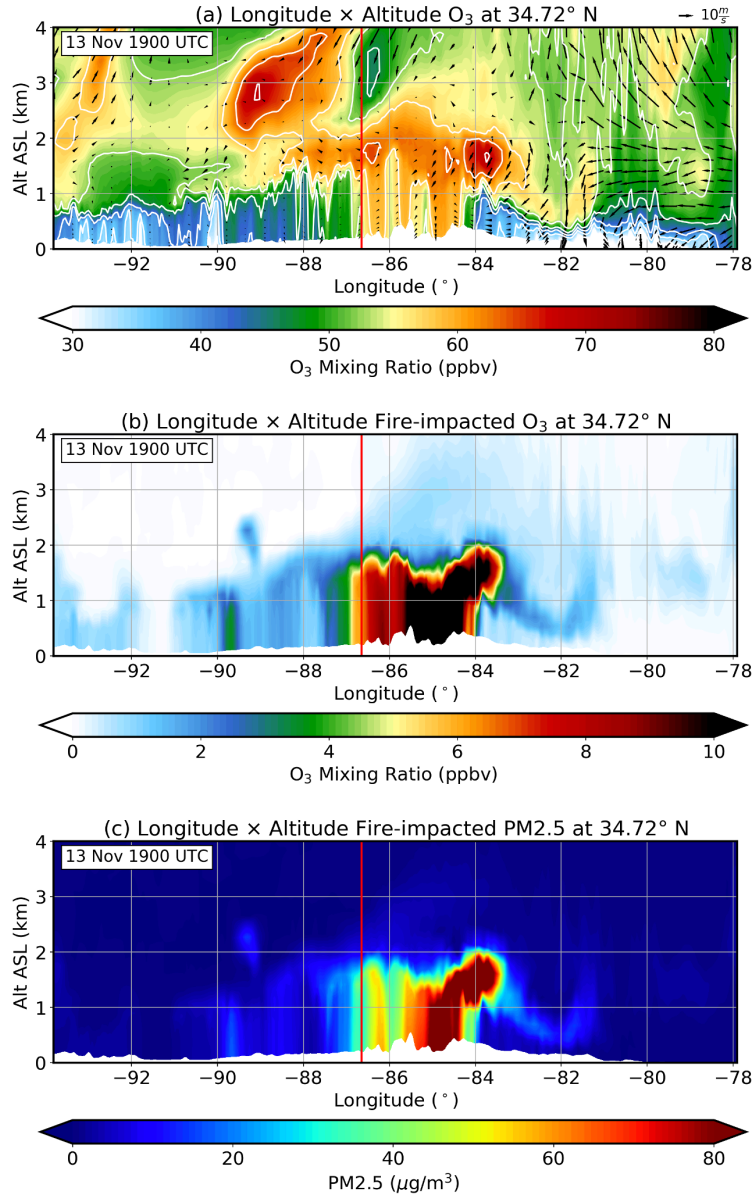


Figure 11. (a) Modeled (FIREcorr) vertical sections of O_3 mixing ratio (ppb) from west to east in SEUS region across Huntsville latitude (34.72° N) at 19 UTC (13 LT) on 12 November 2016 at 0-4 km ASL altitude. Solid red line denotes the longitude of Huntsville. Arrows indicate modeled direction and speed of horizontal wind. (b) Same as Figure a, but for fire-impacted (FIREcorr minus CTRL) O_3 mixing ratio. Note the colorbar range is different from Figure a. (c) Same as Figure b, but for fire-impacted $PM_{2.5}$ concentration ($\mu g/m^3$).



632

Figure 12. Same as **Figure 11**, but for 19 UTC (13 LT) on 13 November 2016.

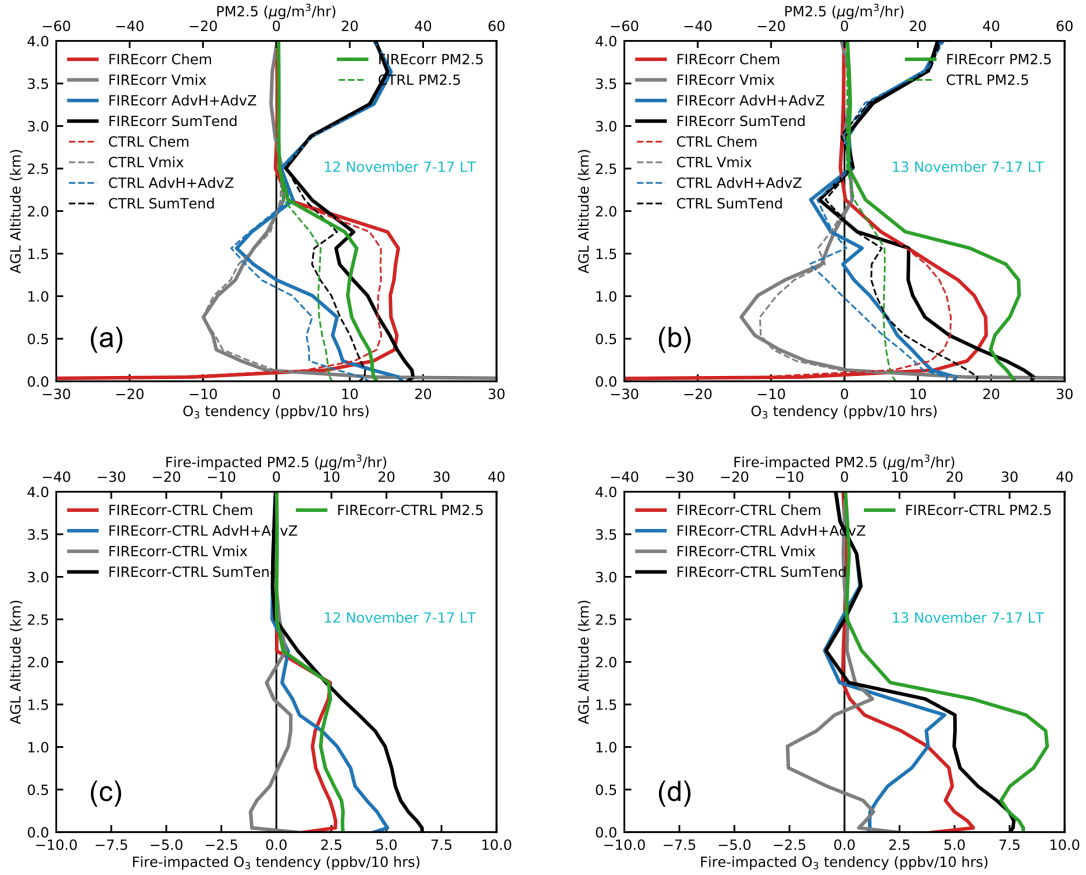


Figure 13. (a) and (b) Process analysis of daytime-integrated vertical ozone tendencies and daytime-averaged PM2.5 over Huntsville in simulations with (FIREcorr, solid lines) and without (CTRL, dashed lines) fire emissions during 7-17 LT on 12 and 13 November, respectively. Processes include chemical reactions (Chem, red), horizontal and vertical advectons (AdvH+AdvZ, blue), vertical mixing (Vmix, gray), and summed tendencies of all processes (SumTend, black). PM2.5 is represented by green lines. (c) and (d) are same as Figure (a) and (b) but for fire-impacted values, calculated by the difference between FIREcorr and CTRL simulations.

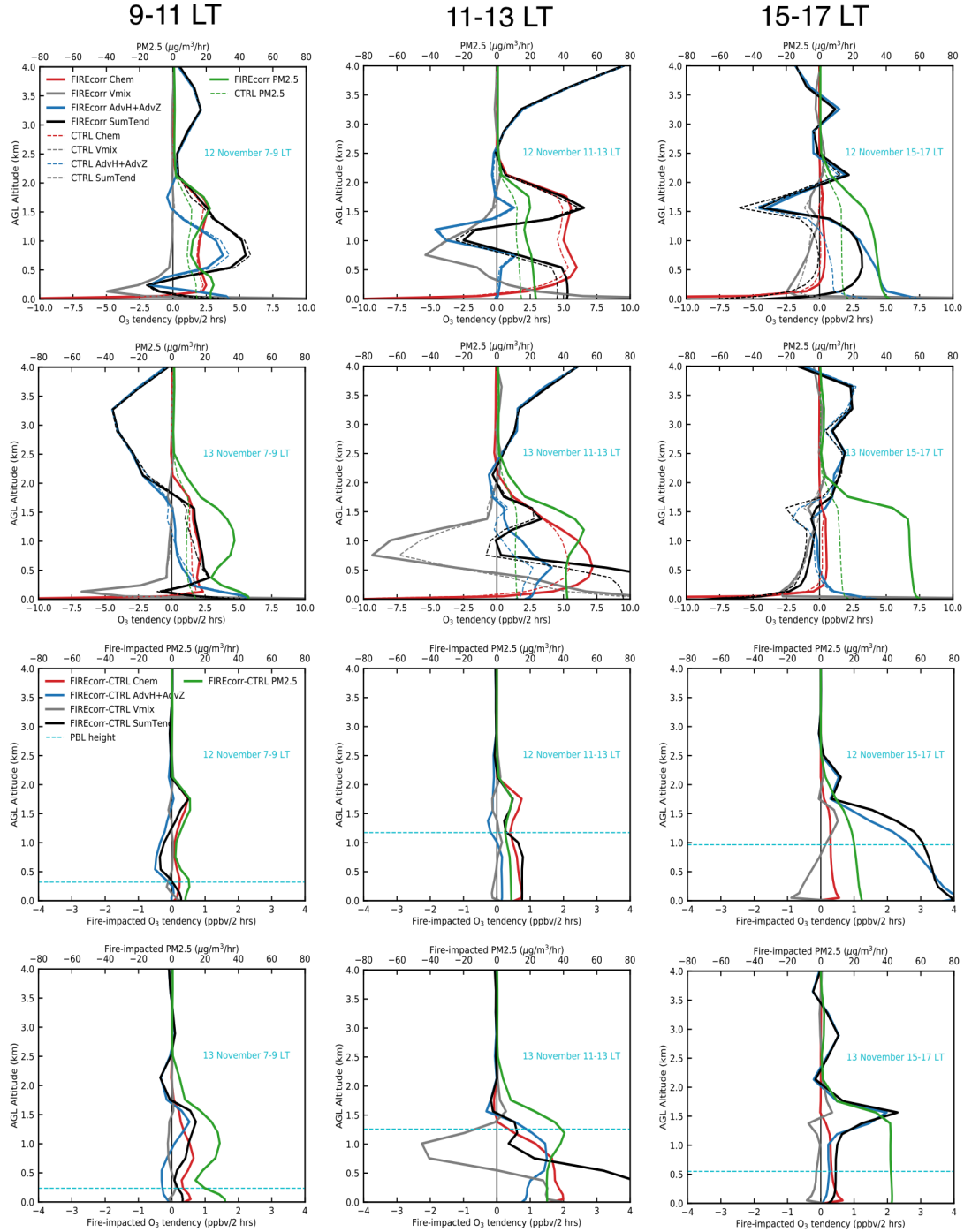
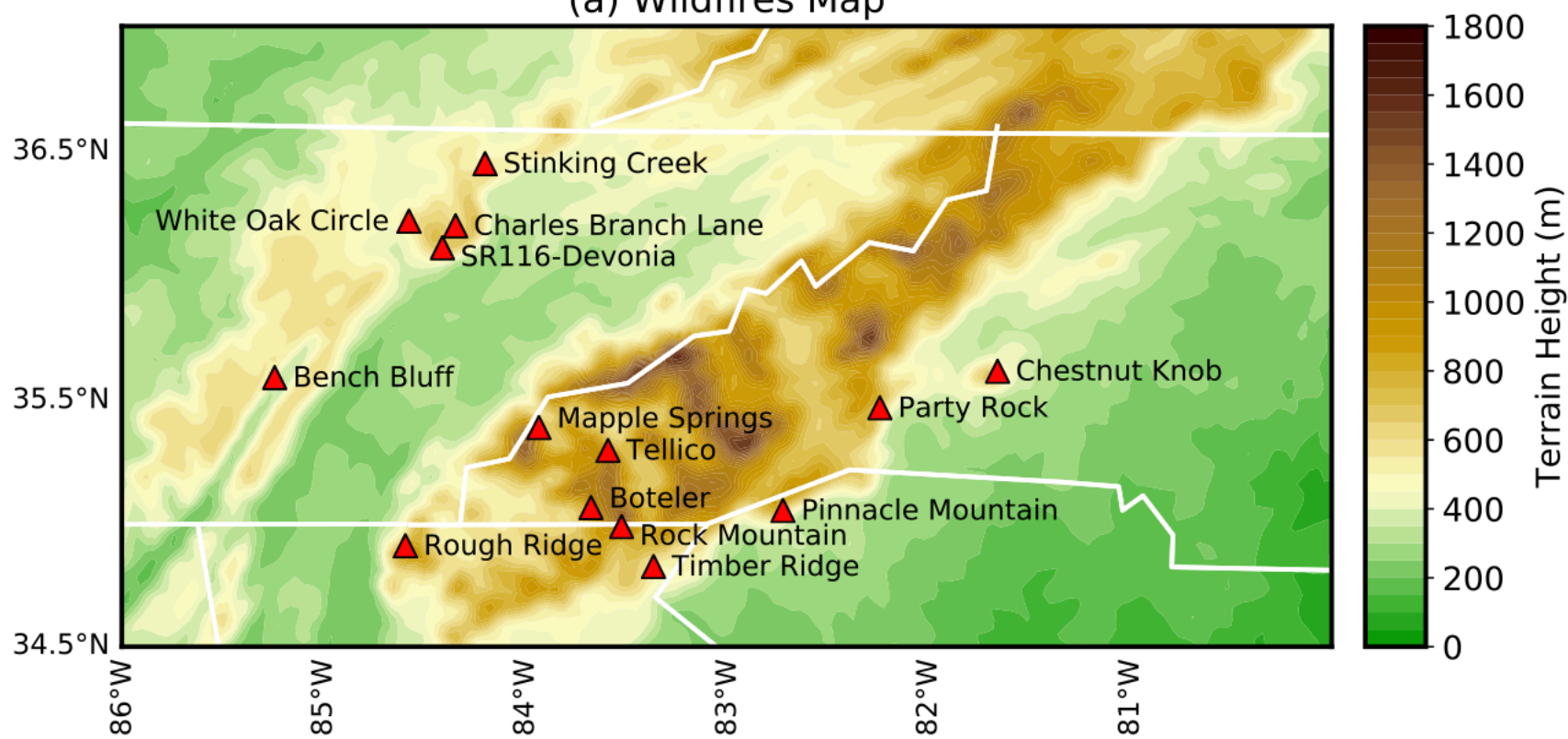


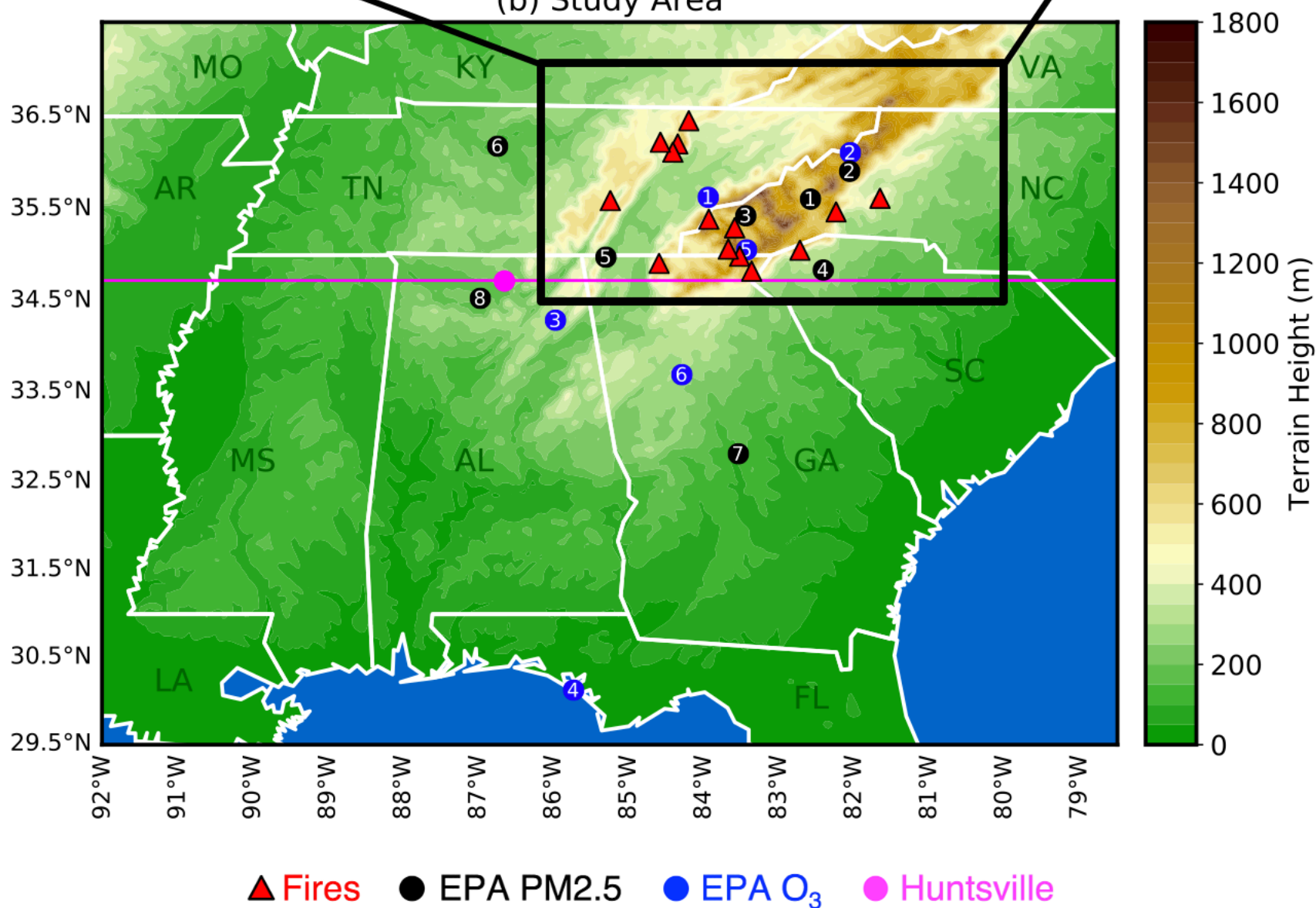
Figure 14. Same as **Figure 13**, but present diurnal variability by integrating 2 hours in 7-9, 11-13, and 15-17 LT on 12 November (row 1, 3) and 13 November (row 2, 4), respectively.

study_area_v2.

(a) Wildfires Map

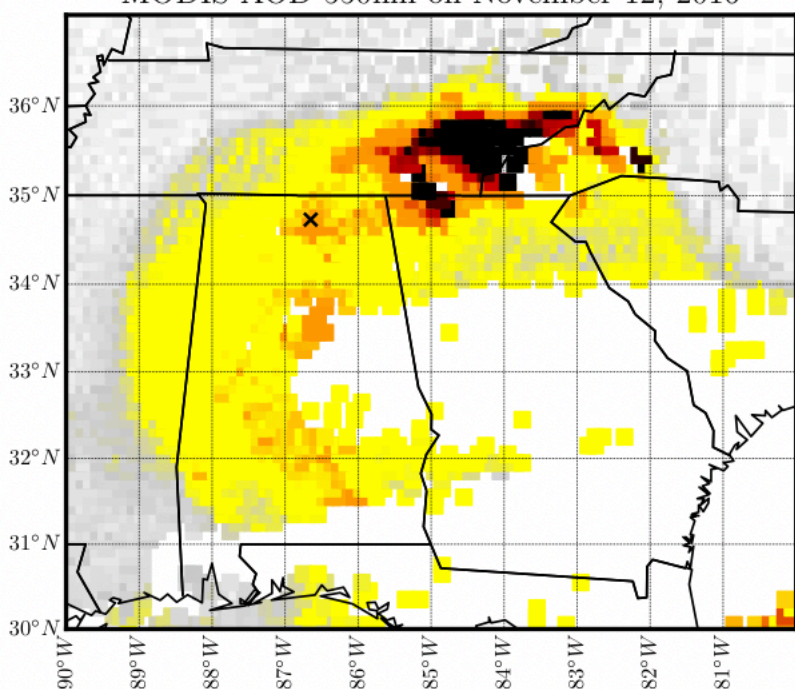


(b) Study Area

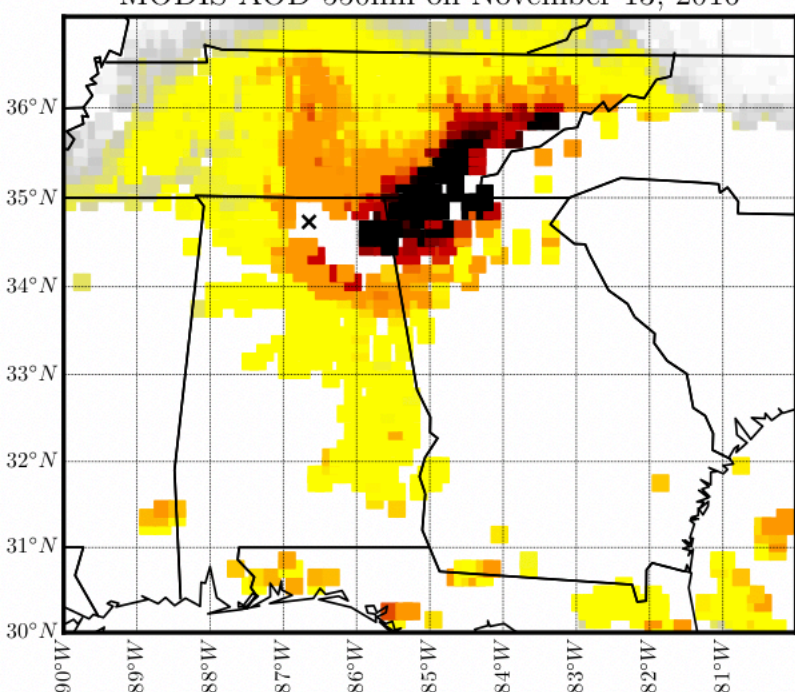


modisAOD.

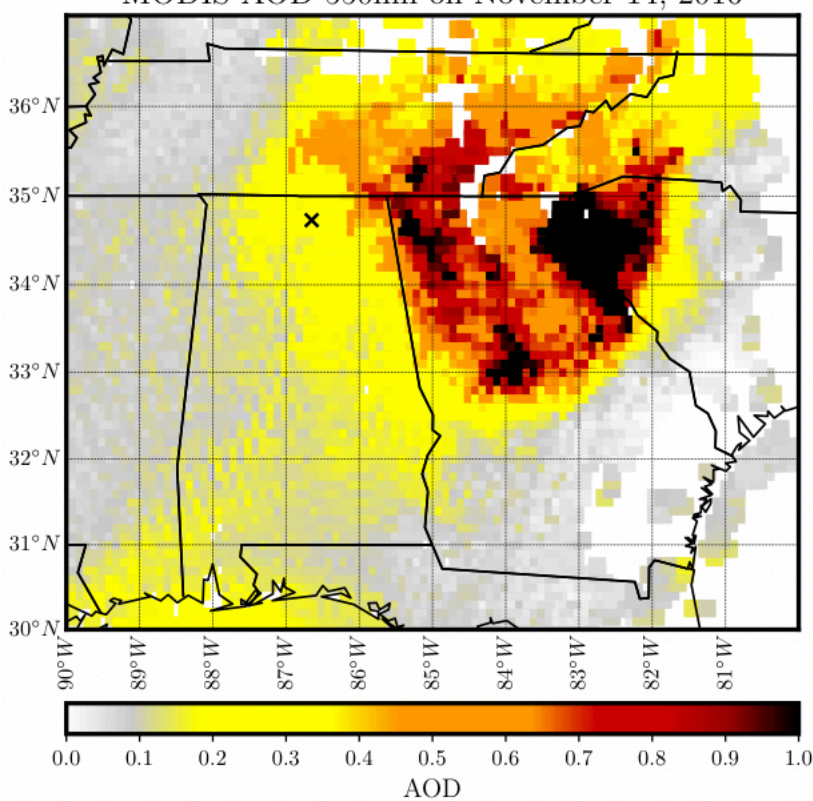
MODIS AOD 550nm on November 12, 2016



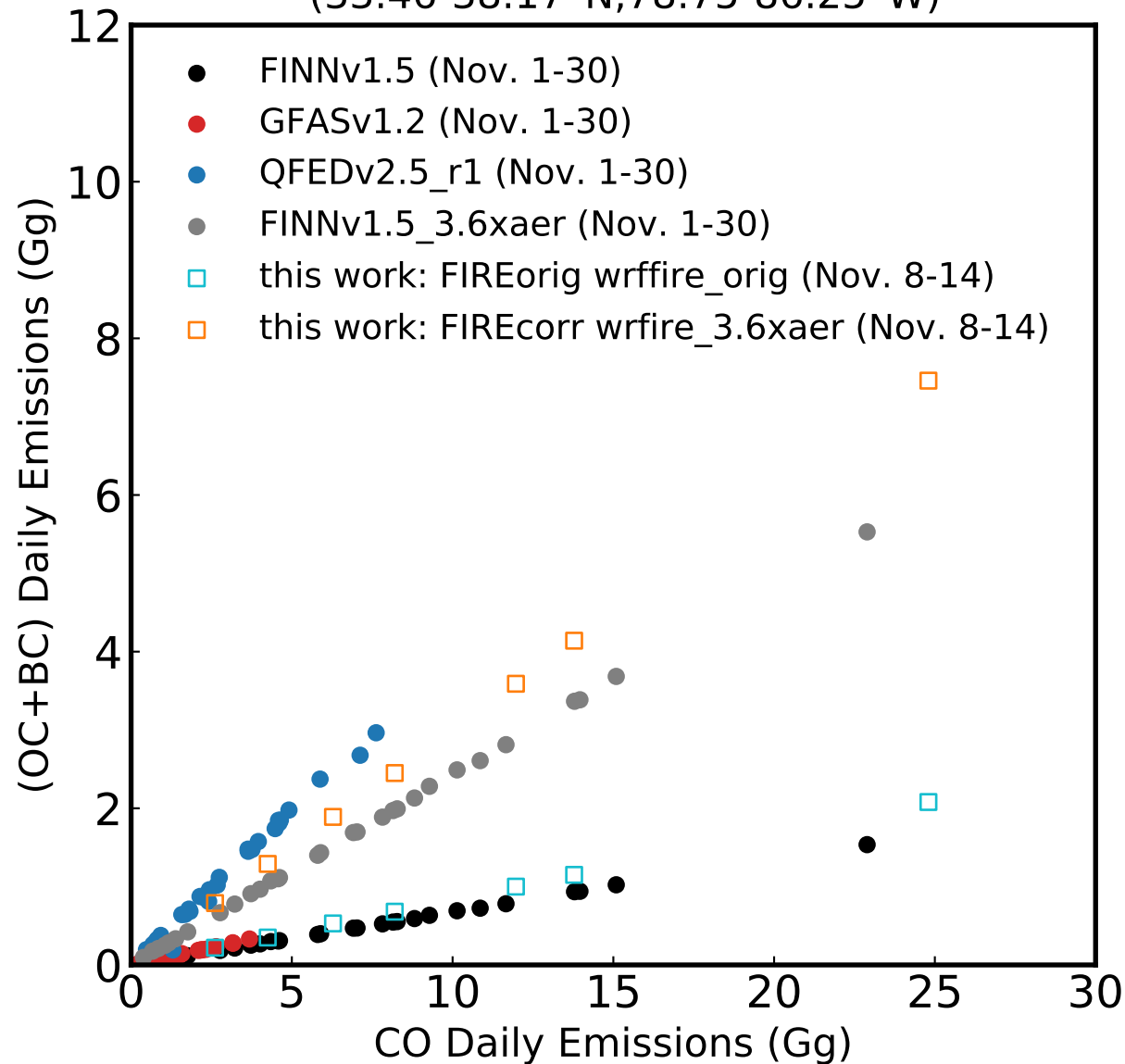
MODIS AOD 550nm on November 13, 2016



MODIS AOD 550nm on November 14, 2016

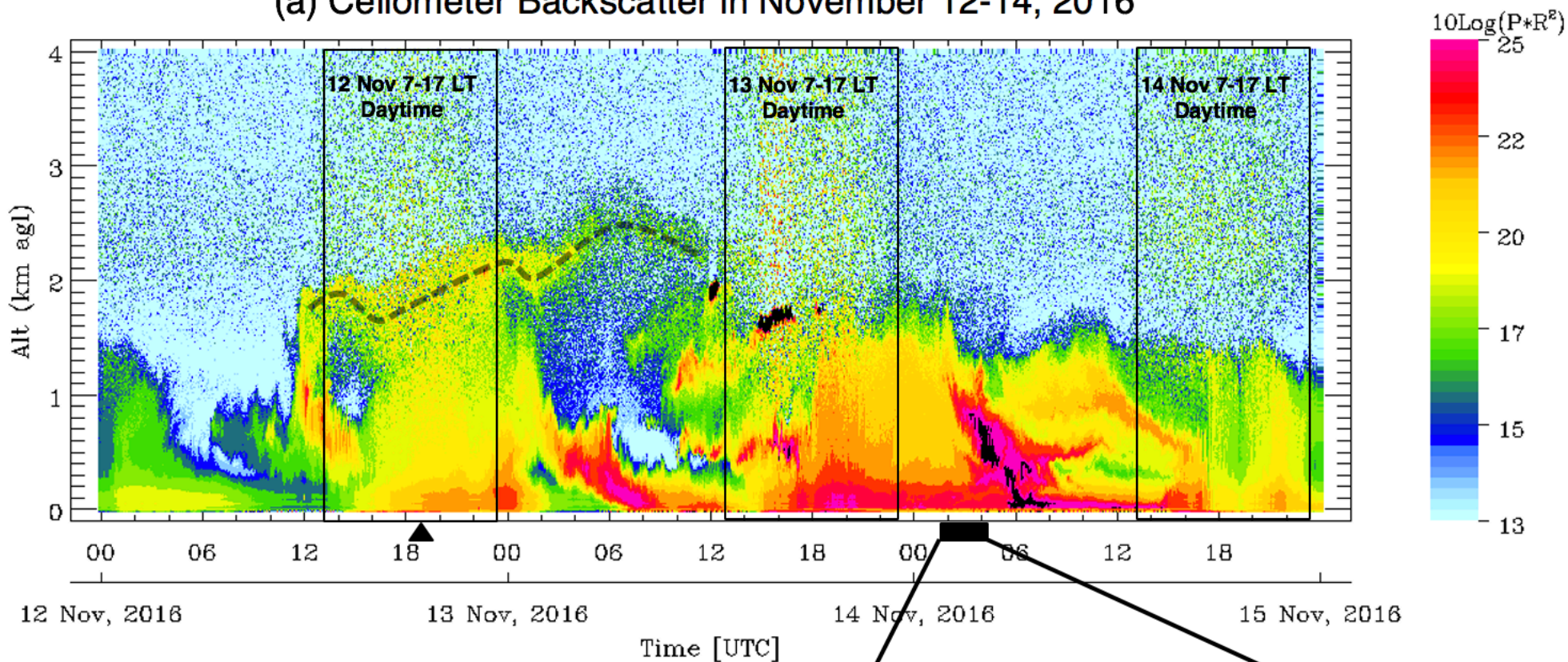


(OC+BC) to CO Emissions in SEUS Wildfire Region
(33.46-38.17°N, 78.75-86.25°W)

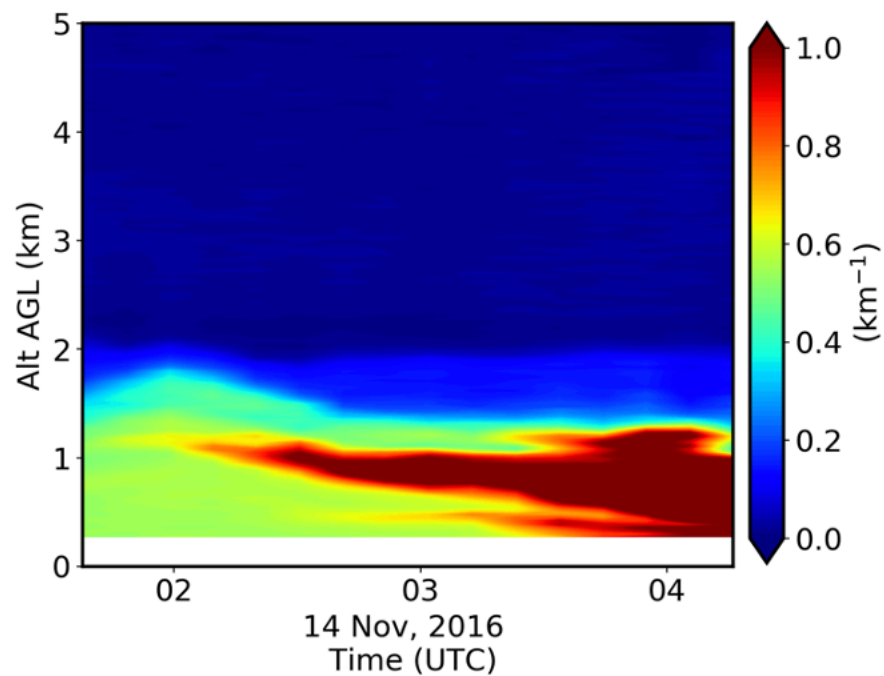


ceilometer_dial_v4.

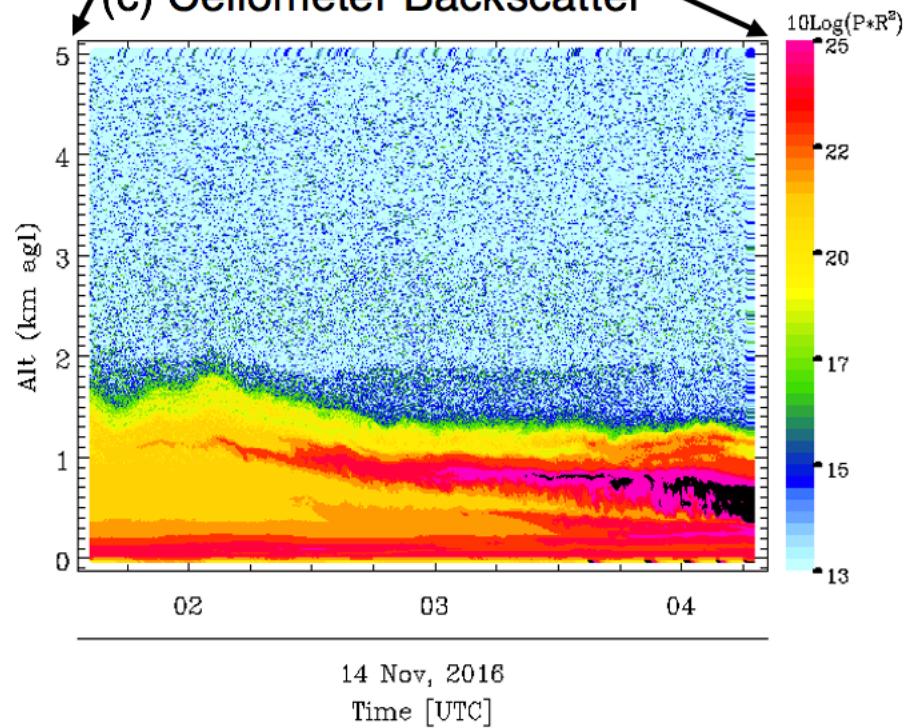
(a) Ceilometer Backscatter in November 12-14, 2016



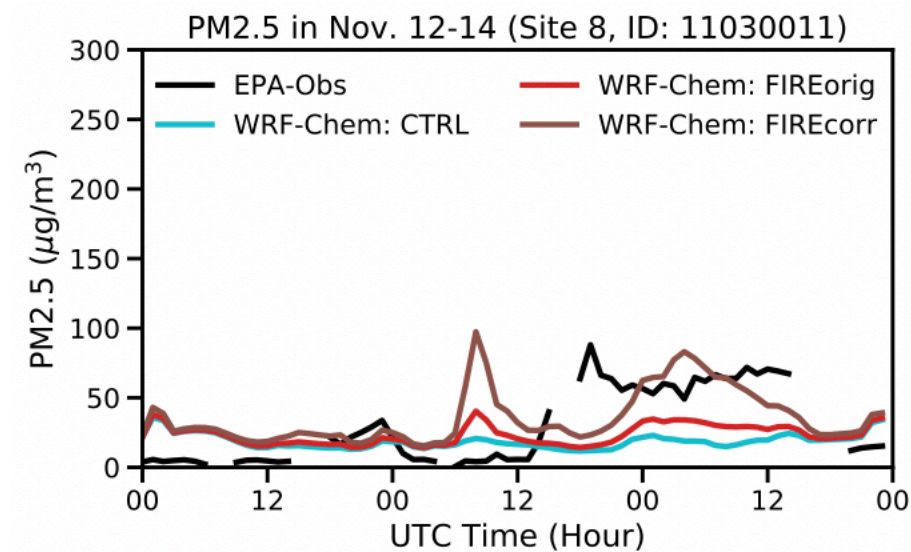
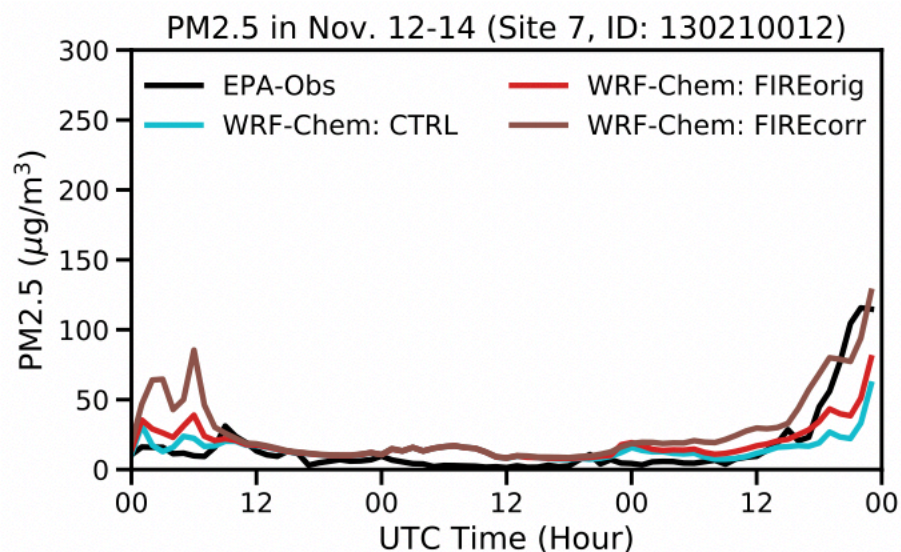
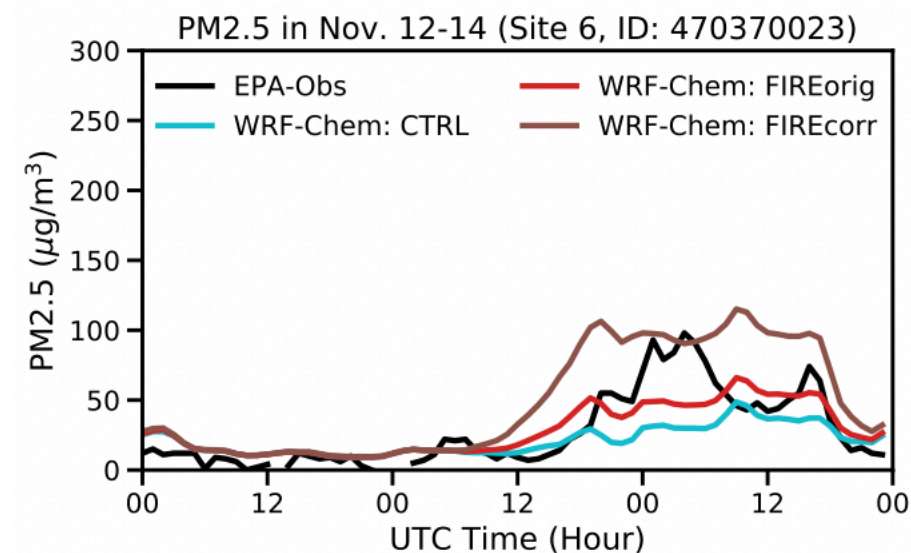
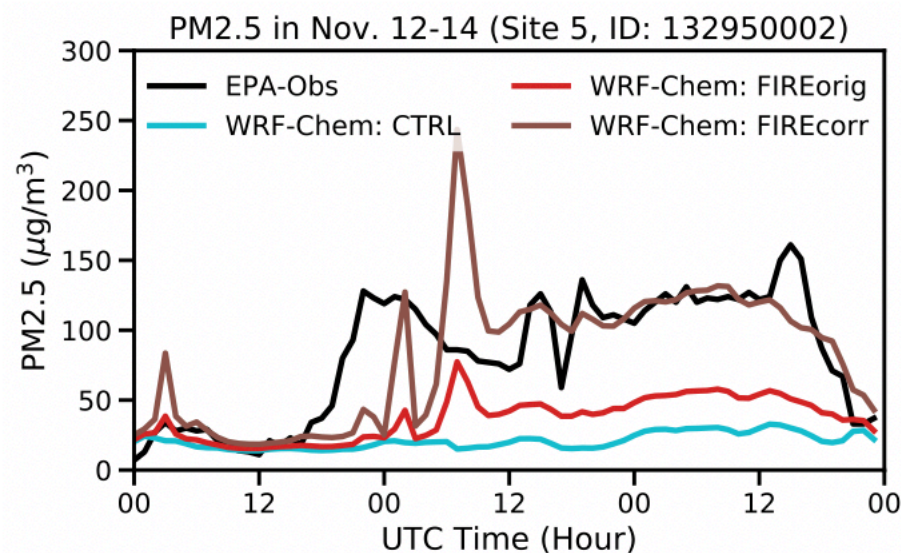
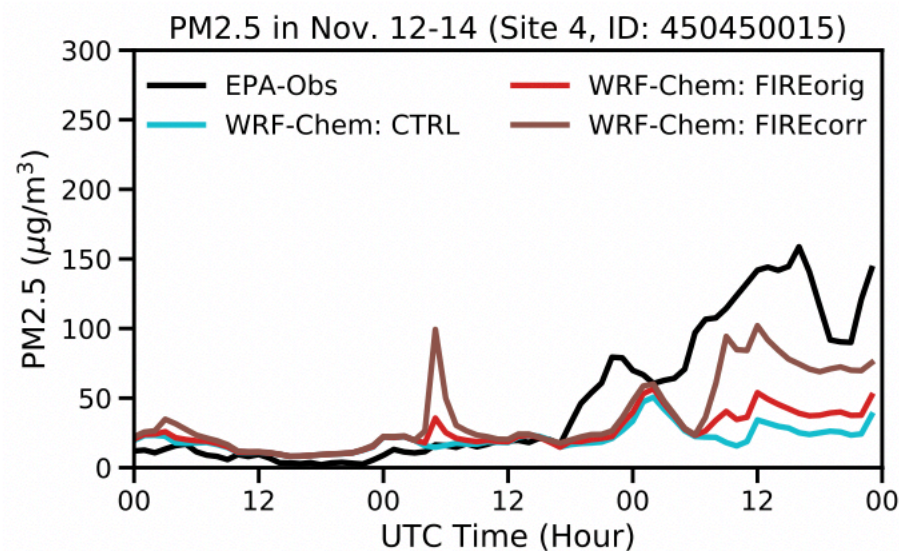
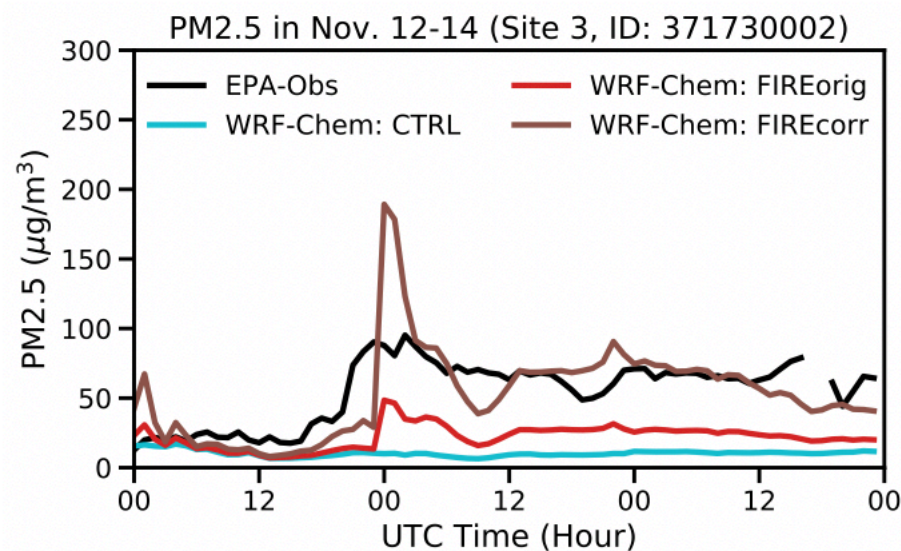
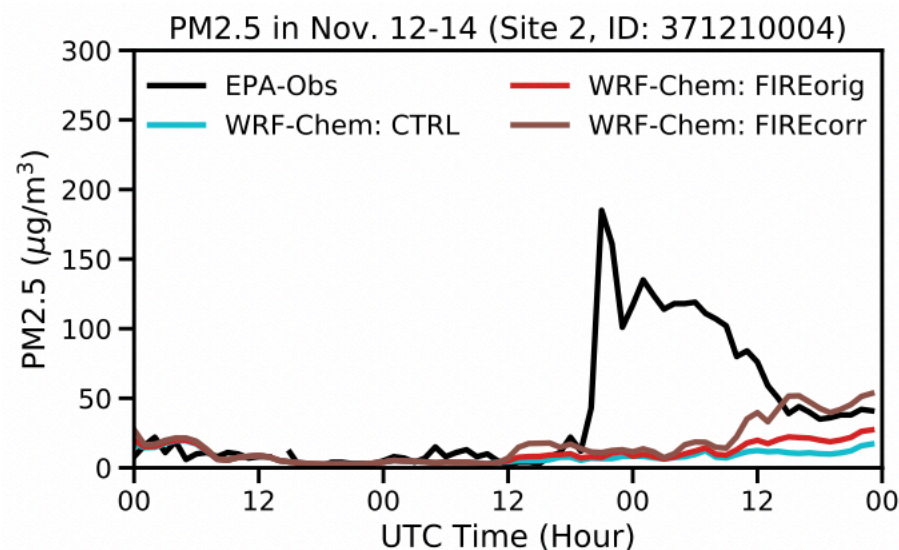
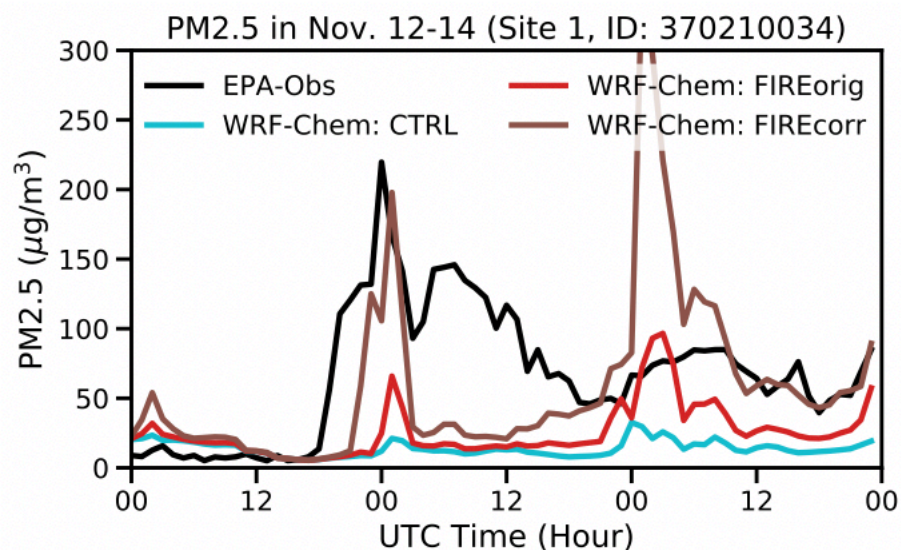
(b) DIAL Aerosol Extinction

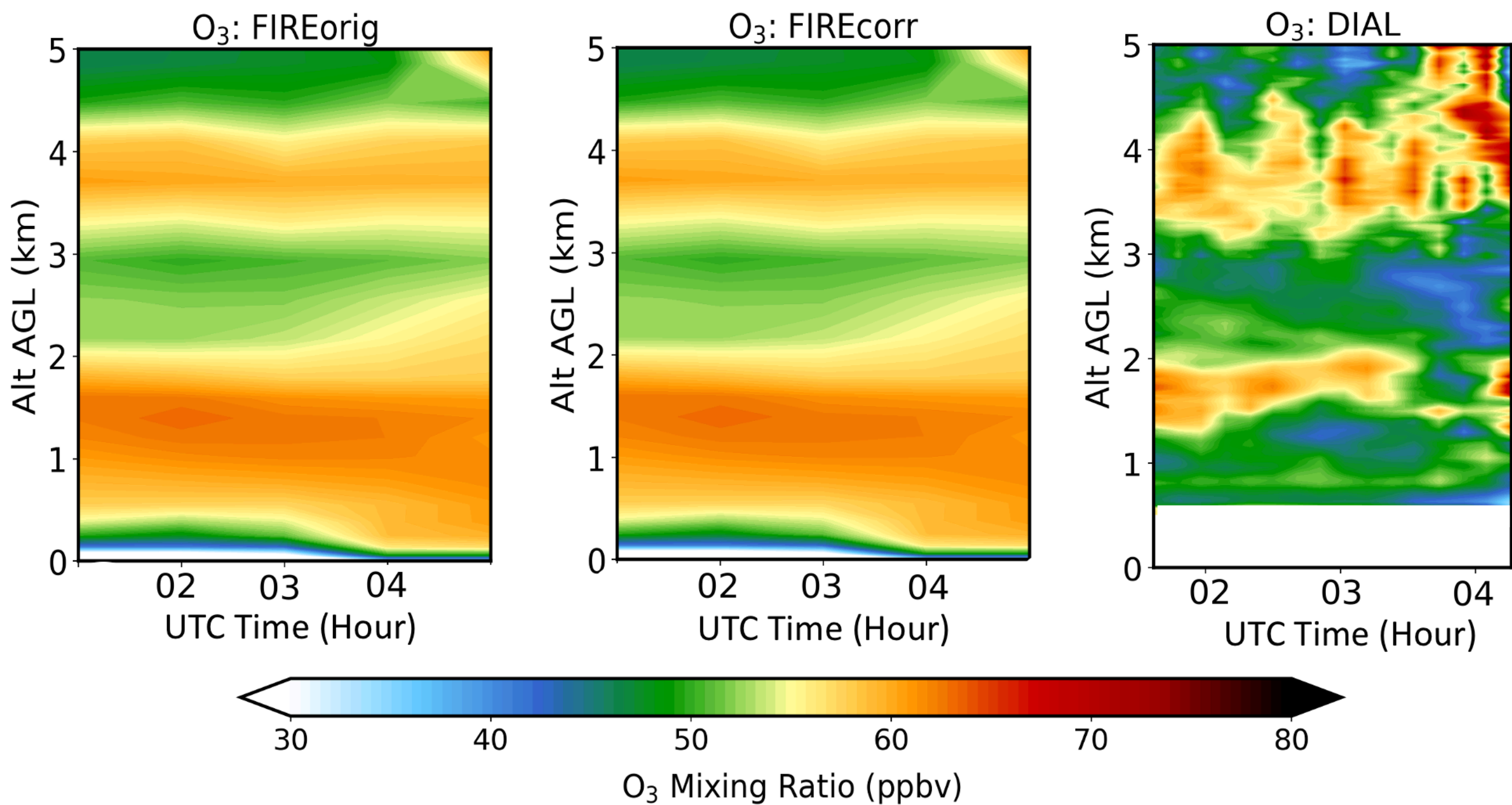
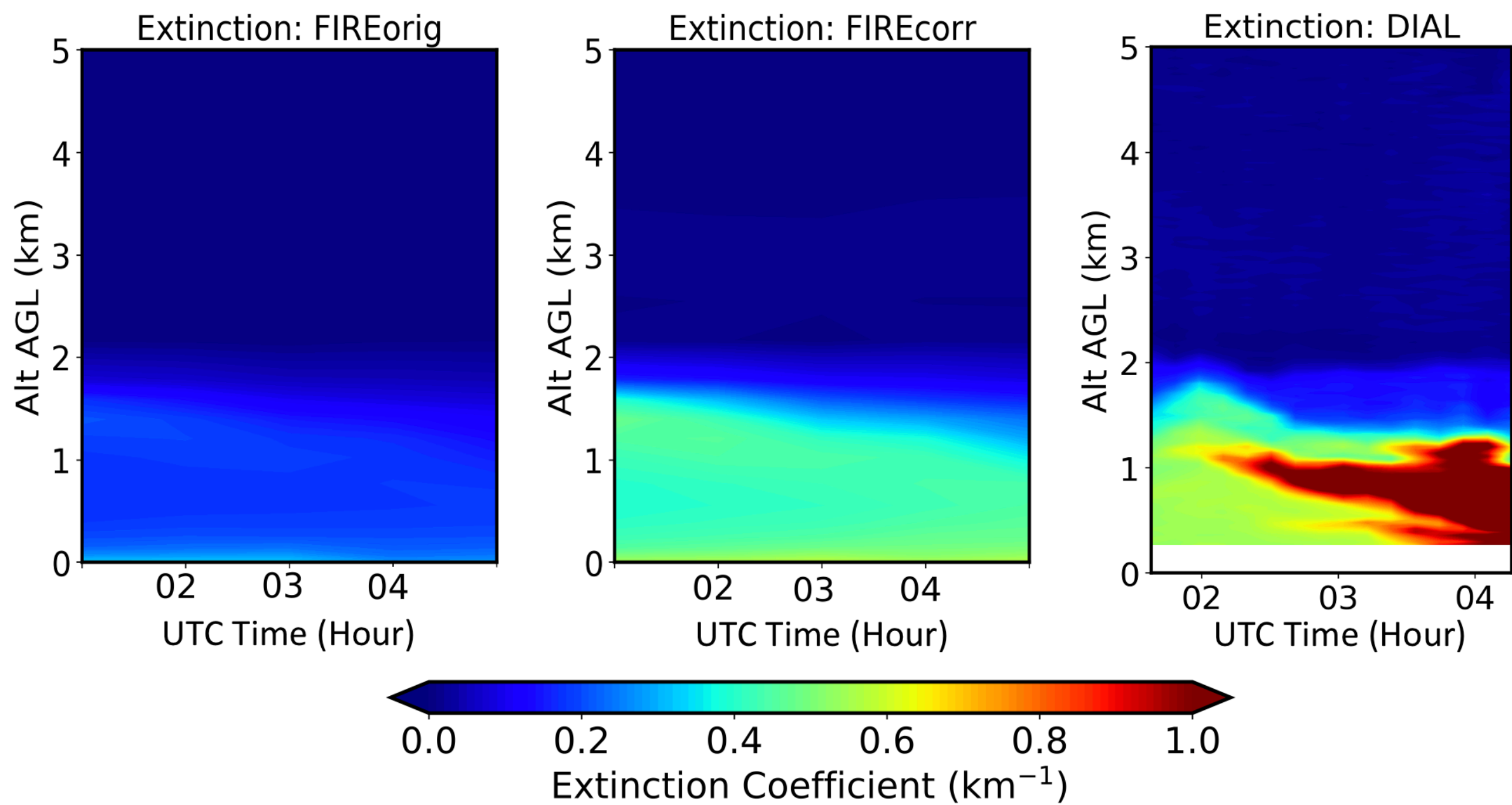


(c) Ceilometer Backscatter



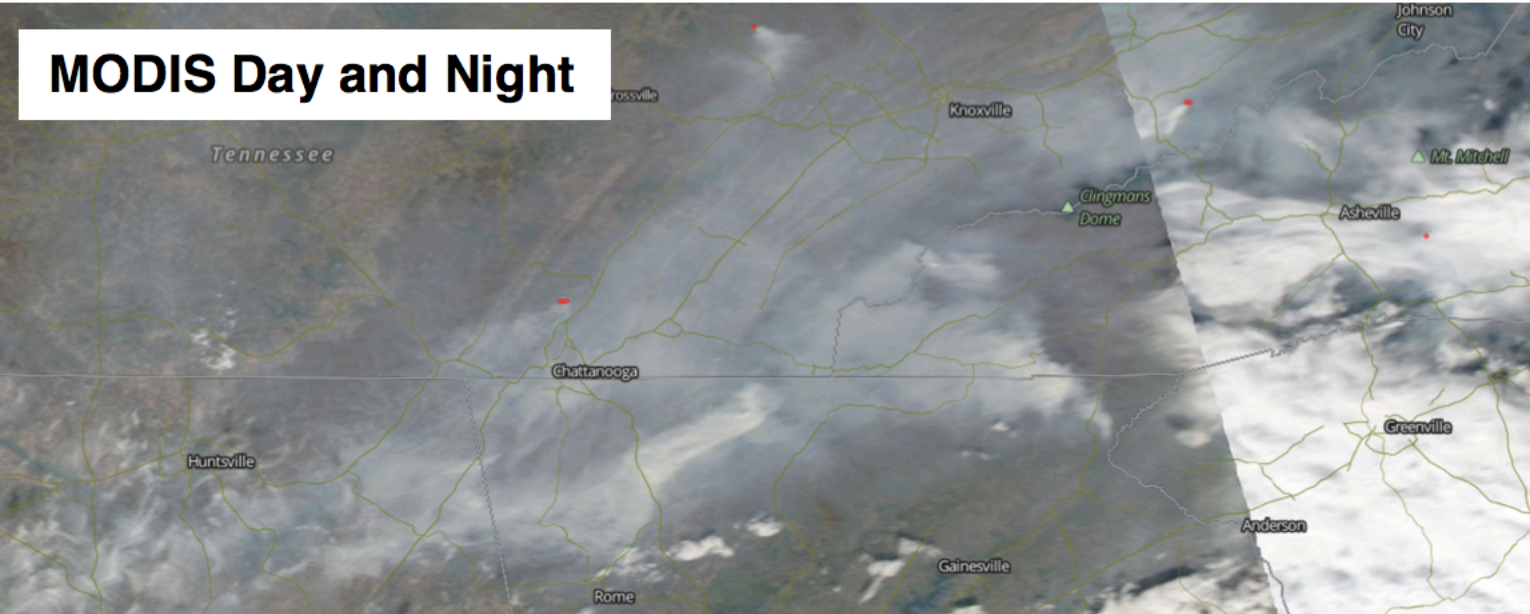
wrfchem_pm25.



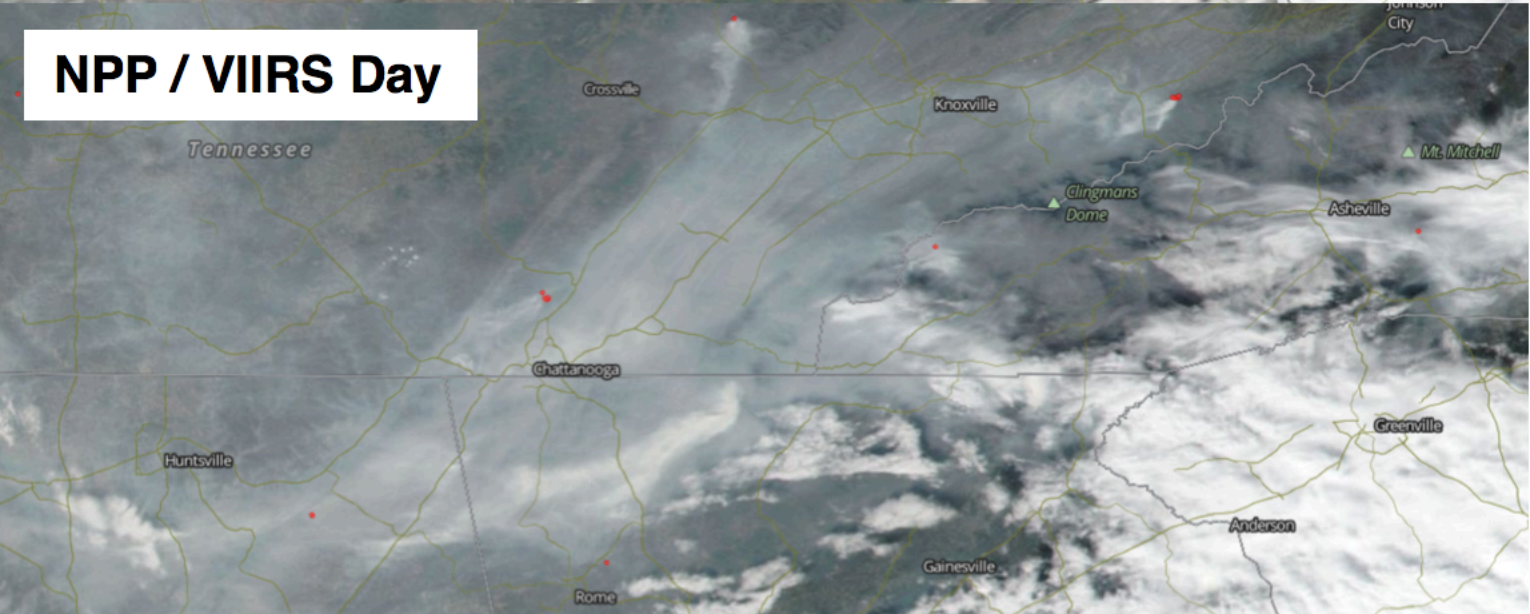


satellite_detection.

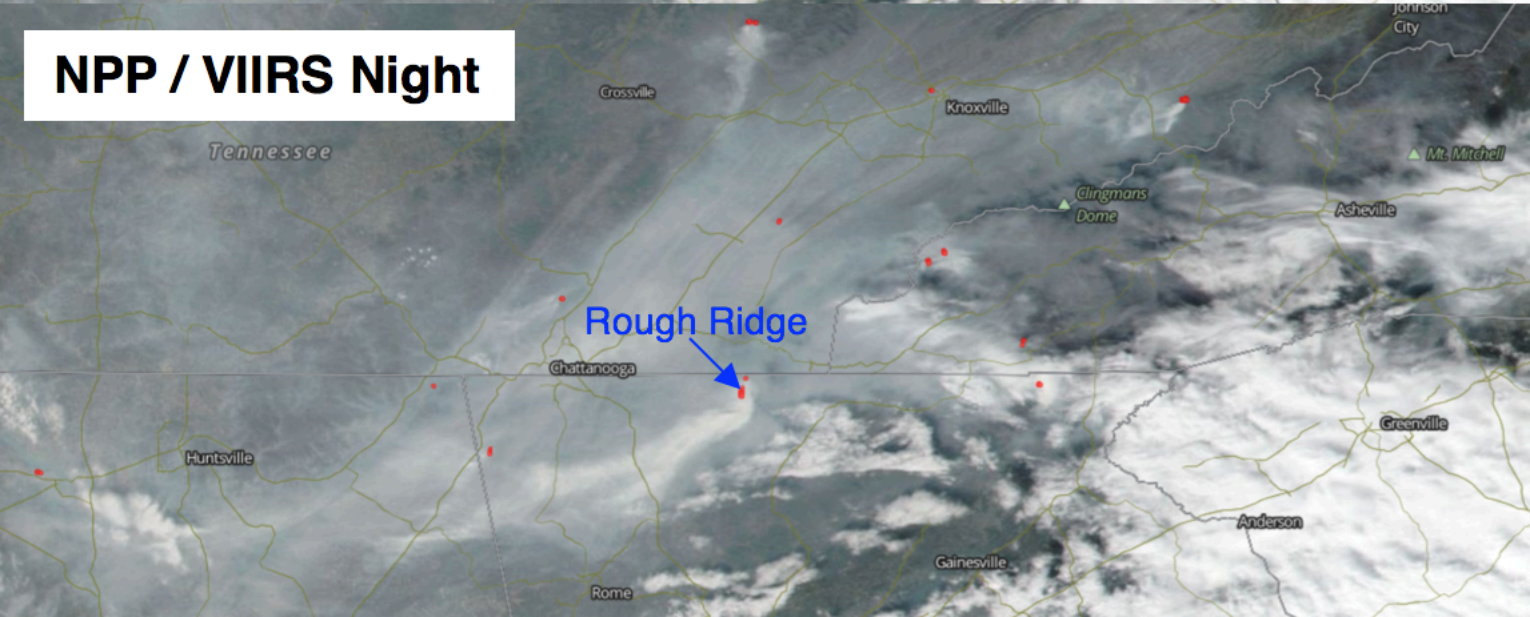
MODIS Day and Night



NPP / VIIRS Day

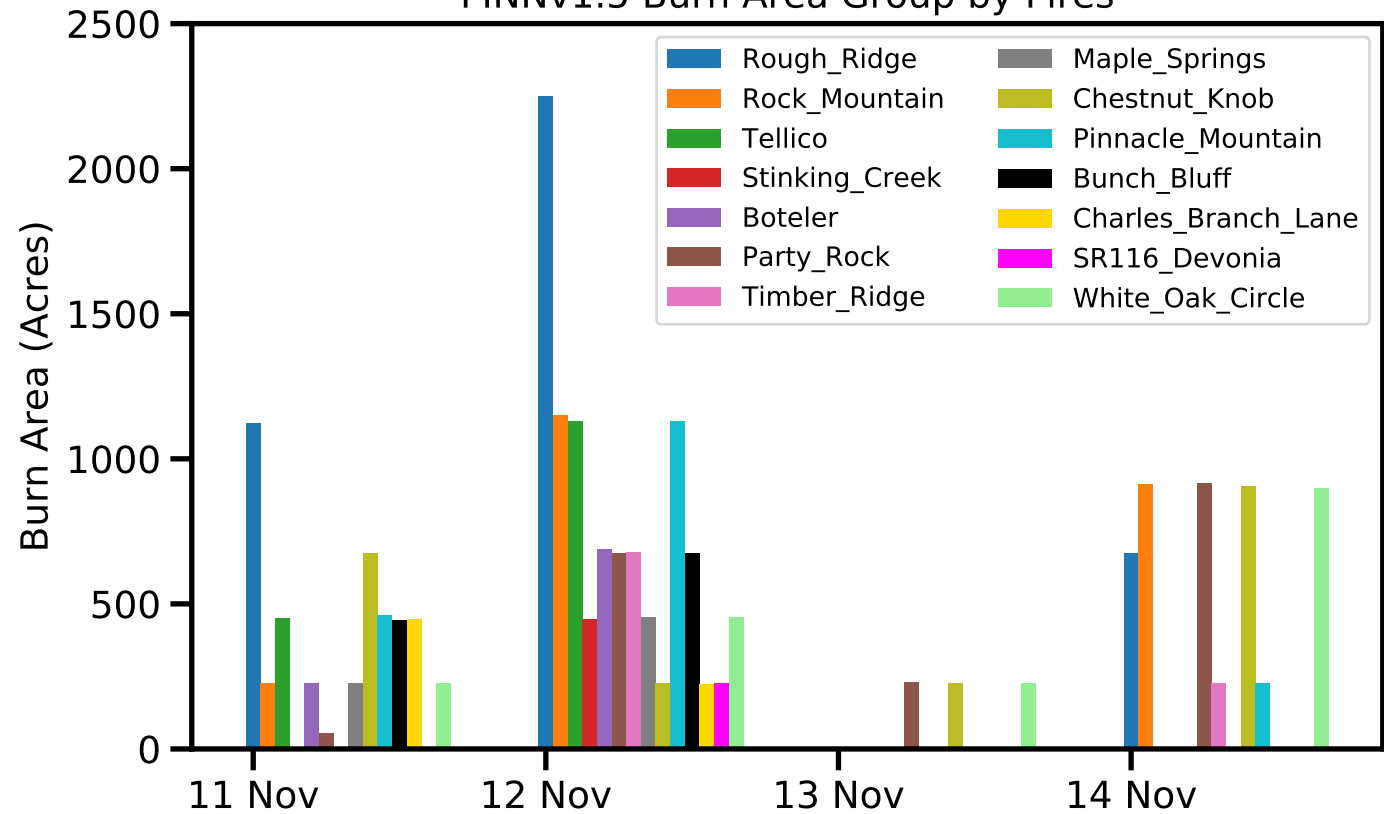


NPP / VIIRS Night

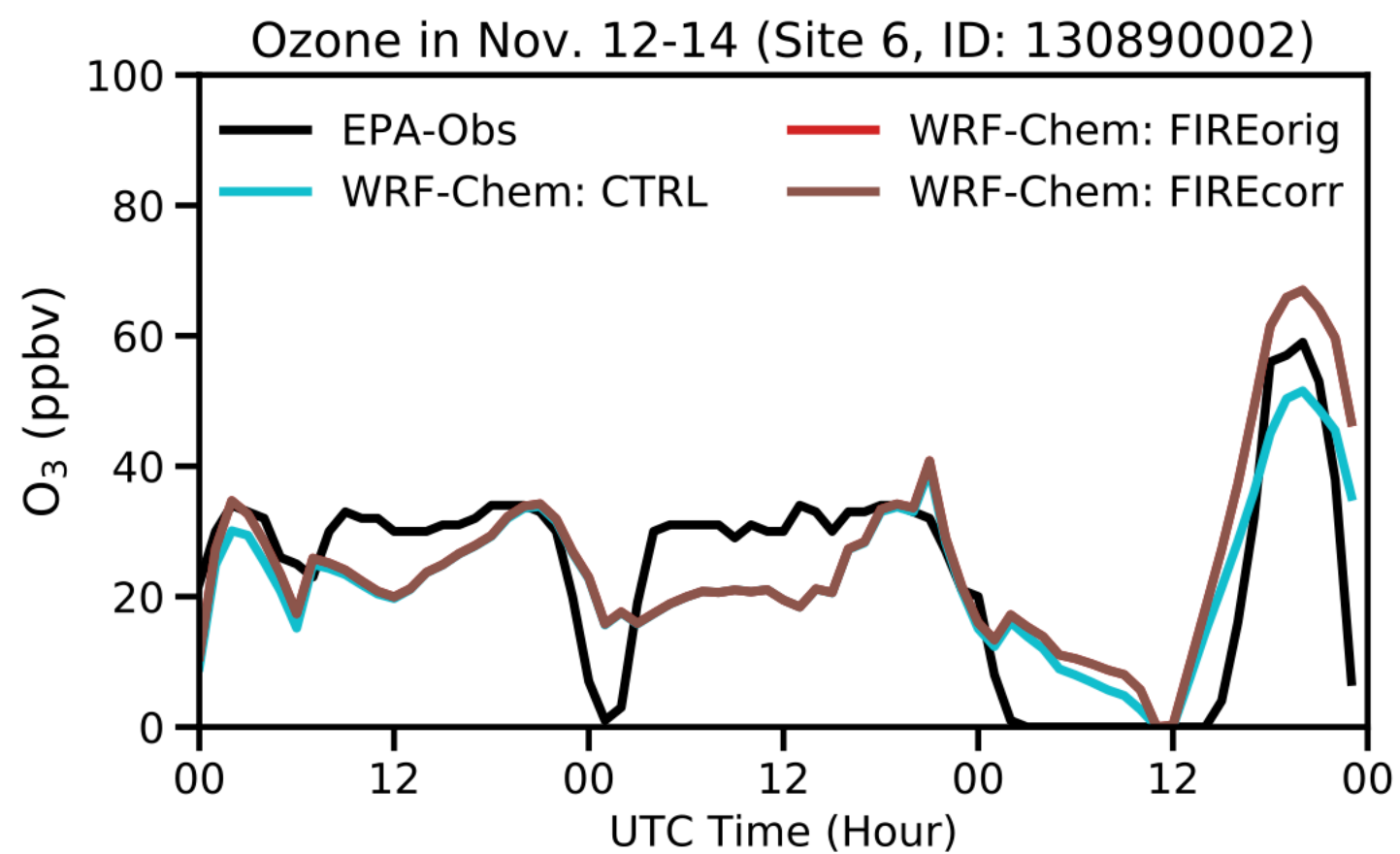
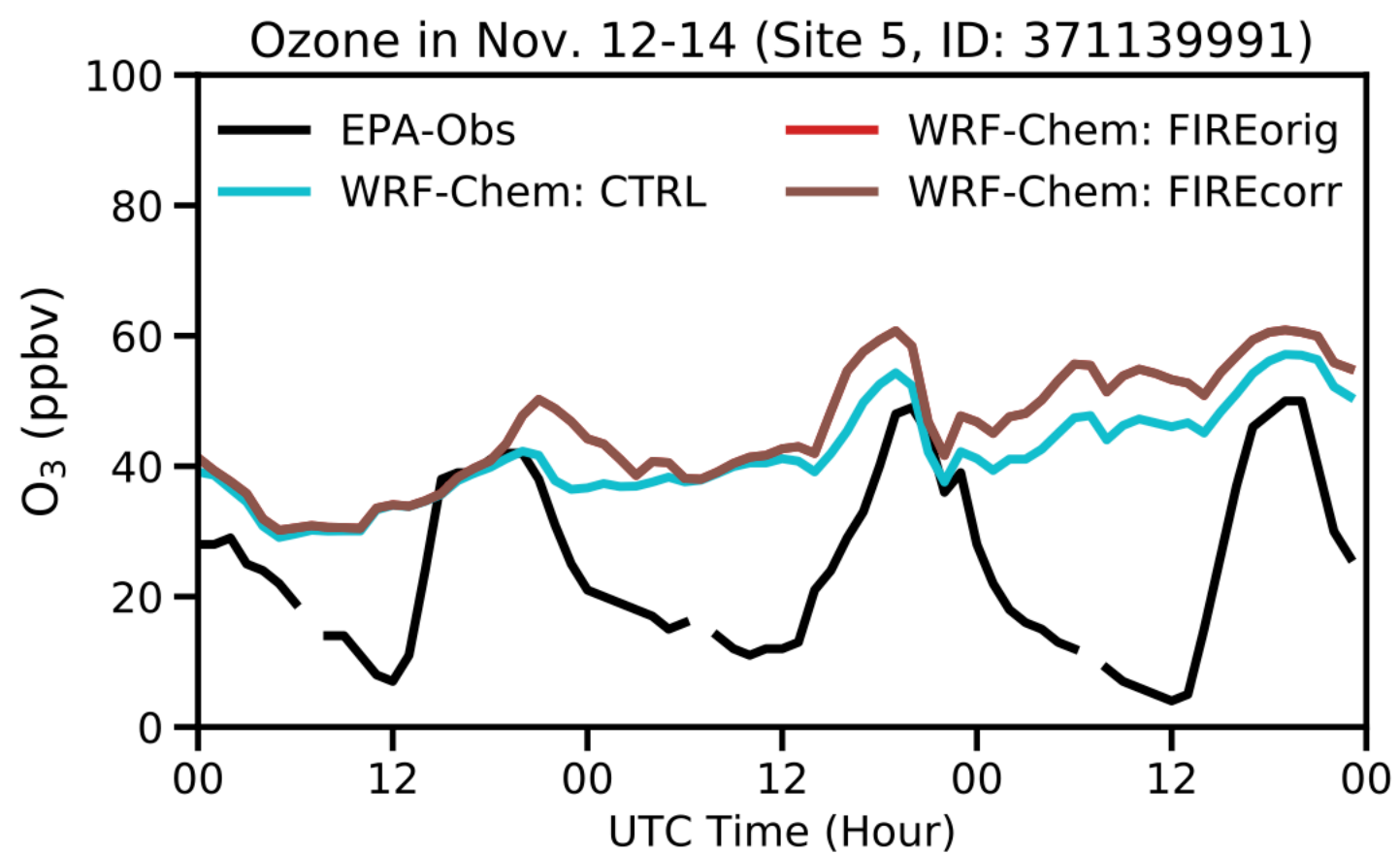
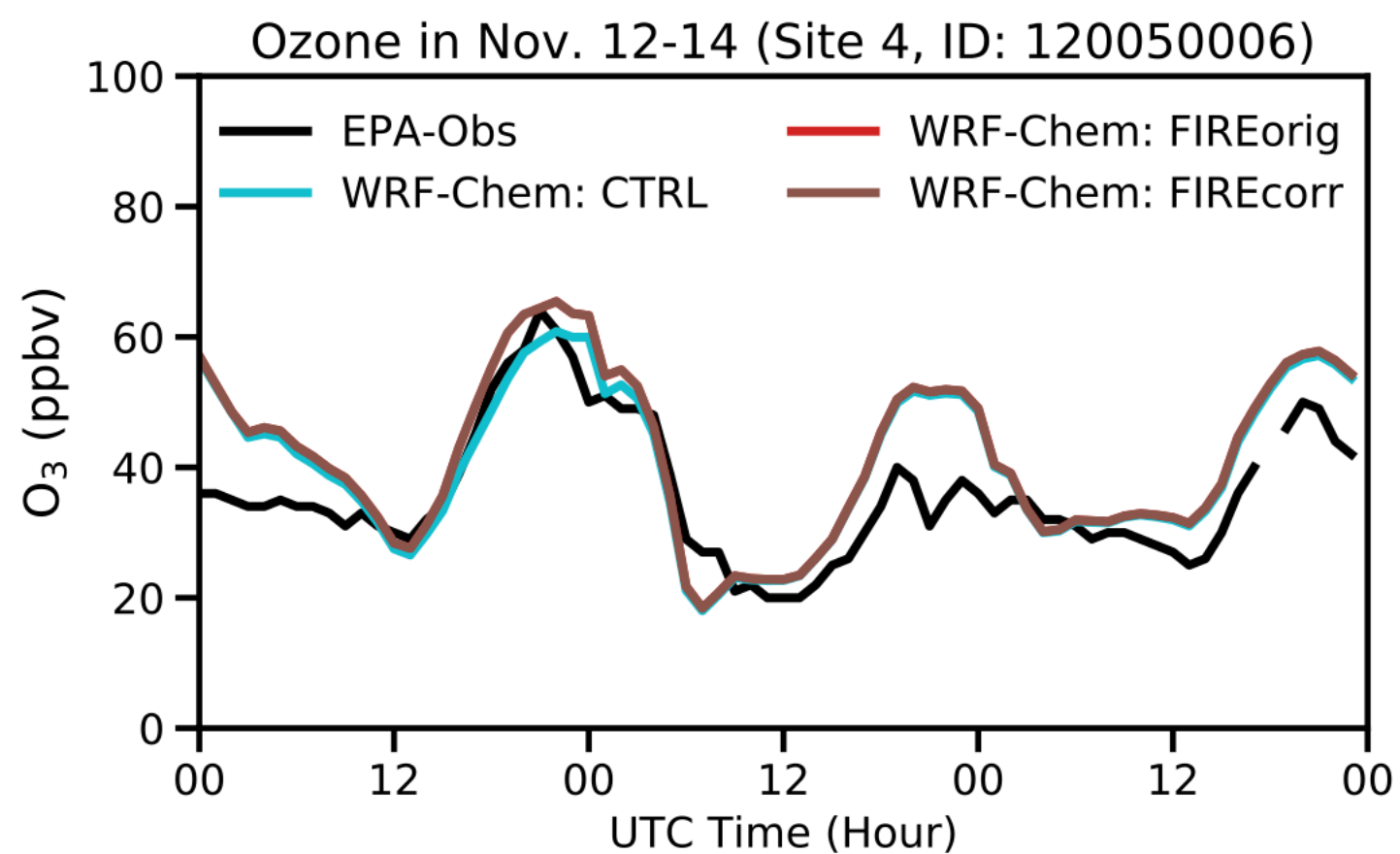
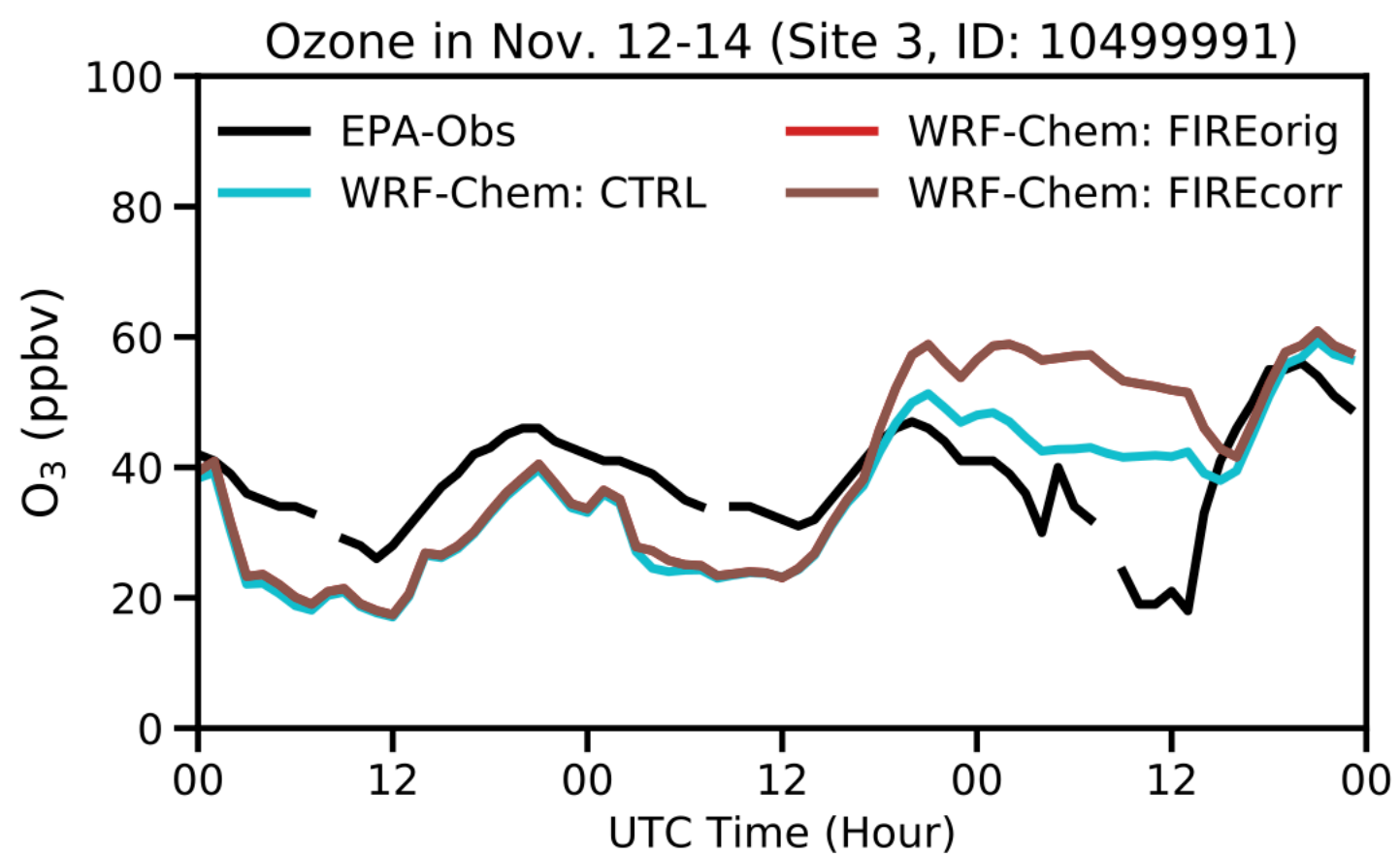
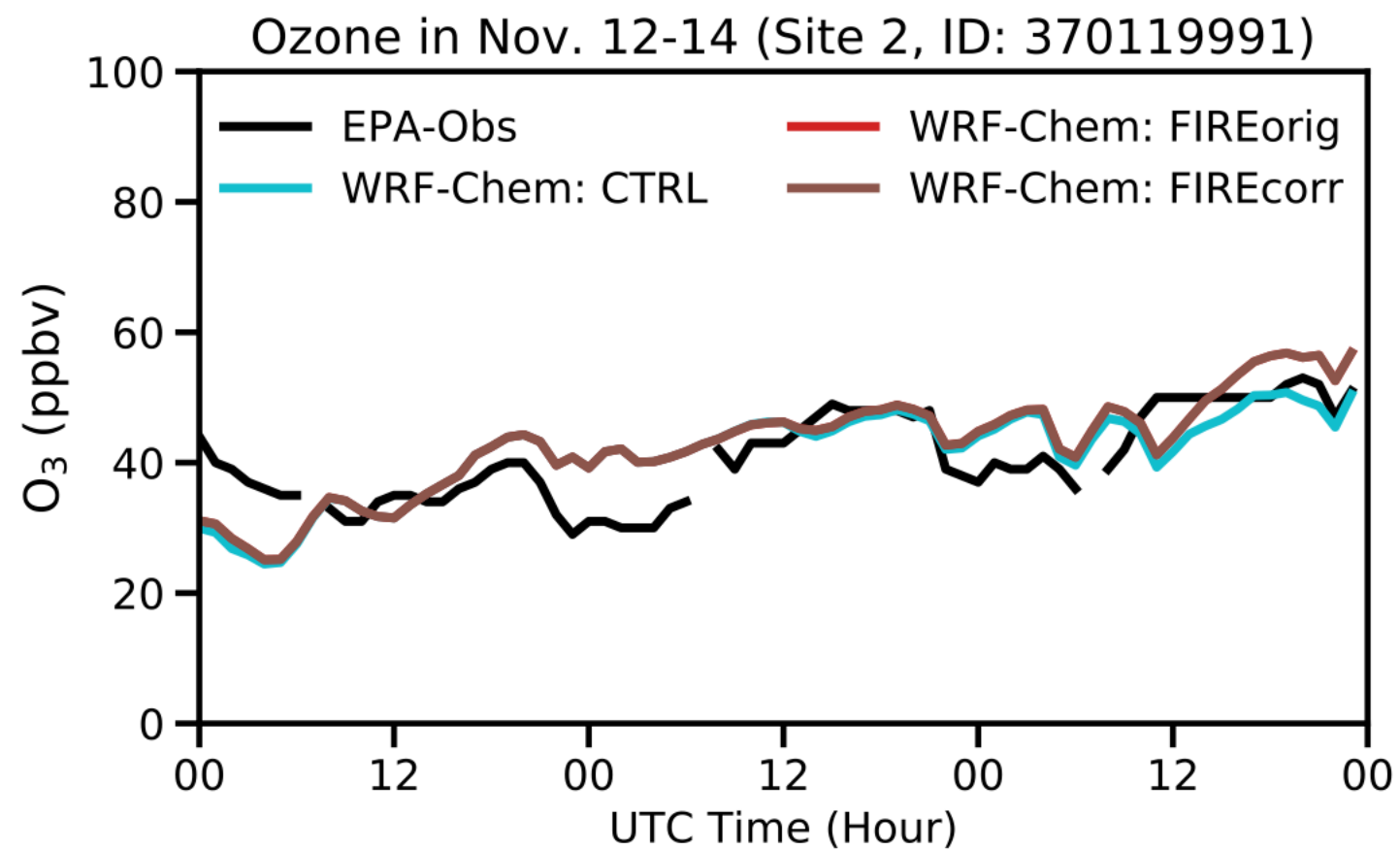
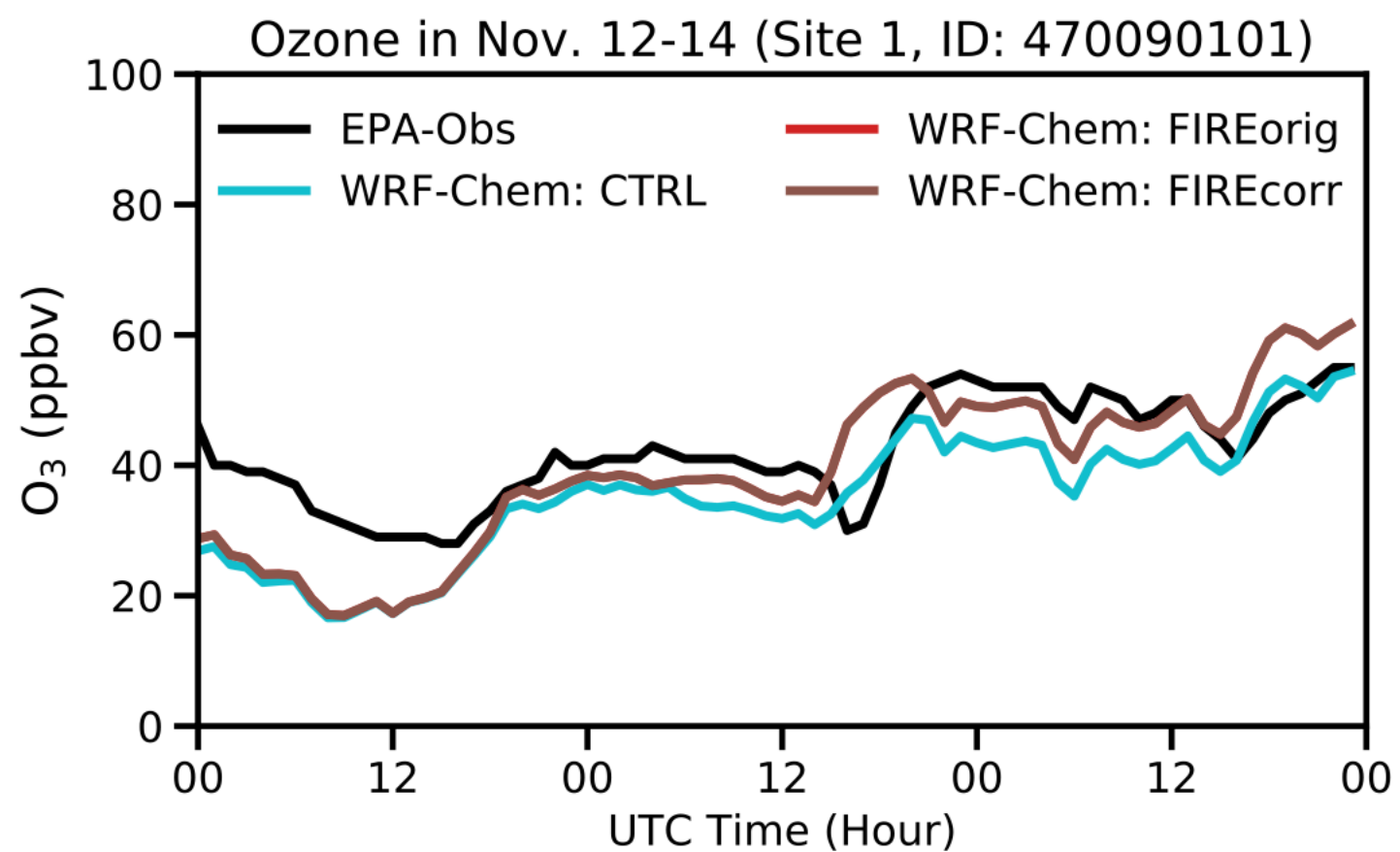


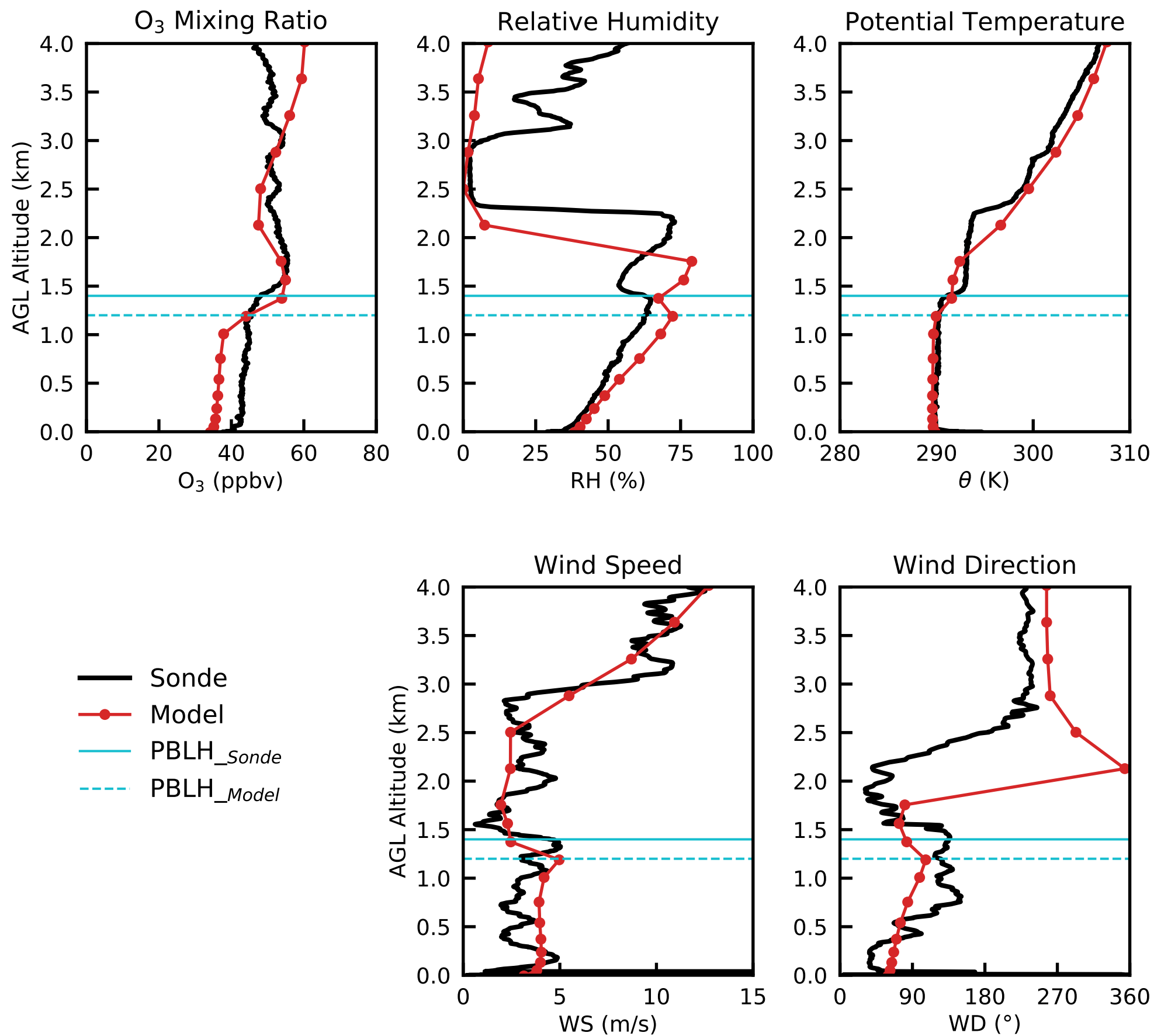
burn_area.

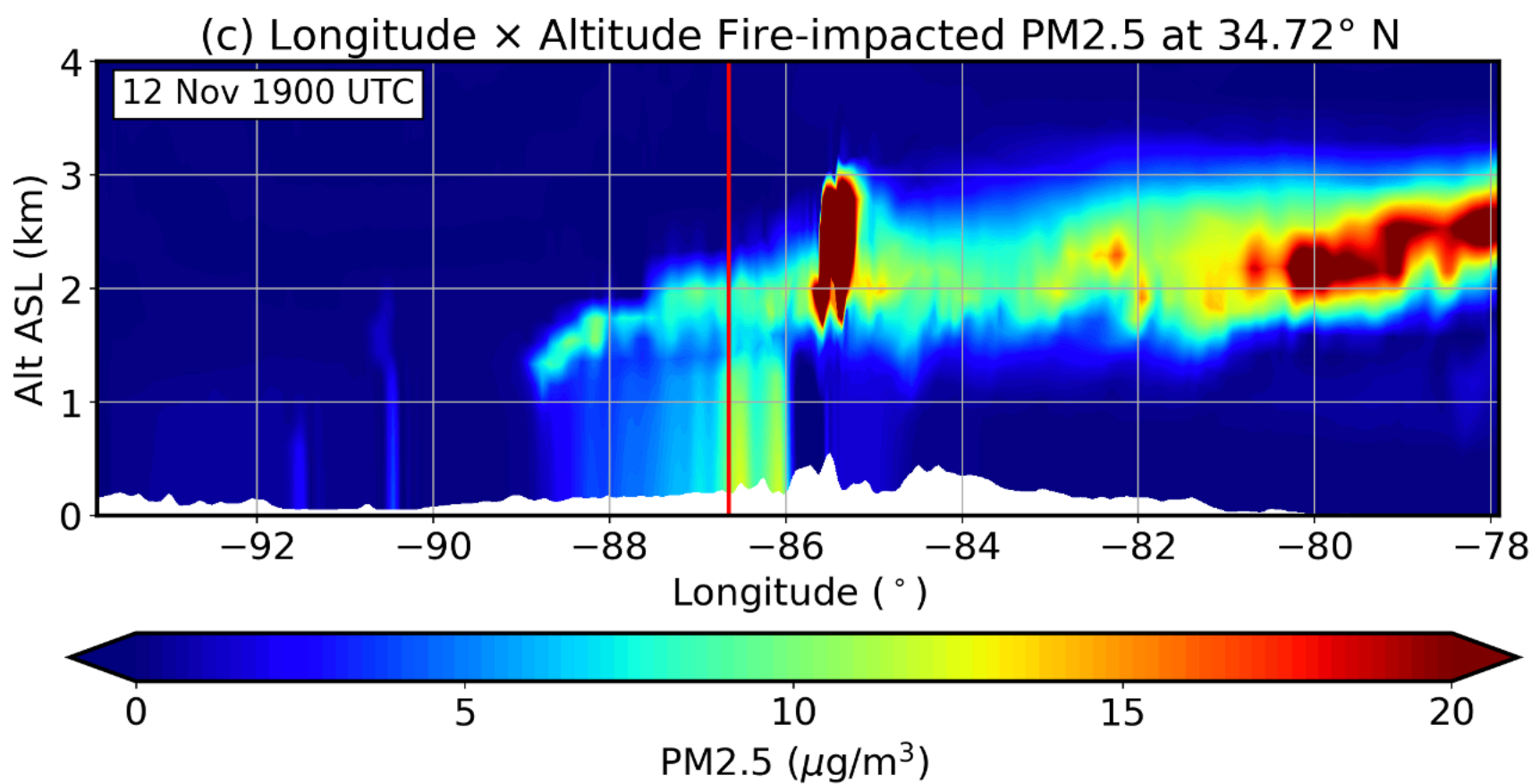
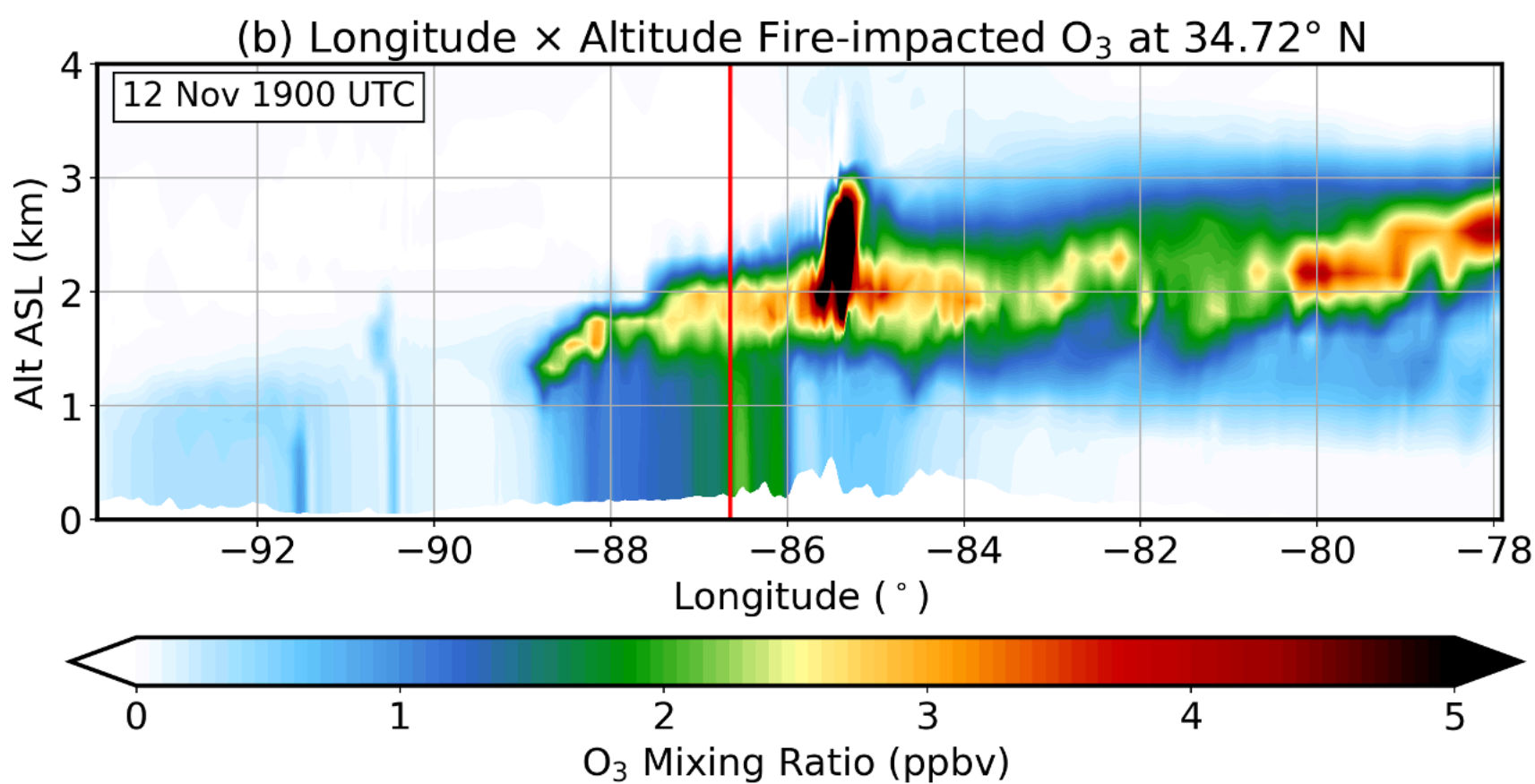
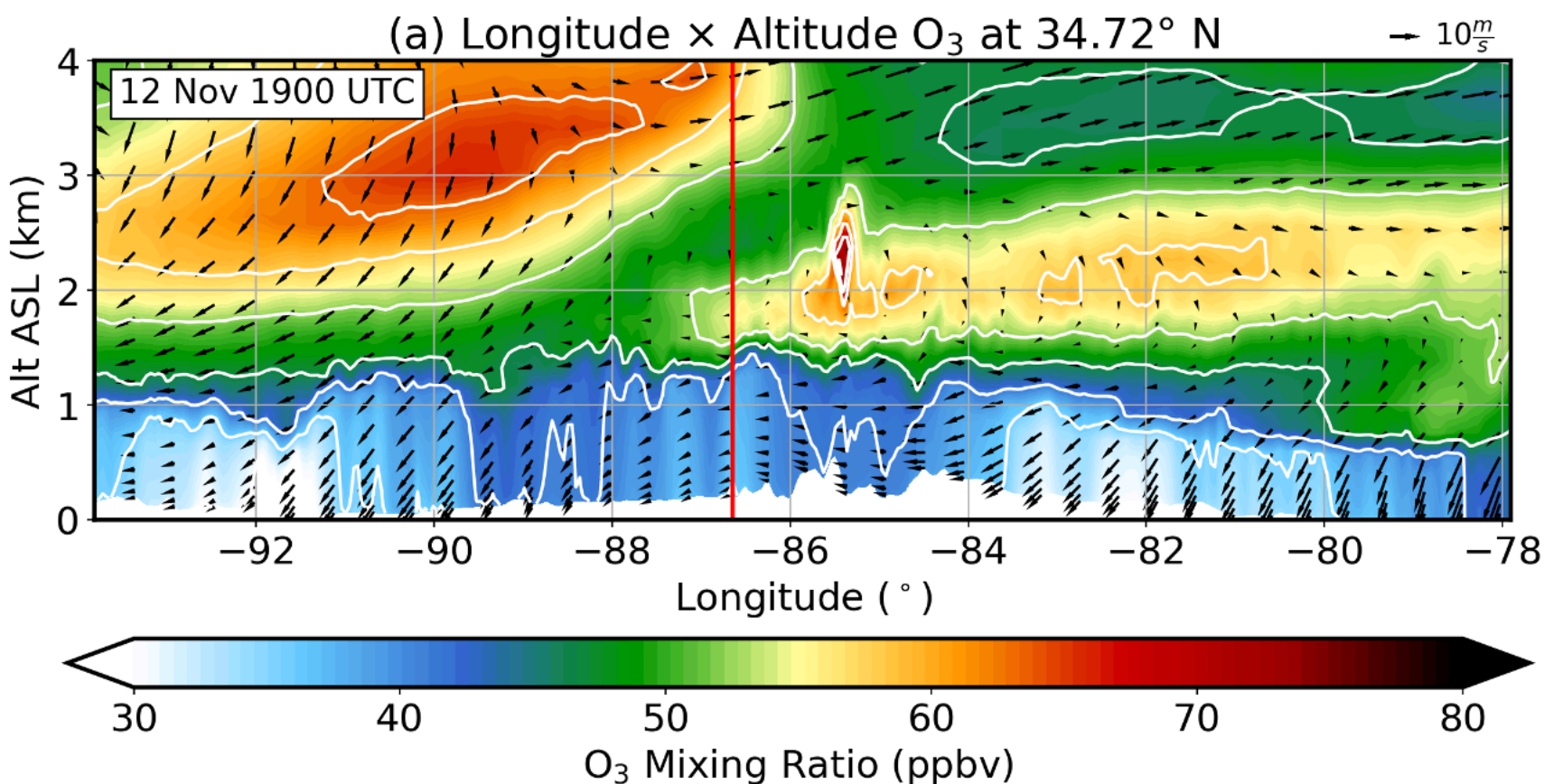
FINNv1.5 Burn Area Group by Fires



wrfchem_ozone_v2.



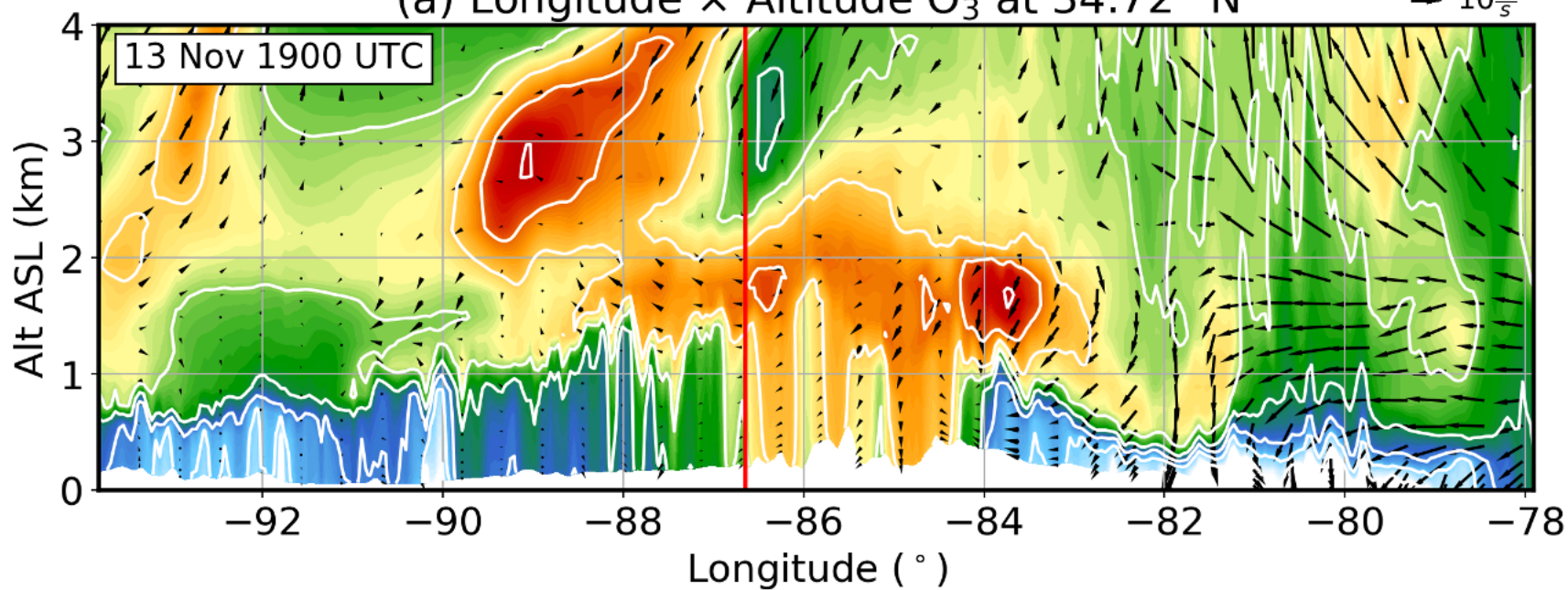




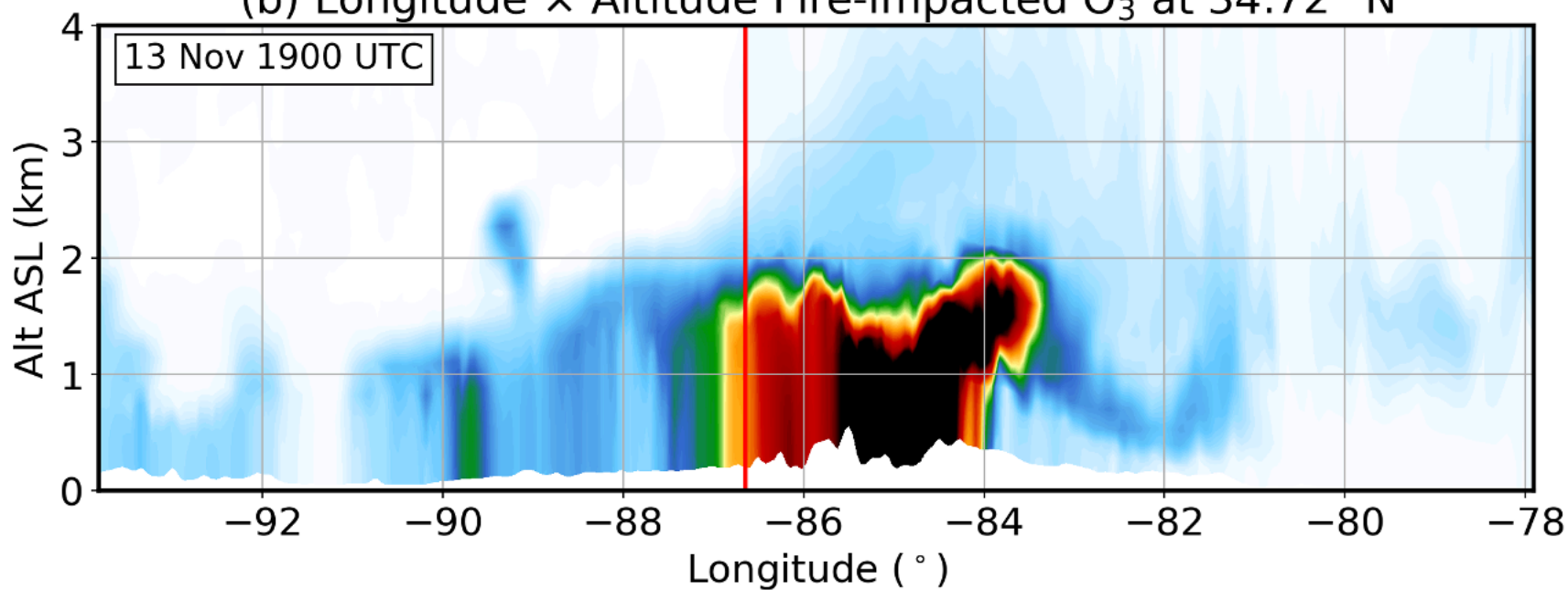
alt_lon_nov13_wofb.

(a) Longitude × Altitude O₃ at 34.72° N

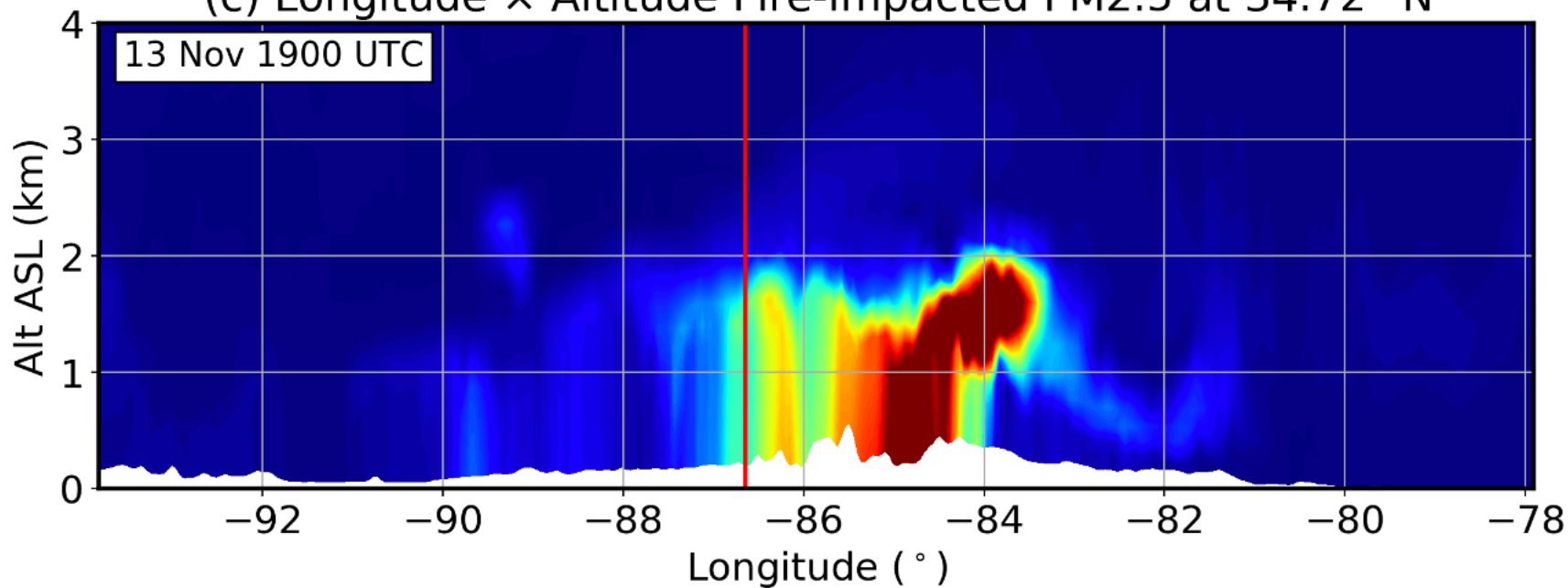
→ 10 $\frac{m}{s}$



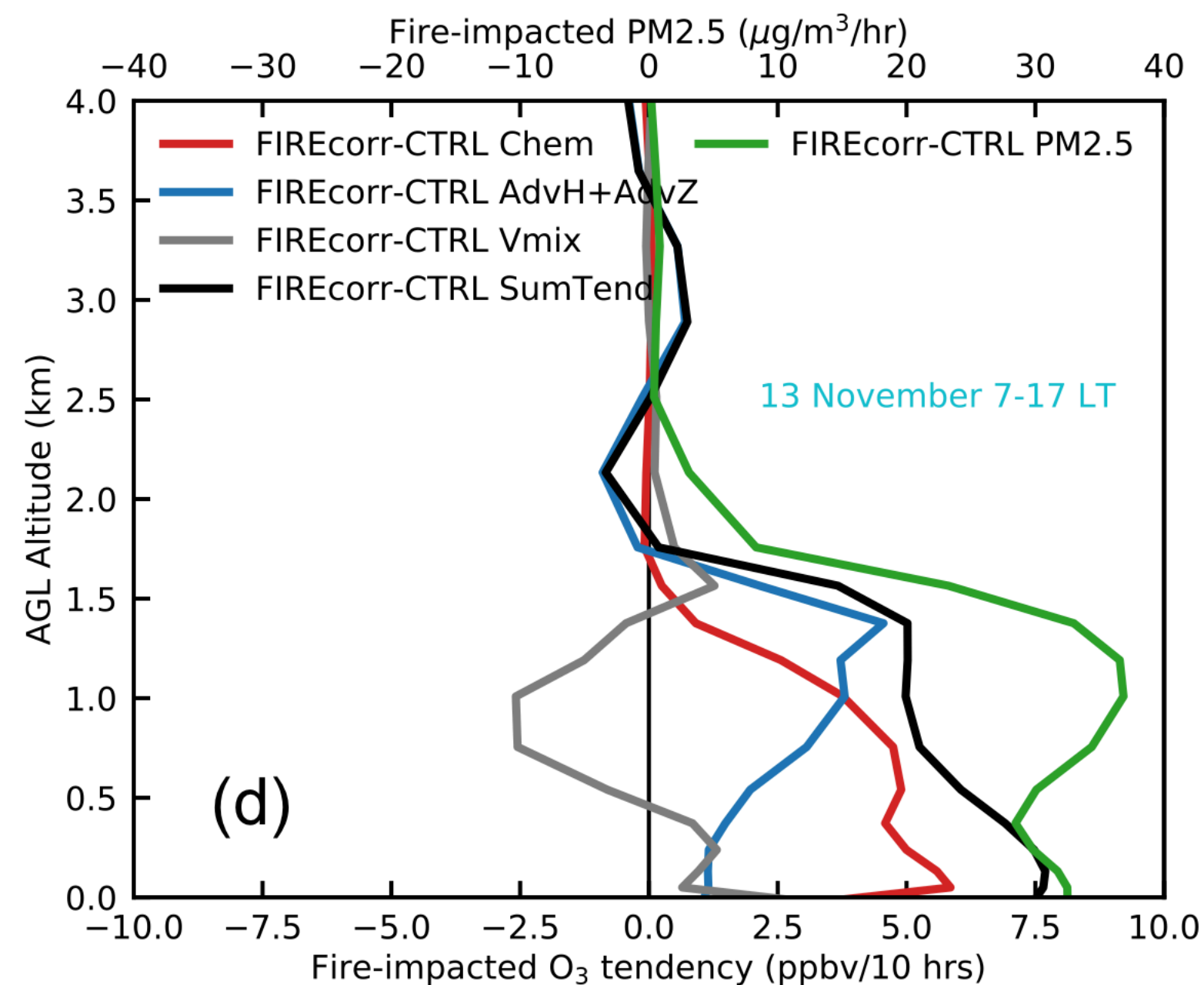
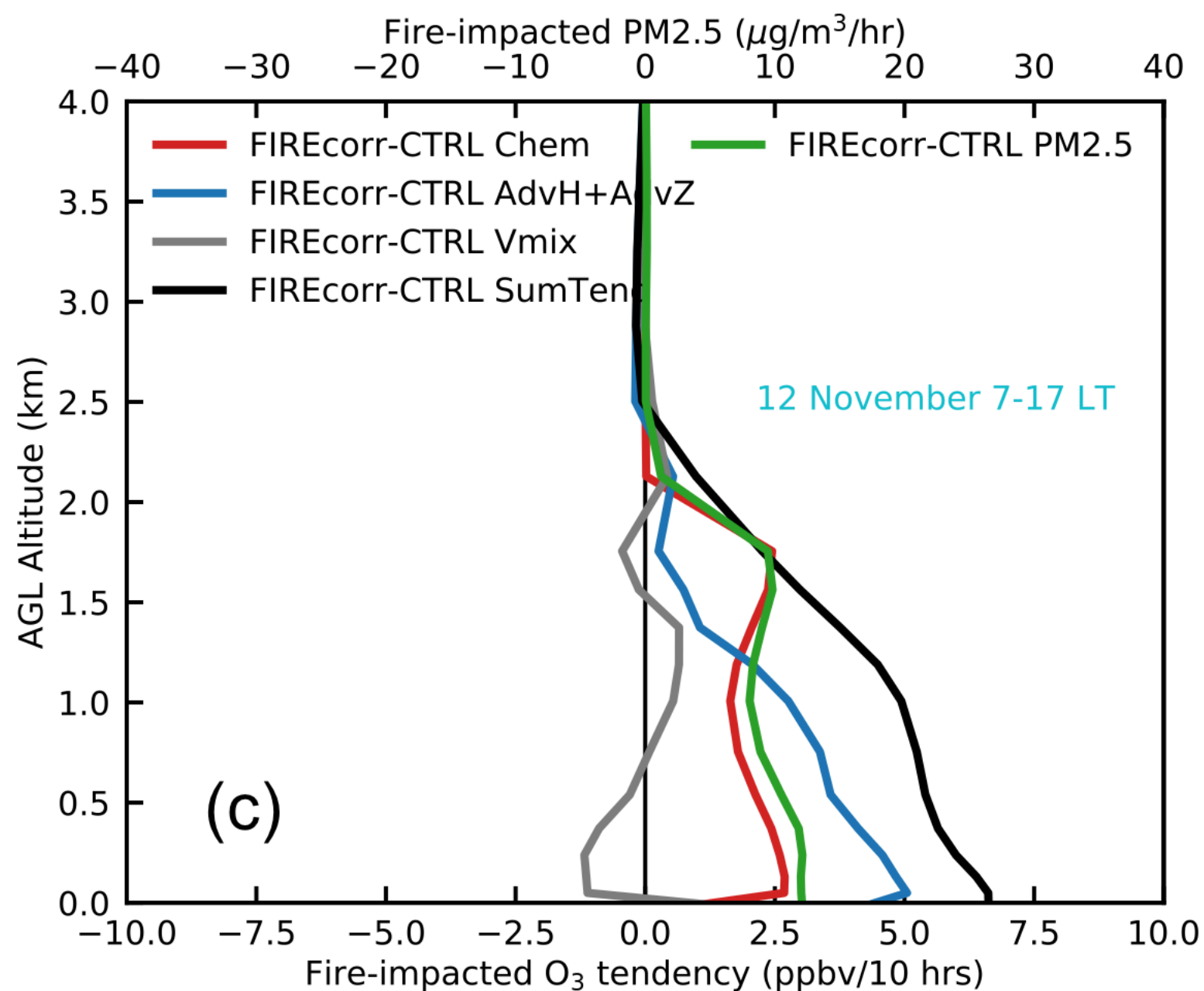
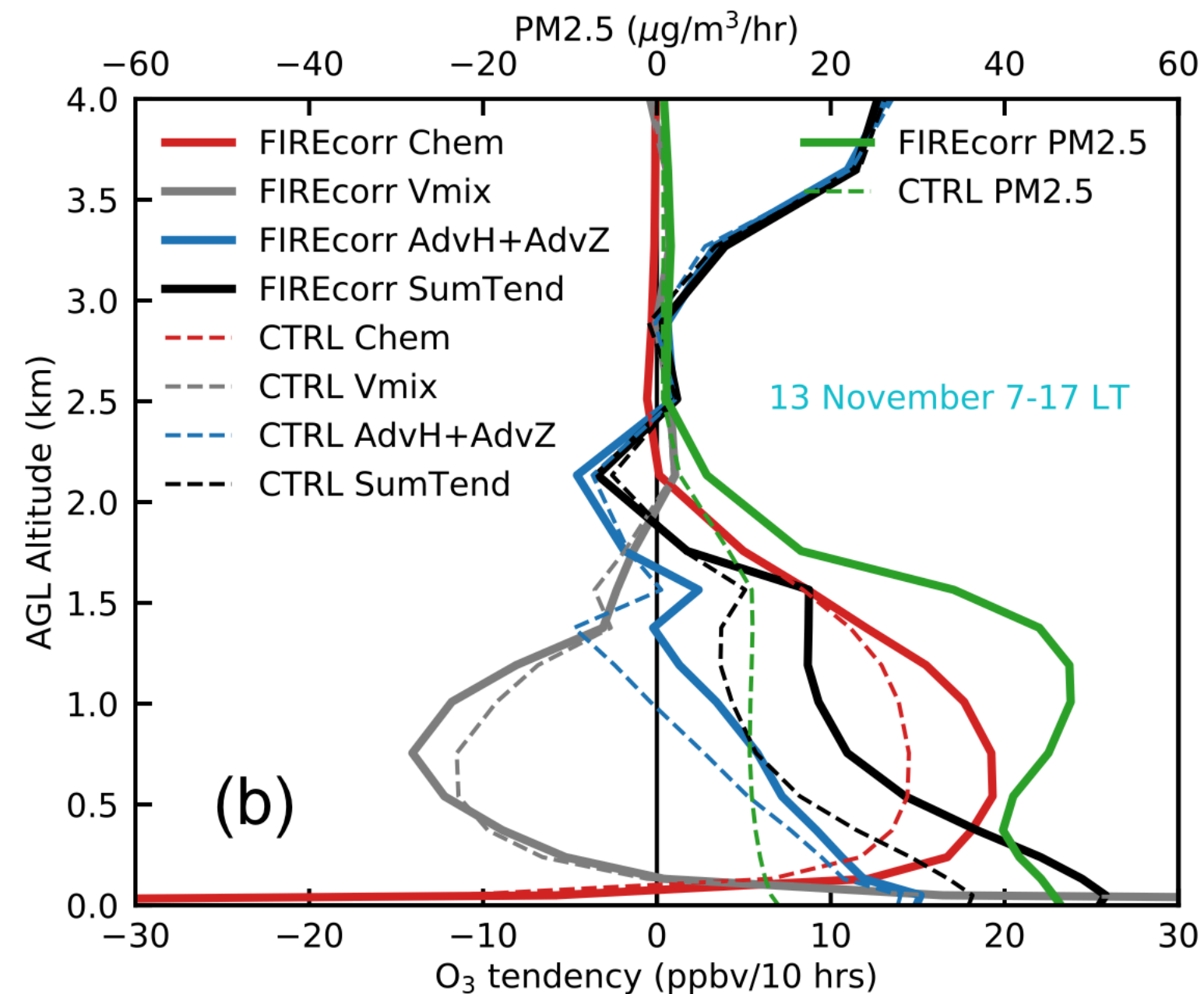
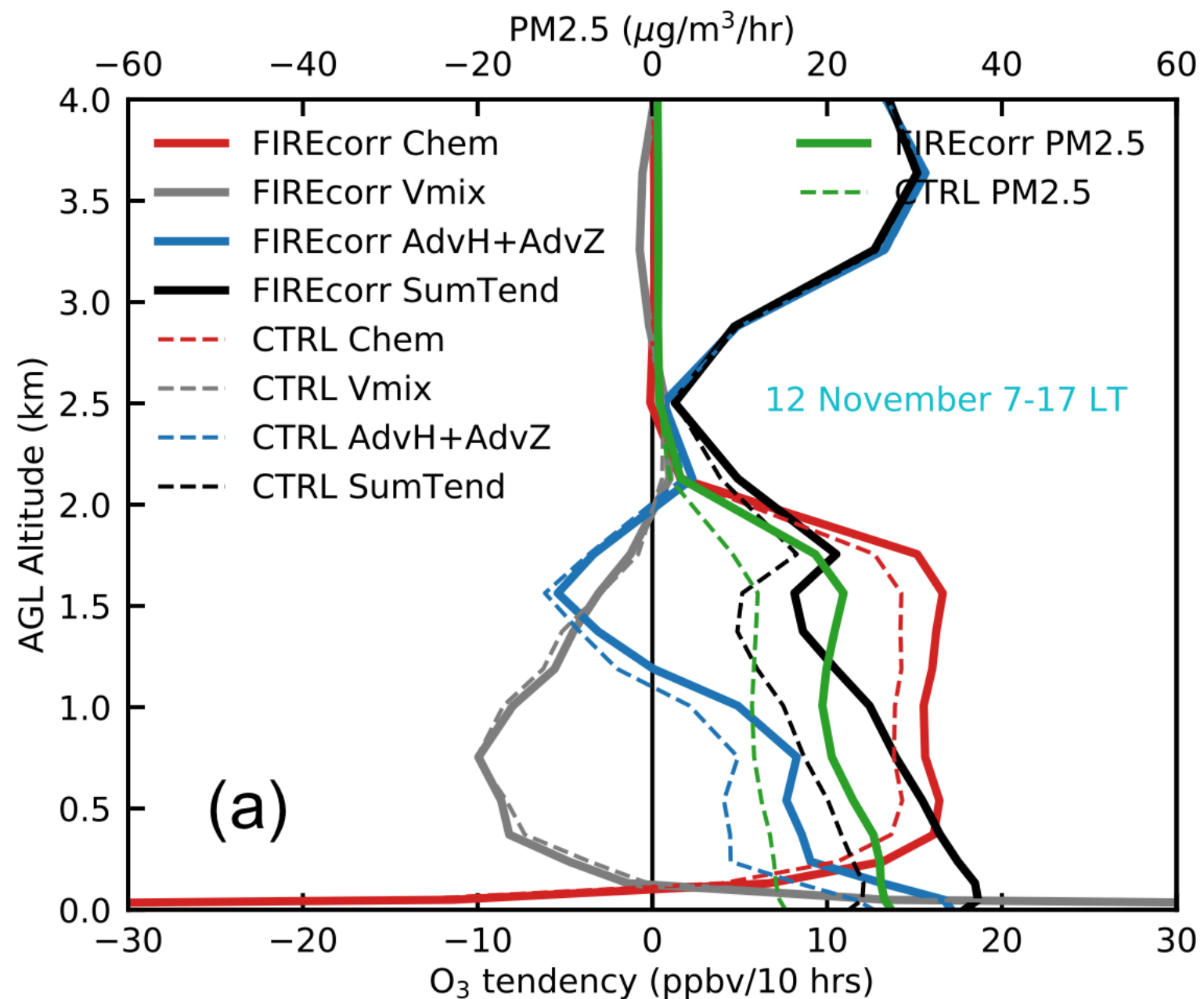
(b) Longitude × Altitude Fire-impacted O₃ at 34.72° N



(c) Longitude × Altitude Fire-impacted PM_{2.5} at 34.72° N

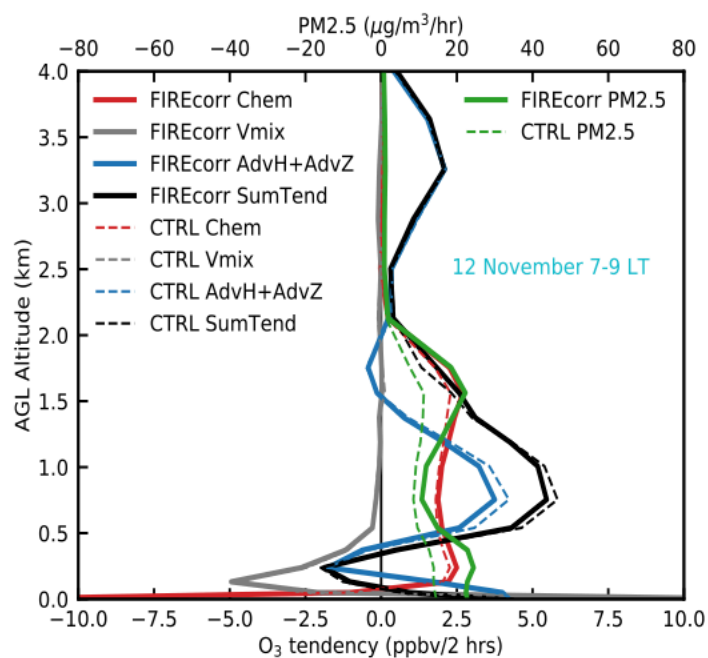


daytime_tendency_v6.

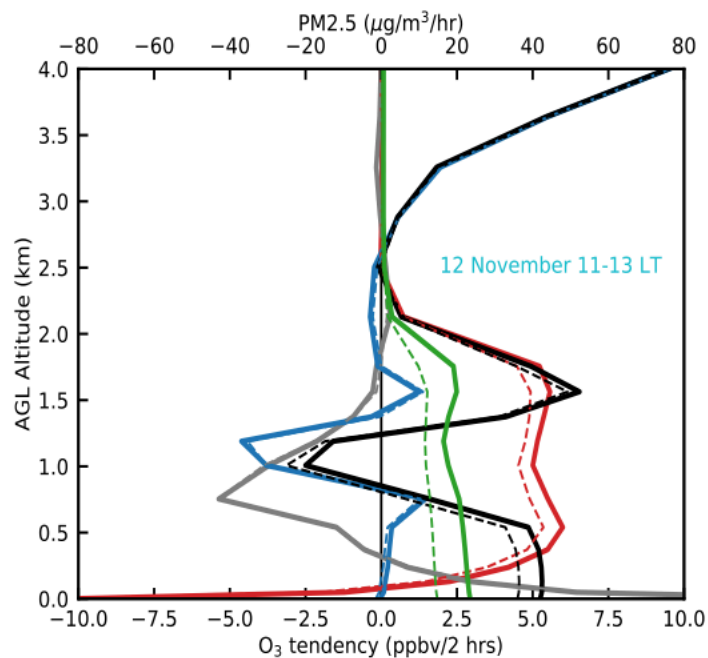


2hr_tendency_v10.

9-11 LT



11-13 LT



15-17 LT

